

**NMR, Water and Plants**



**Promotor** : dr. T. J. Schaafsma,  
hoogleraar in de moleculaire fysica

**Co-referent:** dr. M. A. Hemminga,  
wetenschappelijk hoofdmedewerker

H. Van As

# NMR, Water and Plants

## Proefschrift

ter verkrijging van de graad van  
doctor in de Landbouwwetenschappen,  
op gezag van de rector magnificus,  
dr. C. C. Oosterlee,  
hoogleraar in de veeteeltwetenschap,  
in het openbaar te verdedigen  
op woensdag 31 maart 1982  
des namiddags te vier uur in de aula  
van de Landbouwhogeschool te Wageningen.

BIBLIOTHEEK  
VAN  
LANDELIJKE HOOGESCHOOL  
WAGENINGEN

ISBN = 157402-03

**BIBLIOTHEEK LH.**

**6 3 MAART 1982**

**ONTV. TIJDSCHR. ADM.**

Then I beheld all the work of God,  
that a man cannot find out the work  
that is done under the sun;  
because though a man labour to  
seek it out, yet he shall not find  
it; yea, farther, though a wise man  
think to know it, yet shall he not  
be able to find it.

The Bible, Ecclesiastes 8:17  
( Spreuken 8:17 )

aan mijn ouders  
aan Janneke,  
Elise en Henrik

NN08201,886

# NMR, Water and Plants

Proefschrift van H. Van As  
Wageningen, februari 1982.

STELLINGEN

1. De puls proton NMR-methode zoals beschreven door Hemminga en De Jager, is geschikt om door middel van het meten van bloedstroming eventueel bloedvatvernauwende en/of -verruimende effecten van geneesmiddelen te bepalen.  
M.A. Hemminga en P.A. de Jager, J. Magn. Reson. 37(1980),1  
Dit proefschrift, hoofdstuk 4
2. Het ontleden van een niet-exponentieel verval bij spin-echo NMR spin-spin relaxatietijd metingen aan water in biologische systemen in een som van e-machten vertoont een grote mate van willekeur; voor de rechtvaardiging van een dergelijke ontleding is onafhankelijke experimentele informatie nodig.  
B.M. Fung, Biochim. Biophys. Acta 497(1977),317  
B.M. Fung en P.S. Puon, Biophys. J. 33(1981),27
3. Het verdient aanbeveling pas van dubbele fluorescentie te spreken als uit excitatiespectra éénduidig blijkt dat de waargenomen fluorescenties van één en dezelfde verbinding afkomstig zijn.  
D.L. Philen en R.M. Hedges, Chem. Phys. Letters 43(1976),358
4. Het is de hoogste tijd dat in de evolutie van de beschrijving van de fysische toestand van water in biologische systemen een scheppende daad wordt gesteld.  
M.J. Tait en F. Franks, Nature 230(1971),91  
P.T. Beall, The Sciences 21(1981),6
5. De theorie ontwikkeld ter verklaring van CIDNP verschijnselen, zoals waargenomen met behulp van NMR aan verbindingen in verdunde oplossing, mag niet zonder meer toegepast worden op reactiecentra van fotosynthetiserende bacteriën.  
R. Kaptein, J. Am. Chem. Soc. 94(1972),6251
6. Het is te betwijfelen of de resultaten verkregen met de methode beshreven door Radda et al., om met behulp van NMR bloedstroomsnelheden te meten, onafhankelijk zijn van de spin-rooster relaxatietijd.  
G.K. Radda, P. Styles, K.R. Thulborn en J.C. Waterton,  
J. Magn. Reson. 42(1981),488
7. Het is waarschijnlijk dat er een eenvoudig verband bestaat tussen de waterpotentiaal en de spin-spin relaxatiesnelheid.  
Dit proefschrift, hoofdstukken 5 en 7
8. Het "Voorontwerp van een wet gelijke behandeling" bevat onvoldoende garanties om te voorkomen dat nieuwe vormen van discriminatie ontstaan.  
Voorontwerp van een wet gelijke behandeling

## VOORWOORD

Voor 1977 was watertransport in planten voor mij een stukje middelbare schoolstof dat allang in het moeras van de vergetelheid was weggezonken en water een zo algemeen aanwezig molecuul, dat ik het hooguit als oplosmiddel of dorstlesser gebruikte. Dankzij velen aan de Landbouwhogeschool, zowel binnen als buiten de vakgroep Moleculaire Fysica, is hierin een wending ten goede gekomen, waarvoor mijn oprechte dank. Marcus Hemminga en Adrie de Jager dank ik voor de vele stimulerende discussies, de uitwisseling van informatie en het beschikbaarstellen van het computer programma, waarmee de simulaties werden berekend. Ik hoop Adrie, dat ik je troetel- en geesteskind (het NMR apparaat) niet al te veel misbruikt heb.

Marga Herweijer, Riet Hilhorst, Idy van Leeuwen-Pannekoek en Johan Reinders dank ik voor hun bijdragen tot dit proefschrift. Ze zijn onontbeerlijk geweest voor de afronding van het onderzoek. De nagedachtenis aan Wim van Vliet is er een van vriendschap.

Mijn promotor, Tjeerd Schaafsma, wil ik in het bijzonder bedanken. Tjeerd, je optimisme en kritische zin hebben mij steeds gestimuleerd. Steeds was je ook bereid om mij met raad en daad ter zijde te staan. Dit proefschrift bewijst dat je oorspronkelijke ideeën goed waren.

Ik wil mijn waardering uitspreken voor de wijze waarop de heer A. Hogeveen en Elly Geurtsen van de afdeling Tekstverwerking vorm hebben gegeven aan dit proefschrift. Geoff Searle corrigeerde van enkele hoofdstukken de Engelse tekst, waarvoor ook dank.

Tenslotte wil ik jouw, Janneke, bedanken dat je al deze tijd als een hulp tegenover mij hebt willen zijn, en zelfs meer dan dat.

Ik spreek de wens uit dat ook dit proefschrift mag strekken tot de eer van de Schepper van hemel en aarde, Die mij de kracht en wijsheid gaf om dit werk te doen, in Wiens vreze het beginsel van de wetenschap is en Die ook in de wetenschapsbeoefening toekomt alle lof, eer, aanbidding en dankzegging.



## CONTENTS

	page
<i>LIST OF ABBREVIATIONS AND FREQUENTLY USED SYMBOLS</i>	xi
<b>1 GENERAL INTRODUCTION</b>	<b>1</b>
<b>2 WATER AND PLANTS</b>	<b>6</b>
2.1 State of water in the cell	6
2.2 Water potential	8
2.3 Water transport in the plant stem	9
References	11
<b>3 PULSED NUCLEAR MAGNETIC RESONANCE IN BIOLOGICAL SYSTEMS</b>	
3.1 Basic theory of pulsed NMR	12
3.2 Mechanisms for the spin-spin relaxation	15
3.2.1 Dipolar interaction	16
3.2.2 Paramagnetic ions	18
3.2.3 Sample heterogeneity	20
3.2.4 Exchange and diffusion	22
3.2.5 Summary	25
3.3 Measurement of $T_2$ , diffusion and flow	25
3.3.1 Method of $T_2$ measurement	25
3.3.2 Effect of diffusion and flow	27
3.4 NMR diffusion measurements in biological samples	29
3.5 NMR flow measurements in biological samples	33
3.5.1 History of <i>in vivo</i> blood flow measurements	33
3.5.2 Pulsed NMR flow measurements	34
3.5.3 NMR flow measurements in plants	36
3.6 $T_2$ and water content	39
References	42

<b>4</b>	<b>FLOW MEASUREMENTS IN MODEL SYSTEMS</b>	
4.1	Introduction	45
4.2	Theory	45
4.2.1	System description	46
4.2.2	Motion of the magnetization in the rotating frame	49
4.2.3	$\pi$ pulses	50
4.2.4	A semi-empirical approach	51
4.2.5	Laminar flow	55
4.2.6	Determination of the flow velocity	57
4.2.7	Determination of $T_2$ and volume flowrate	58
4.3	Some comments on the semi-empirical approach	59
4.3.1	Approximations	59
4.3.1.1	Distribution of the r.f. field	60
4.3.1.2	Off-resonance effects on the effective r.f. field	60
4.3.1.3	Sampling time	61
4.3.1.4	Effect of $T_1$ relaxation and diffusion	63
4.3.2	Comparison between theoretical approaches	63
4.4	Experimental	68
4.5	Results and Discussion	70
4.5.1	Calibration	70
4.5.1.1	The need of a linear field gradient	70
4.5.1.2	Effect of $T_1$ and $T_2$ relaxation	72
4.5.1.3	Effect of flow profile	75
4.5.2	Determination of $T_2$ and volume flowrate	75
4.5.2.1	Effect of $T_1$	75
4.5.2.2	Off-resonance signal of stationary water	80
4.5.3	Optimum experimental conditions	82
4.6	Conclusions	83
4.7	Acknowledgement	84
	References	85
<b>5</b>	<b>FLOW MEASUREMENTS IN PLANTS</b>	
5.1	Introduction	86
5.2	Experimental	87

5.2.1	NMR flow measurements	87
5.2.2	NMR T <sub>2</sub> measurements	88
5.2.3	Plant material	89
5.3	Results and discussion	89
5.3.1	Stem segments	89
5.3.2	Intact plants	96
5.4	Conclusions	103
5.5	Acknowledgement	103
	References	104
6	<i>COMPARISON OF FLOW MEASUREMENTS WITH NMR, HEAT PULSE AND BALANCE METHOD</i>	
6.1	Introduction	105
6.2	Experimental	106
6.2.1	NMR flow measurement	106
6.2.2	Heat pulse flow measurement	107
6.2.3	Balance volume flowrate measurement	107
6.2.4	Cross-sectional area	108
6.2.5	Plant material	108
6.3	Results	108
6.4	Discussion	112
6.5	Acknowledgement	114
	References	114
7	<i><sup>1</sup>H SPIN-ECHO NUCLEAR MAGNETIC RESONANCE IN PLANT TISSUE. I. EFFECT OF Mn(II) AND WATER CONTENT IN WHEAT LEAVES</i>	
7.1	Introduction	115
7.2	Materials and methods	116
7.3	Results and discussion	117
7.4	Conclusions	120
	References	121
8	<i>APPLICATION OF NMR FLOW MEASUREMENTS</i>	122
	<i>SUMMARY</i>	126
	<i>SAMENVATTING</i>	128
	<i>CURRICULUM VITAE</i>	131

LIST OF ABBREVIATIONS AND FREQUENTLY USED SYMBOLS

A	-	cross-sectional area
$B_0$	-	static magnetic field
$B_1$	-	radio frequency field
C	-	calibration constant relating $\bar{v}$ and $t_{\max}^1$
CPMG	-	Carr-Purcell-Meiboom-Gill
D	-	(self-)diffusion coefficient
$D_1$	-	theoretical value of $S(t_{\max})$ at $t_{\max}=0$
EPR	-	electron paramagnetic resonance
FETS	-	fast-exchange two-state
FID	-	free induction decay
g	-	electron g factor
G	-	magnetic field gradient
$G(\tau)$	-	autocorrelation time
$H_0$	-	height of signal of stationary water at $t=0$
$\hbar$	-	$h/2\pi$ , where $h$ is Planck's constant
$\vec{I}$	-	angular momentum vector
I	-	nuclear spin quantum number
$J(\omega)$	-	spectral density function
k	-	Boltzmann's constant
$L_{\text{eff}}, l$	-	(effective) length of the r.f. coil
$M_0, M$	-	magnetization
NMR	-	nuclear magnetic resonance
$P_f, P_b$	-	free, bound water fraction
Q	-	volume flowrate
R	-	vessel radius
$R_1, R_2$	-	spin-lattice, spin-spin relaxation rate
Re	-	Reijnold's number
$S(t)$	-	signal amplitude as function of time
$t_p$	-	duration of a r.f. pulse
S	-	electron spin quantum number
$T_1, T_2$	-	spin-lattice, spin-spin relaxation time

$\bar{v}$	-	mean linear flow velocity
V	-	amount (volume) of flowing water in r.f. coil
$\alpha$	-	rotation angle due to a r.f. pulse
$\gamma$	-	gyromagnetic ratio
$\tau$	-	time between two r.f. pulses
$\tau_a$	-	mean residence time in site a
$\tau_D$	-	diffusional correlation time
$\tau_e$	-	correlation time for scalar interactions
$\tau_r$	-	rotational correlation time
$\tau_t$	-	translational correlation time
$\tau_s$	-	electron spin relaxation time
$\psi$	-	water potential
$\vec{\mu}$	-	magnetic moment
w	-	precession frequency in a magnetic field

## 1 GENERAL INTRODUCTION

Plants require water; deprived of it, they will wilt and die. In fact, the typical land plant consumes prodigious quantities of water, much more than any of the other substances that enter it. Most of this water does not remain within the plant, but passes through the plant to the atmosphere. This process is called *transpiration*. Water transport over long distances primarily occurs through a system of capillaries called *xylem*. The xylem forms an extra-protoplasmic pathway for solute flow, consisting in particular of water, ions and certain organic solutes upwards from the root to transpiring surfaces of shoot system. In contrast, there is a second pathway through the sieve elements of the *phloem*. Within this system concentrated solutes such as carbohydrate produced by photosynthetically active structures flow to sink regions of various kinds in which these solutes are consumed for growth or stored in fruits or other reservoirs.

The seemingly wasteful consumption of water through transpiration is essential to the growth of plants. In nature and even in agriculture, it is a rare and fortunate plant that enjoys an optimum supply of water throughout its lifecycle. Without irrigation, most crops are inhibited, often seriously, from achieving full growth and development.

Out of all process controlling the growth of wild or cultured plants there is perhaps no single factor that is more crucial and none more amenable to our intervention (at least in principle) than that of control over transpiration in plants. Also in horticulture (greenhouses) this becomes increasingly important as energy costs are rising and transpiration as well as uptake of water in the roots require large amounts of energy.

The transpirational process is one of the factors contributing to the water balance of the plant, beside uptake, transport and storage of water; these processes are strongly mutually coupled [1]. The rate of water transport in the xylem in combination with water

content of the surrounding stem tissue are useful parameters to study and control the water balance, especially in relation to the effects of environmental factors such as light intensity, air humidity, CO<sub>2</sub> concentration, soil- and air temperature on crop production. In addition, these parameters may be used for selection of breeds which combine favourable parameters for the water balance and low energy use.

Several methods have been used to study water transport and -content [2].

Concerning water transport, either the mean linear flow velocity  $\bar{v}$  or the volume flowrate  $Q$  of the movement of water in the vascular system in plant stems has been measured. The major existing methods are:

- injection and monitoring of dyes or radio-active tracers (e.g. [3]). These methods are highly sensitive but cannot measure flow after equilibrium has been reached. Also, it is uncertain if the transport rate of tracers represents the actual rate of water flow, since dyes or radio isotopes are absorbed at the vessel's surface [3].
- heat pulse methods, measuring the unbalance created by net water transport through plant stems by a unit containing a heat injecting resistor and two temperature sensors symmetrically placed around the injector [4,5]. This method cannot measure absolute flowrates, but only changes. It does not provide reliable figures on the volume of waterflow per unit of time. The time-resolution is relatively long (5-10 min.).
- the magnetohydrodynamic technique, where a magnetic field perpendicular to the flow generates a small induction voltage in a direction at right angles both to the flow and the field, due to the movement of charged particles [6,7]. The voltage measured by means of an electronic detection system is directly proportional to magnetic flux density, to the internal radius of the vessels and to the instantaneous velocity of the stream. The method can be used for instantaneous (repetitive) as well as continuous (steady state) measurements. A disadvantage of this method is the need of a relatively high flow velocity.

- the weight balance method, by which the loss of weight of the plant per unit of time is determined by a sensitive balance (e.g. [8]). The method requires isolation of the plant and surrounding soil and is vulnerable to air-currents. It has a time-resolution of a few minutes. In contrast to the previous mentioned methods this method yields volume flowrates. This is also obtained by a related method based on lysimeters [2]. Increase in plant weight by CO<sub>2</sub> and/or water uptake introduces errors in determining the actual volume flowrate through the plant stem.

None of these methods detects the movement of water itself, however, and many are invasive. Nuclear magnetic resonance (NMR) does not have these disadvantages, and has been shown to be a suitable technique to study liquid flow [9]. To measure flow in plant stems the technique must be able to measure linear flow velocities in the range of 1-30 mm/s [2], and must be able to discriminate between a small fraction of flowing water (2-10%) and a large amount of stationary water in the plant stem tissue. Two different pulsed NMR methods have been developed satisfying these conditions [10,11], the first of which is a difference method and requires that the amount and physical properties of stationary water do not change in the course of the measurements. In Chapter 5 we show that this situation in plants clearly cannot be obtained.

The second method [11] does not have this disadvantage and allows determination of flow in a single experiment. This NMR method has the following advantages:

- it is non-destructive and non-invasive. Whereas the first advantage is obvious, the importance of the second is not generally realized. Some plants react excessively to mechanical or electrical contact, and it must be suspected that most if not all plants exhibit some change in one or more rate-processes upon such contact.
- it allows instantaneous as well as continuous measurements.
- it selectively measures flowing water only and does not record stationary water. In addition it measures the movement of the water molecules itself by "labelling" and monitoring the protons of the water molecules.
- the method is insensitive to air-currents after the sample remains in a fixed position in the magnet.



- as will be shown in Chapter 4, the method permits measurement of linear as well as volume flowrates after non-destructive calibration using a glass capillary system.
- the method, when used to perform instantaneous measurements, allows a high time-resolution (3-10 s).

The disadvantages of this NMR method are:

- intrinsic low sensitivity of NMR.
- the NMR apparatus is relatively expensive in comparison to alternative methods, described before.

The method can equally well be applied to liquid flow in other biological objects than plants, e.g. for the measurement of blood flow (see Chapter 8) and the circulation of body fluids in human and animals. Finally, there appears to be no technical barrier for the measurement of spatially resolved flow patterns in various objects, using a combination of flow measurements by pulsed NMR and zeugmatography.

For the determination of the water content, several methods have been used and are still in use [2], but they are either invasive, indirect, or destructive. Already in 1961 it has been shown that NMR can be used to determine the water content of grain [12]. From basic theory of NMR (see Chapter 3), it follows that the NMR signals are proportional to the amount of protons in the detector of the NMR apparatus. In Chapter 7 it is demonstrated that these signals can indeed be related to the water content. In addition the dynamical information in these NMR signals (see Chapter 3), can be used to distinguish various water fractions in the tissue with different physical properties, e.g. surface-bound, exchanging or bulk water fractions.

Thus NMR flow measurements can be used to selectively measure flowing water only, without interference of the stationary tissue water, whereas by choosing a different pulse-sequence stationary water content can be monitored in the same experiment, without replacing the plant. This is a great advantage of the non-destructive NMR method over the existing other methods.

The goal of this Thesis is to describe the application (and its limits) of the pulsed NMR method to plant stems. Chapter 2 summarizes the process of watertransport in plants and the physical state of

water in the cell. Basic NMR theory as well as NMR pulse sequences to determine flow, diffusion and water content in biological systems are presented and reviewed in Chapter 3. Chapter 4 presents a detailed description and discussion of the NMR method to determine flow in plant stems, showing that linear flow velocity as well as volume flowrate can be determined simultaneously, yielding in addition an estimate of the effective cross-sectional area of the transport vessels. NMR flow measurements in stem segments and in intact plants are reported in Chapters 5 and 6. Chapter 5 explains the reason for some negative results and discusses the results of simultaneous flow measurements and water content monitoring. A comparison between the results of flow measurements obtained with NMR, the heat pulse and weight balance method is presented in Chapter 6.

Throughout this Thesis we are concerned with transport of water in the xylem. The phloem transport is downwards, which should give rise to an opposite sign of the NMR signal with respect to that of the upwards xylem transport. Phloem transport has not been observed, due to its much lower velocity.

#### REFERENCES

1. R.O. Slatyer, "Plant-Water Relationships" (Academic Press, New York, 1967).
2. B. Slavik, "Methods of Studying Plant Water Relations", Ecological Studies, Vol. 9 (Springer-Verlag, Berlin, 1974).
3. S.C. van de Geijn, Thesis, Utrecht, The Netherlands (1976).
4. B. Huber, Ber. Deut. Bot. Ges. 50 (1932), 89.
5. K. Schurer, H. Griffioen, J.G. Kornet, G.J.W. Visscher, Neth. J. Agric. Sci. 27 (1979), 136.
6. D.W. Sheriff, J. Exp. Bot. 23 (1972), 1086.
7. D.W. Sheriff, J. Exp. Bot. 25 (1974), 675.
8. P. Tegelaar, A.F. van der Wal, Neth. J. Pl. Path. 80 (1974), 77.
9. D.W. Jones, T.F. Child, in "Advances in Magnetic Resonance" (J.S. Waugh, ed.), Vol. 8, p.p. 123-148 (Academic Press, New York, 1976).
10. M.A. Hemminga, P.A. de Jager, A. Sonneveld, J. Magn. Reson. 27 (1977), 359.
11. M.A. Hemminga, P.A. de Jager, J. Magn. Reson. 37 (1980), 1.
12. S.V. Kuznetsov, Vestnik Selskokhoz. Nauki 6 (1961), 117 (from ref. 2).

## 2 WATER IN PLANTS

This Chapter summarizes some characteristics of water transport in the plant stem and the physical state of water in the plant cell, in order to define some basic concepts underlying the main results of this Thesis.

Water transport and -balances in plants and its parts have been treated in several reviews [1-6], on which the last parts of this Chapter are based. The state of water in the cell is reviewed in ref. 5-9.

### 2.1 STATE OF WATER IN THE CELL

Biological tissues contain 60-90 percent water and living organisms are absolutely dependent on water in a variety of ways. Nevertheless, basic knowledge about the physical state of cellular water is rather limited. There are two classical viewpoints about cellular water:

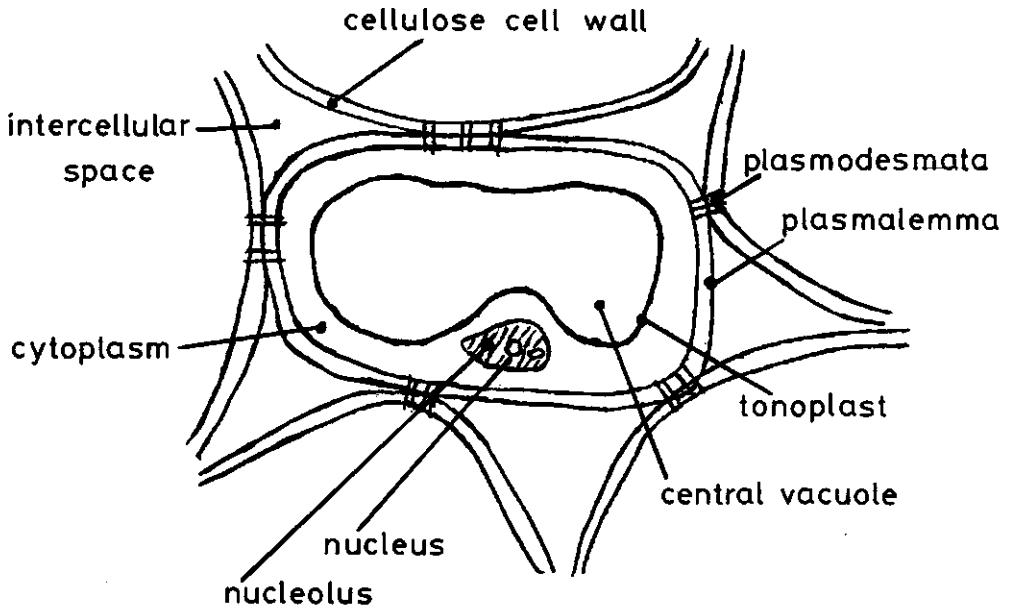


Fig. 1 Structure of a vacuolated plant cell (adapted from [10]).

(i) most water in the cell is considered to be in the free liquid state (bulk water); then, a living cell is equivalent to a dilute aqueous solution surrounded by a semipermeable membrane. In a vacuolated plant cell (Fig. 1) the cytoplasm is considered as such a semipermeable membrane. Following this model, it has been thought that the total cell behaves as an osmometer, an idea which is still in use [1], (ii) on the other hand there is also experimental evidence that the cellular water partially or totally exists in a physical state significantly different from normal liquid water. Water, ions and biopolymers inside the cell form a highly ordered phase.

Hechter [11], discussing these classical concepts, concluded that both ideas are partly correct and partly wrong.

For water near interfaces there is considerable evidence that there exists indeed a structurally changed boundary layer of water, called hydration water. The water molecules in the hydration layer of biological macromolecules exhibit restricted motion due to a significant decrease in translational and rotational degrees of motion by interaction with the macromolecules. Clifford [7] has described

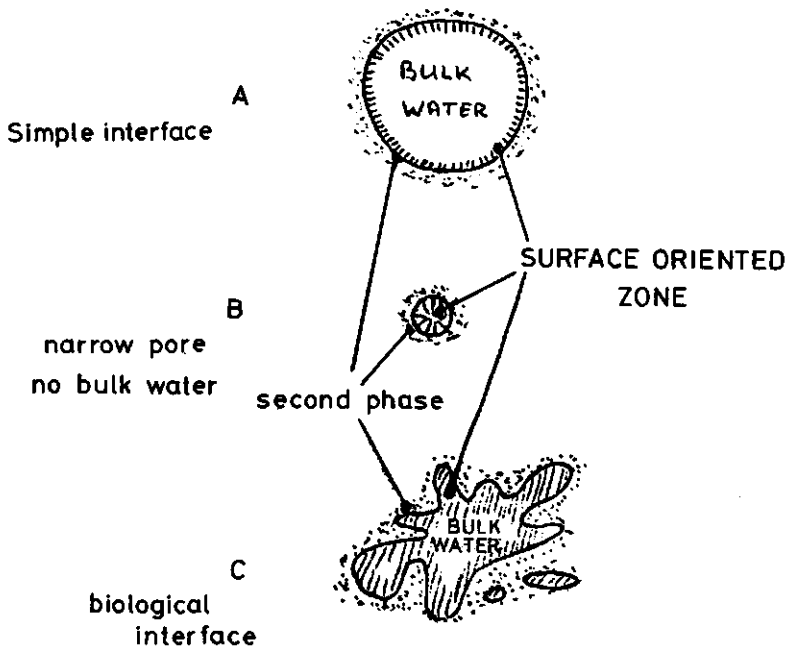


Fig. 2 Possible surface environments: (A) surface in contact with bulk water, (B) thin films and narrow pores, (C) particular surface in biological material. (adapted from [7]).

the effect of surface environments on the behaviour of water, as illustrated in Fig. 2. In A there is simply an interface between bulk water and a second phase, which may be solid, liquid, or vapour. In B there is a thin layer of water between two interfaces, not allowing sufficient space for the development of bulk water structure. In biological material surfaces are usually more like C: the surface available for adsorption is many times the superficial surface area and water molecules exist in spaces comparable with molecular dimensions.

## 2.2 WATER POTENTIAL [4]

In plant physiology, it is customary to express the free energy content of water by the *water potential*  $\psi$ . Derivations of water potential from strict thermodynamic principles can be found in [1] and [4]. For our purposes, it is sufficient to define water potential as the free energy per unit volume of water, assuming the potential of pure water to be zero under standard conditions.

Because water potential increases with temperature, it is important to maintain constant temperature during a series of measurements. In contrast, water potential is lowered below that of pure water by dissolved solutes and also by the binding of water to surfaces by matrix forces. Since these effects are considered to be mutually independent, the water potential of a solution ( $\psi$ ) can be expressed as

$$\psi = \psi_s + \psi_m \quad (2.1)$$

where  $\psi_s$ , the *solute potential*, is the reduction in water potential due to dissolved solutes (negative),  $\psi_m$ , the *matrix potential*, is the reduction in water potential due to matrix forces (negative) and thus  $\psi$  will be negative. Consequently, in the soil-plant-atmosphere system, water potentials are usually negative, and water flows towards regions with more negative values.

In plant tissue, water potentials may be increased by hydrostatic pressure and, therefore, eqn. 2.1 must be modified to give

$$\psi = \psi_s + \psi_m + \psi_p \quad (2.2)$$

where  $\psi_p$ , the *pressure potential*, is the increase in water potential due to hydrostatic pressure (positive). Since  $\psi_p$  is positive, the resulting water potential is less negative than would be expected if only solute and matrix effects were considered.

### 2.3 WATER TRANSPORT IN THE PLANT STEM

Longitudinal water transport in the plant stem is primarily located in the vascular system, where it moves from the xylem terminals in the root to those in the leaf. In principle, the whole cross-sectional area of the root or the stem is available for transport. However, the flow through cell walls in the stem pathway can, at least under normal conditions, be neglected. The permeability of the protoplast is assumed to be 50 times less than that of the cell wall [2,3] and consequently this pathway can also be neglected with respect to vascular transport. This does not mean that transverse water transport is absent in the stem. This has been demonstrated, by adding isotopically labelled water to the root medium [12], causing the water in the xylem to be rapidly replaced by the labelled water, concomitant with a slow progressive replacement of water in the remainder of the outer stem tissue.

In a freely-transpiring plant, water evaporates from the moist walls of epidermal and mesophyll cells in the interior of the leaves and is lost to the atmosphere through the stomata. As water loss proceeds, the water potential in the leaf apoplast falls below that of the leaf cells and also below the water potential in the xylem and the soil. (The apoplast is defined as the non-living parts of the plant, e.g. xylem, cell walls, etc.). This results in the rapid withdrawal of water from leaf cells and a lowering of cell water potential. Although there is continuity of liquid water between leaf and soil via the xylem, equalization of water potential throughout the plant by upward water movement can not occur very rapidly because there is a resistance to hydraulic flow in the plant/soil system. Consequently, transpiration establishes a water potential gradient causing flow of water from the soil to the leaf.

The flow of water to a transpiring leaf in response to a water potential gradient has been described by an expression analogous to Ohm's Law [13]. In a symplified form this results in

$$Q = \frac{\psi_{rs} - \psi_{leaf}}{R} \quad (2.3)$$

where  $Q$  is the volume flowrate of the water moving from soil to leaf,  $\psi_{rs}$  is the water potential of the soil at the root surface,  $\psi_{leaf}$  is the water potential of the transpiring leaf, and  $R$  is the resistance to hydraulic flow between the root surface and the site of evaporation. For a simple plant (e.g. a seedling),  $R$  can be divided into a series of component resistances within the plant:

$$R = r_{root} + r_{stem} + r_{leaf} \quad (2.4)$$

where  $r_{root}$  is the resistance to flow between the root and the lumen of the xylem,  $r_{stem}$  is the resistance in the xylem (root, stem and leaf), and  $r_{leaf}$  is the resistance to flow across the leaf to the evaporation site. Of those quantities,  $r_{leaf}$  and  $r_{root}$  have been considered as the most important resistances. Experimentally, it has been found that the resistance in the xylem vessels depends on the lumen wall surface sculptures [14].

When a plant is transpiring rapidly ( $\psi_{soil} - \psi_{rs}$ ) and ( $\psi_{rs} - \psi_{leaf}$ ) cannot exceed values of 10 - 30 bar (1 bar =  $10^5$  Pa) whereas ( $\psi_{leaf} - \psi_{air}$ ) varies between 100 and 2000 bar [4]. Therefore, as long as steady state flow is maintained, leaf diffusive resistance controls the rate of water throughout the soil-plant-atmosphere system as well as transpiration rate.

Great care must be exercised in applying this model to the behaviour of plants. Most plants do not consist of a single root, stem and leaf in series; they should rather be considered as a number of root axes, branches and leaves attached in parallel to a single (or multiple) stem. Another difficulty is that water can be withdrawn into, or released from, storage reservoirs (e.g. stem or leaf tissue, fruits, etc.) at different points along the pathway, thus altering the flowrate. In Chapter 5 we show, that cells bordering the xylem in the stem and root system lose water during periods of water stress (e.g. during the day) and adsorb water during the night. This problem can be overcome by extending the electrical analogy to include capacitance, as well as resistance in the soil, stem and leaves;

the exchange of water with storage reservoirs is then analogous to charging and discharging an electrical capacitance. Such a model has been proposed in [5].

An indication of the value of the average maximum velocities of water transport in xylem is given in [15]. In mm/s  $\bar{v}$  is 0.3 - 0.6 in ferns, 0.33 in evergreen conifers, 0.27 - 1.7 in leafy trees with scattered porous wood (e.g. birch, beech, lime), 3.9 - 12.2 in ring porous wood (oak, ask trees), 2.8 - 16.7 in herbs and 42 in lianes.

#### REFERENCES

1. R.O. Slatyer, "Plant-Water Relationships" (Academic Press, New York, 1967).
2. M.B. Russell, J.T. Woodley, in "Growth in Living Systems" (M.X. Zarrow, ed.) p.p. 695 - 722 (Basic Books, New York, 1961).
3. P.E. Weatherley, in "The Water Relations of Plants" (A.J. Ruttan, F.H. Whitehead, eds.) p.p. 85 - 100 (Blackwell, London, 1963).
4. A.H. Fitter, R.K.M. Hay, "Environmental Physiology of Plants" (Academic Press, London, 1981).
5. H. Meidner, D.W. Sheriff, "Water and Plants" (Blackie, Glasgow, 1976).
6. G. Peschel, in "Water and Plant Life: Problems and Modern Approaches" (O.L. Lange, L. Kappen, E.D. Schulze, eds.), Ecological Studies, Vol. 19, p.p. 6 - 18 (Springer-Verlag, Berlin, 1976).
7. J. Clifford, in "Water - A Comprehensive Treatise" (F. Franks, ed.), Vol. 5, p.p. 75 - 132 (Plenum Press, New York, 1975).
8. H.J.C. Berendsen, idem, p.p. 293 - 330.
9. F. Franks, Phil. Trans. R. Soc. London B 278 (1977), 89.
10. J. Sutcliffe, "Plants and Water" (Edward Arnold, London, 1968).
11. O. Hechter, Annal. New York Acad. Sci. 125 (1965), 625.
12. O. Biddulph, F.S. Nakayama, R. Cory, Plant Physiol. Lancaster 36 (1961), 429.
13. T.H. van der Honert, Disc. Faraday Soc. 3 (1948), 146.
14. A.A. Jeje, M.H. Zimmermann, J. Exp. Bot. 30 (1979), 817.
15. B. Slavik, "Methods of Studying Plant Water Relations", Ecological Studies, Vol. 9, p. 223 (Springer-Verlag, Berlin, 1974).



## 3 PULSED NUCLEAR MAGNETIC RESONANCE SPECTROSCOPY IN BIOLOGICAL SYSTEM

Reviews on the NMR pulse method and the theory of relaxation have been published [1-6,13]. Hence, this Chapter does not contain a detailed treatment of methods, theory and interpretation of pulsed NMR. Only the necessary background for the Chapters 4 - 8 of this thesis is provided, as well as short reviews on some special applications of NMR, i.e. self-diffusion and flow measurements. In addition, the relationship between the relaxation parameters and water content, emphasizing biological systems, is shortly discussed.

## 3.1 BASIC THEORY OF PULSED NMR

Most nuclei possess the property of *spin*, characterized by an angular momentum vector  $\vec{I}$  and a magnetic moment  $\vec{\mu}$  related by

$$\vec{\mu} = \gamma \hbar \vec{I}, \quad (3.1)$$

where  $\gamma$  is the gyromagnetic ratio, a constant for a given nucleus;  $\hbar$  is  $h/2\pi$  where  $h$  is Planck's constant. When a nucleus of spin  $I$  is placed in a static magnetic field  $\vec{B}_0$ , the magnetic interaction between the nuclear magnetic moment  $\vec{\mu}$  and  $\vec{B}_0$  gives rise to  $(2I + 1)$  equidistant energy levels, with a separation

$$\Delta E = \gamma \hbar B_0 \quad (3.2)$$

For protons ( $^1\text{H}$ ), the only nuclei considered in this thesis,  $I = \frac{1}{2}$ .

At thermal equilibrium, nuclei are distributed among the energy levels according to a Boltzmann distribution. This results in a macroscopic *magnetization*  $\vec{M}_0$  along the direction of  $\vec{B}_0$ . For a sample containing  $N$  nuclei, the equilibrium magnitude of  $\vec{M}_0$  is given by [2]

$$|M_0| = N\gamma^2\hbar^2 I(I + 1)B_0/3kT \quad (3.3)$$

We shall find it adequate in our treatment of pulse phenomena to deal almost entirely with the macroscopic magnetization by a classical description [1]. A complete theoretical description, in a quantum mechanical formalism, is given in several textbooks [2-4].

Bloch et al. [5] found that the motion of macroscopic magnetization in the presence of an applied magnetic field  $\vec{B}$  could be explained in terms of phenomenological differential equations. The classical equation of motion for the magnetization is given by

$$d\vec{M}/dt = \gamma\vec{M} \times \vec{B} \quad (3.4)$$

describing a precession of the magnetization around the magnetic field vector  $\vec{B}$  at an angular frequency  $\vec{\omega} = -\gamma\vec{B}$ . The precession frequency of  $\vec{M}$  in  $B_0$  is called the Larmor frequency  $\omega_0$ . In order to stimulate spin transitions, the frequency of the electromagnetic radiation must be equal to the frequency of the Larmor precession according to  $\omega = -\gamma B_0$ . This is the *resonance condition*.

In NMR experiments, commonly a rotating frame of reference  $\{x', y', z'\}$  is defined for which the  $z'$  axis has the same direction as the  $z$  axis in a laboratory frame, coinciding with the direction of  $\vec{B}_0$ . The frame  $\{x', y', z'\}$  rotates at an angular frequency  $\omega$  ( $\omega \cong \omega_0$ ) around  $\vec{B}_0$  (Fig. 1).

(a)

(b)

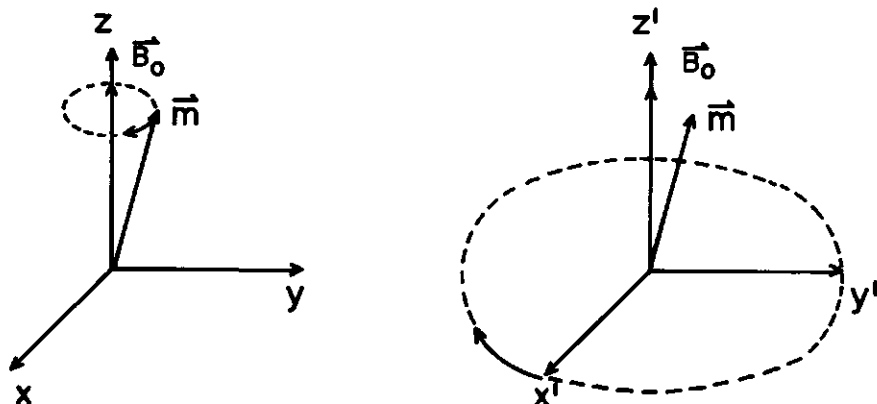


Fig. 1 Magnetization  $\vec{M}$  in a laboratory frame (a) and a rotating frame (b), when  $\omega = \omega_0$

The equation of motion (Eqn. 3.4) in the rotating frame becomes

$$d\vec{M}'/dt = \vec{M}' \times \gamma(\vec{B}' + \vec{\omega}/\gamma) = \vec{M}' \times \gamma\vec{B}'_{\text{eff}} \quad (3.5)$$

On resonance  $\vec{\omega} = -\gamma\vec{B}_0$ . When  $\vec{B}' = \vec{B}_0$ ,  $\vec{M}'$ , the magnetization in the rotating frame, is constant. When we apply in addition to  $\vec{B}_0$  a radio frequency field  $B_1$ , with angular frequency  $\vec{\omega}$ , perpendicular to  $\vec{B}_0$  (i.e. in the  $x, y$  plane), the effective field in the rotating frame becomes  $\vec{B}_1$ , and the magnetization rotates around  $\vec{B}_1$  at an angular frequency  $\gamma B_1$ . During a time  $t_p$  the angle over which  $\vec{M}$  rotates is

$$\alpha = \gamma B_1 t_p \quad (\text{radians}) \quad (3.6)$$

Strictly speaking, this relation only holds for the exact resonance frequency. It can be shown however, that the condition (3.6) holds relatively well even when the resonance condition is not exactly fulfilled, provided the  $B_1$  pulse is sufficiently strong and its rise time short (a few  $\mu\text{s}$ ).

If the  $B_1$ -field is switched off at the moment when  $\alpha = 90^\circ$ , the pulse in question is a  $90^\circ$  ( $\frac{1}{2}\pi$ ) pulse. Correspondingly, if the length of the pulse is chosen in such a way that  $\alpha = 180^\circ$ , the pulse is called a  $180^\circ$  ( $\pi$ ) pulse (Fig. 2).

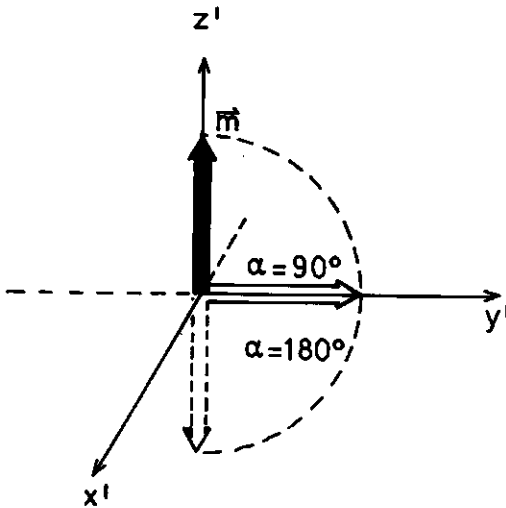


Fig. 2 The  $90^\circ$  and  $180^\circ$  pulses.

After the pulse,  $B_1$  is absent and  $B_{\text{eff}} = 0$ . Because  $\vec{M}$  is no longer in its equilibrium state, nuclear magnetic relaxation processes ensure its return to the equilibrium value  $\vec{M}_0$ . Bloch [5] has described the motion of the components of magnetization by the following equations:

$$dM_x/dt = -M_x(t)/T_2 \quad \text{or} \quad M_x(t) = M_x(o)\exp(-t/T_2) \quad (3.7a)$$

$$dM_y/dt = -M_y(t)/T_2 \quad \text{or} \quad M_y(t) = M_y(o)\exp(-t/T_2) \quad (3.7b)$$

$$d(M_z - M_0)/dt = -(M_z(t) - M_0)/T_1 \quad \text{or} \quad M_z(t) = (M_z(o) - M_0)\exp(-t/T_1) \quad (3.7c)$$

The terms  $-M_{x,y}/T_2$  and  $-(M_z(t) - M_0)/T_1$  represent the tendency of the magnetization to return to its equilibrium value, i.e. nuclear magnetic relaxation. The time constant  $T_1$  refers to the return of  $M_z$  to its equilibrium value  $M_0$ ;  $T_1$  is called the *spin-lattice* or the *longitudinal relaxation time*.

The transverse component of  $\vec{M}$  decays exponentially with the time constant  $T_2$ , the *spin-spin* or the *transverse relaxation time* (also called the phase coherence time). In fact, the spin-lattice relaxation time  $T_1$  characterizes the exchange of energy between the spin system and the degrees of freedom of the lattice whereas the spin-spin relaxation time  $T_2$  characterizes the exchange of magnetic energy inside the spin system, i.e., without a global change of the equilibrium magnetization. The latter characterizes the mean life time of the spins in a given energy state, due to the exchange of magnetic energy between the spins.

As shown in eqns. 3.7a-c  $\vec{M}$  approaches equilibrium exponentially. However, because of the heterogeneity of biological systems, the nuclear relaxation is in general not characterized by a single exponential decay, but by a sum of exponentials, each with its characteristic relaxation time. This situation applies also to the results for plant samples as described in this thesis (Chapter 7).

### 3.2 MECHANISMS FOR THE SPIN-SPIN RELAXATION

The NMR relaxation times of water in biological samples, which have been widely used to measure the physical properties of this water, are affected by many factors and in general a straightforward

theoretical interpretation of the observed relaxation behaviour is therefore impractical. In this section we will give the mechanisms and dynamic processes which cause nuclear relaxation, especially in biological tissue. In favourable cases one of these mechanisms or dynamic processes dominates the relaxation behaviour and interpretation of the data is quite simple. Unfortunately, in most biological tissues this is not the case and approximations must be made to explain the relaxation measurements.

### 3.2.1 Dipolar interaction

One of the most important mechanisms for nuclear magnetic relaxation involves magnetic dipole-dipole interaction. Due to this interaction a magnetic nucleus experiences a small local field  $B_{loc}$ , produced by the neighbouring nuclear magnets [1]:

$$B_{loc} = \sum_i \frac{\mu_i}{r_i^3} (3\cos^2\theta_i - 1) \quad (3.8)$$

where  $r_i$  is the internuclear distance, and  $\theta_i$  the angle between  $\vec{r}$  and the magnetic field. This interaction may be intra- or inter-molecular.

Secondly, molecules are in thermal translational and rotational motion, and atoms, or even groups of atoms, may change places within or between molecules. Due to these motions, the local magnetic field  $\vec{B}_{loc}$  experienced by a particular nucleus continuously varies in time. If  $\vec{B}_{loc}$  fluctuates at a suitable frequency it may induce transitions between spin states similar to those caused by the external resonance frequency field. Thermal motions in a liquid cover a wide spectrum characterized by the 'spectral density' function  $J(\omega)$  [6], which represents the power at frequency  $\omega$ .  $J(\omega)$  is the Fourier transform of the so-called autocorrelation function  $G(\tau)$ , measuring the persistence of the fluctuations of the motion. Frequently  $G(\tau)$  drops off exponentially with a decay time  $\tau_c$ , which is called the correlation time. It is the time taken for a typical fluctuation to die away. In many cases,  $\tau_c$  uniquely defines the  $J(\omega)$  of the local field. For translational motion  $\tau_c$  can be considered as the time

needed for a molecule to make a displacement corresponding to its diameter; similarly, for rotational motion,  $\tau_c$  can be viewed as the time needed to make a rotation through an angle of one radian; for collisions  $\tau_c$  is the average time between molecular collisions.

If we assume that a single correlation time characterizes the molecular rotation, the dipole-dipole interaction for two identical nuclei with  $I = \frac{1}{2}$  gives rise to nuclear spin relaxation, with relaxation times:

$$\left(\frac{1}{T_1}\right)_{\text{intra}} = \frac{3\gamma^4 \hbar^2}{10 r^6} \left\{ \frac{\tau_c}{1 + \omega_0^2 \tau_c^2} + \frac{4\tau_c}{1 + 4\omega_0^2 \tau_c^2} \right\} \quad (3.9a)$$

$$\left(\frac{1}{T_2}\right)_{\text{intra}} = \frac{3\gamma^4 \hbar^2}{20 r^6} \left\{ 3\tau_c + \frac{5\tau_c}{1 + \omega_0^2 \tau_c^2} + \frac{2\tau_c}{1 + 4\omega_0^2 \tau_c^2} \right\} \quad (3.9b)$$

where  $r$  is the internuclear distance and  $\tau_c$  is the rotational correlation time. For the translational motions involved in intermolecular interactions, the general expressions for  $\left(\frac{1}{T_1}\right)_{\text{inter}}$  and  $\left(\frac{1}{T_2}\right)_{\text{inter}}$  are similar to eqns. 3.9a-b, where the rotational correlation time  $\tau_c$  must be replaced by the translational correlation time  $\tau_t$  [2].

For fast rotational motion ( $1/\tau_c \gg \omega_0$ ),  $T_1$  equals  $T_2$  and both are inversely proportional to  $\tau_c$ . This condition is commonly met in aqueous solution at room temperature, where  $\tau_c$  for water molecules is of the order of  $10^{-11}$  s. As the correlation time  $\tau_c$  increases, the component of the local fluctuating field at the resonance frequency  $\omega_0$  decreases, tending to zero when  $\omega_0 \tau_c \gg 1$ .  $T_1$  now becomes proportional to  $\tau_c$  and increases once more as the magnitude of  $\tau_c$  increases.  $T_2$ , however, continues to decrease linearly with  $\tau_c$ , because  $T_2$  is also sensitive to low frequency fluctuations, until the molecular motion slows down so much that it reaches the rigid lattice condition. When water molecules interact with macromolecules in solution or with membranes the rotational and translational motion slows down considerably, causing  $T_1$  and  $T_2$  to become different, and resulting in a value of  $T_2$  much less than for free water.

In analyzing relaxation measurements it is a standard procedure to include only intramolecular dipolar interactions. However, evidence has been presented that intermolecular dipolar interactions

between water molecules, especially in the hydration layer, and protons of the macromolecules may have a significant or dominant contribution in the relaxation mechanism [e.g. 7-9]. There is an additional effect that may influence the observed nuclear magnetic relaxation: diffusion through local gradients in the magnetic field, due to local differences in the magnetic susceptibility, as found for heterogeneous systems [10]. However, it has been concluded that in biological tissues this effect is small and often can be neglected [9].

### 3.2.2 Paramagnetic ions

A significant effect on nuclear relaxation times in biological tissues can be attributed to paramagnetic ions in solution, resulting from the dipolar interaction between electron and nuclear spins and the scalar interaction depending on the unpaired electron density at the position of the nucleus. The relaxation times of nuclei bound near a paramagnetic site are given by the equations of Solomon (11) and Bloembergen (12),

$$\frac{1}{T_{1M}} = \frac{2}{15} \left( \frac{y_I^2 g^2 S(S+1) \beta^2}{r^6} \right) \left\{ \frac{3\tau_c}{1+w_I^2 \tau_c^2} + \frac{7\tau_c}{1+w_S^2 \tau_c^2} \right\} + \frac{2}{3} S(S+1) \left( \frac{A}{\hbar} \right)^2 \left\{ \frac{\tau_e}{1+w_S^2 \tau_e^2} \right\} \quad (3.10a)$$

$$\frac{1}{T_{2M}} = \frac{1}{15} \left( \frac{y_I^2 g^2 S(S+1) \beta^2}{r^6} \right) \left\{ 4\tau_c + \frac{3\tau_c}{1+w_I^2 \tau_c^2} + \frac{13\tau_c}{1+w_S^2 \tau_c^2} \right\} + \frac{1}{3} S(S+1) \left( \frac{A}{\hbar} \right)^2 \left\{ \frac{\tau_e}{1+w_S^2 \tau_e^2} + \tau_e \right\} \quad (3.10b)$$

where  $\omega_I$  and  $\omega_S$  are the nuclear and electron Larmor precession frequencies respectively,  $S$  is the electron spin,  $g$  the electron  $g$  factor (a dimensionless constant),  $\beta$  the electron Bohr magneton,  $r$  the distance between the nucleus and the paramagnetic ion,  $A/\hbar$  the electron-nuclear hyperfine coupling constant, and  $\tau_c$  and  $\tau_e$  the correlation times characterizing the modulation of the dipolar and scalar interactions, respectively. These are given by

$$\frac{1}{\tau_c} = \frac{1}{\tau_s} + \frac{1}{\tau_M} + \frac{1}{\tau_r} \quad (3.11)$$

and

$$\frac{1}{\tau_e} = \frac{1}{\tau_s} + \frac{1}{\tau_M} \quad (3.12)$$

where  $\tau_M$  is the life-time of a nucleus at the binding site,  $\tau_r$  is the rotational correlation time of the bound paramagnetic ion, and  $\tau_s$  is the electron-spin relaxation time.

When fast chemical exchange occurs of water molecules in the bulk water and those near a paramagnetic site, the observed relaxation times can be shown to be

$$\frac{1}{T_{1,obs}} = \frac{1-f}{T_{1w}} + \frac{f}{T_{1M}} \quad (3.13a)$$

$$\frac{1}{T_{2,obs}} = \frac{1-f}{T_{2w}} + \frac{f}{T_{2M}} \quad (3.13b)$$

where  $f$  is the fraction of time that each proton spends in the coordination shell of the paramagnetic ion. If  $n$  is the coordination number,  $N$  is the concentration of paramagnetic species, and  $N_H$  is the molar concentration of protons we have  $f=n/N_H$ . Neglecting  $T_{1w}$  and  $T_{2w}$ , the relaxation times in pure water, eqn. 3.13 becomes

$$\frac{1}{T_{1,obs}} = \left(\frac{N}{N_H}\right) \frac{n}{T_{1M}} \quad (3.14a)$$

$$\frac{1}{T_{2,obs}} = \left(\frac{N}{N_H}\right) \frac{n}{T_{2M}} \quad (3.14b)$$

showing a linear dependence of both  $1/T_{1,obs}$  and  $1/T_{2,obs}$  on  $N$  (Chapter 7). From eqn. 3.10 it can be seen that  $1/T_{1,obs}$  and  $1/T_{2,obs}$  are also roughly proportional to  $\mu_{eff}^2$ , the mean square magnetic moment of the paramagnetic species, which is about a thousand times larger for electrons than for protons, causing a very effective relaxation mechanism.

In biological tissues one is mainly concerned with the ions  $Cl^-$ ,  $Na^+$ , and  $K^+$ . At physiological concentrations, the effect of these ions on the relaxation times of pure water is usually very small and can in general be neglected [14,15]. However, in biological tissue these ions can influence the relaxation time of water by osmosis, affecting the water content of the tissue, and - at high



ionic concentrations - by a direct effect of these ions on the water structure [16,17].

### 3.2.3 Sample heterogeneity

The measurement and interpretation of nuclear relaxation in biological tissue is also complicated by tissue heterogeneity, both on a macroscopic and on a microscopic scale [18]. In this respect, we can distinguish regions with e.g. different cell size, different water content, different chemical composition. Furthermore, these regions are spatially organized in a non-random manner, they contain molecules of different sizes, and - finally -, water and ions may be distributed throughout the system in a non-uniform way, as indicated in Fig. 3. Water molecules may exchange between regions A and B at a rate that is a function of the self-diffusion coefficient of water in each region and of the potential barrier constituted by the interface separating the two regions.

On a microscopic scale the heterogeneity influences the time constants of the different dynamic processes that characterize the

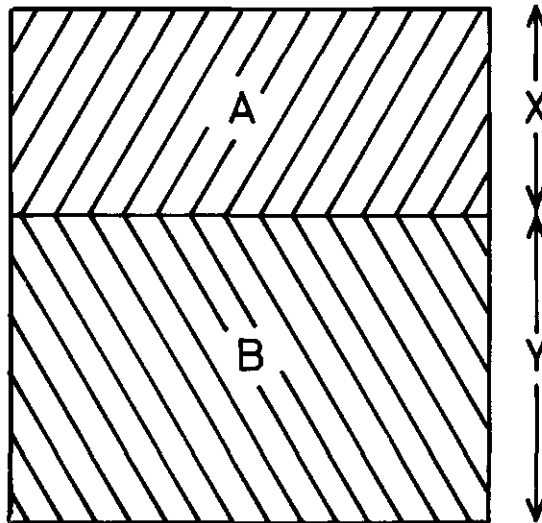


Fig. 3 Schematic illustration of large scale heterogeneity. Distinct regions (e.g. A and B) of the material may have differing compositions (e.g. water contents), geometries and dimensions (e.g. X, Y, etc.) and may also differ in e.g. degrees of order and anisotropy in internal structure (from Packer [18]).

motion of the water molecules and proton exchange in such systems. Fig. 4 gives a schematic illustration of two interacting regions  $\alpha$  and  $\beta$  on a microscopic scale [18]. The shaded regions  $\alpha$  and  $\beta$  represent two macromolecular structures characterized by dimensions  $d$ ,  $x$ ,  $y$ , orientations  $\theta_\alpha$  and  $\theta_\beta$  defined with respect to an external reference axis, and correlation times for tumbling  $\tau_m$ . The distance  $d$  is often much larger than the size of a water molecule, and in systems where the macromolecules concerned are structural components such as in collagen,  $\tau_m$  can be very long or even infinite. In protein solutions  $\tau_m$  will reflect the tumbling of the protein molecule in part or as a whole. The water molecules can undergo a variety of motions in such a system as illustrated in Fig. 4.

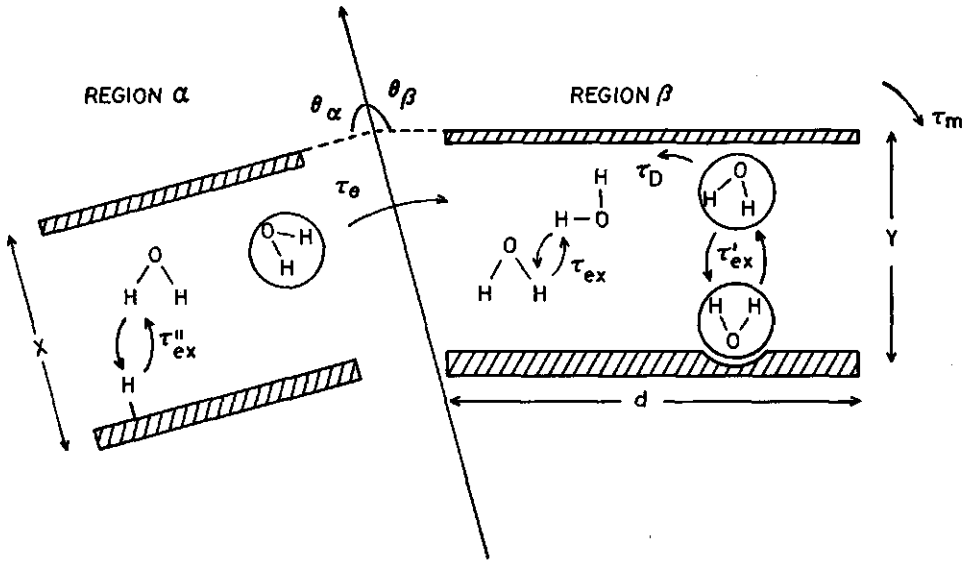


Fig. 4 A schematic illustration of small scale heterogeneity and various dynamic processes which may be experienced by water in a biological system (from Packer [18]).

Water molecules outside the region of influence of the macromolecules diffuse, rotate and exchange protons with characteristic times  $\tau_D$ ,

$\tau_r$  and  $\tau_{ex}$  respectively. Water molecules interacting with the macromolecules tumble anisotropically, this process being represented by a collective correlation time  $\tau_r'$  and have a lifetime in this state designated by  $\tau_{ex}'$ . Water molecules may diffuse from one region to another, their lifetime in a given region being  $\tau_\theta$  ( $\sim d^2/2D_s$ ), with  $D_s$  the self-diffusion coefficient, while the exchange of protons with the macromolecules corresponds to a lifetime of  $\tau_{ex}''$ . Water molecules near the macromolecular surface move in an anisotropic potential which remains almost unchanged during the reorientation of a water molecule, resulting in an anisotropic magnetic interaction, mainly of dipolar nature which is not averaged out to zero during the reorientation time of such a water molecule. Water molecules outside the region of influence of the macromolecules, the bulk liquid water, also experience at any instant an anisotropic potential, but the axes defining this anisotropy changes direction as fast as individual molecules reorient, consequently the effects due to an anisotropic potential are generally averaged out on the NMR timescale. As is evident from Fig. 4 the dynamics of water in biological tissue contains many different processes and a full description is virtually impossible without making suitable approximations.

#### 3.2.4 Exchange and diffusion

In biological tissues each region (i.e.  $\alpha$  and  $\beta$ , fig. 4) will probably contain a number of different types of binding sites which give rise to different values of e.g. correlation times and relaxation times. If  $\tau_{ex}'$  for each such site were sufficiently large then the observed nuclear relaxation would contain a superposition of relaxation rates of free and the total of bound sites. By exchange processes however, the nuclear relaxation of the different sites is completely or partially averaged, depending on the rate of exchange. For the fast exchange condition ( $\tau_{ex}' \ll T_{2b}$ , where b is the bound site) in a single region assuming only a single type of binding site, the observed relaxation time becomes [19]

$$T_2^{-1} = P_f T_{2f}^{-1} + P_b T_{2b}^{-1} \quad (3.15)$$

where  $f$  refers to the free (bulk) water and  $P_f$ ,  $P_b$  are the mole fractions of the free and bound water, respectively. For a system with exchange between two sites  $a$  and  $b$ , the relaxation times depend on the exchange rates ( $\tau_a^{-1}$  and  $\tau_b^{-1}$ ) and the relaxation times of the sites in the absence of exchange ( $T_{2a}$  and  $T_{2b}$ ) as given by [20-22]

$$T_{2I,II}^{-1} = \frac{1}{2} [T_{2a}^{-1} + T_{2b}^{-1} + \tau_a^{-1} + \tau_b^{-1}] \pm [(S + \sigma)^2 + \frac{1}{\tau_a \tau_b}]^{\frac{1}{2}} \quad (3.16)$$

$$\text{with } S \equiv \frac{1}{2} (T_{2a}^{-1} - T_{2b}^{-1}) \quad (3.17)$$

$$\text{and } \sigma \equiv \frac{1}{2} (\tau_a^{-1} - \tau_b^{-1}) \quad (3.18)$$

The fractions are given by  $P_a = \tau_a / (\tau_a + \tau_b)$ .

In this description the chemical shift difference between the two states (the difference in the Larmor precession frequency) has been neglected. However, in considering the relaxation rates we must also take into account that the exchange process itself causes an additional relaxation mechanism because the nuclei experience time-dependent magnetic fields by exchange between different environments. This results in a dependence of the nuclear relaxation times on the chemical shift differences and, in the case of a  $T_2$  measured via the Carr-Purcell-Meiboom-Gill method [23,24 and Section 3.3], on the pulse separation  $2\tau$  of the  $\pi$ -pulses [21,22 and references cited therein]. For  $2\tau\delta \ll 1$ , where  $\delta$  is the chemical shift difference, the effect of the chemical shift disappears, resulting in eqn. 3.16. On the other hand, for  $2\tau\delta \gg 1$ ,  $T_2^{-1}$  is given by [21,22]

$$T_{2I,II}^{-1} = \frac{1}{2} (T_{2a}^{-1} + T_{2b}^{-1} + \tau_a^{-1} + \tau_b^{-1}) \pm p \quad (3.19)$$

where  $p$  can be calculated from

$$(p + iq)^2 = (i\delta + s + \sigma)^2 + (\tau_a \tau_b)^{-1} \quad (3.20)$$

and  $S$  and  $\sigma$  are defined in eqns. 3.17 and 3.18. The physical reason for the dependence of  $T_2$  on the pulse spacing  $2\tau$  may be explained as follows. During the time  $\tau$  after an echo, the magnetizations  $M_A$  and  $M_B$  rotate in the rotating frame with an angular frequency  $-\delta$  and  $+\delta$ , respectively.  $M_A$  and  $M_B$  have a phase difference  $2\tau\delta$  after

time  $\tau$ , in the absence of exchange. As a result, the observed relaxation times vary with increasing  $2\tau$  between the limiting values given by eqn. 3.16 and eqn. 3.19. Therefore, a comparison of  $T_2$  relaxation times should take into account the experimental pulse spacing  $2\tau$ .

The dependence of  $T_2$  on  $2\tau$  in plant tissue such as bean leaves and apple pulp has been demonstrated by Fedotov et al. [25]. From these measurements these authors concluded that (in terms of Fig. 4)  $\tau_r'$  is of the order of  $10^{-8}$  s,  $\tau_{ex}''$  varies from  $3.5 \times 10^{-3}$  s for maize leaves to  $9.5 \times 10^{-3}$  s for onion bulb, and  $\tau_{ex}' \geq 10^{-4}$  s. In all measured plant tissues these authors observed only a single relaxation time for  $T_1$  and  $T_2$ , in contrast to the measurements reported in this Thesis (Chapter 7).

So far, exchange between two sites has been considered assuming that any water molecule at any instant has equal probability to be found in either one of the two sites. This situation is clearly not met in heterogeneous systems. The discrete jumps of a water molecule or a proton between two well-defined sites can then be generalized to random, quasicontinuous displacements, as in free diffusion. It depends on the distance over which the tissue is homogeneous, the presence of diffusion barriers and the diffusion coefficient, which kind of relaxation behaviour is observed: a single relaxation time for more homogeneous tissues with unrestricted diffusion or a distribution of relaxation times for more complex systems. A full theoretical description, in which many exchange sites with different relaxation times are incorporated, has not yet been developed.

Recently, Brownstein [26] and Brownstein and Tarr [27] applied a simple theory based on a diffusion equation using the bulk diffusivity of water [28,29] to explain the multi-exponential decay seen in nuclear relaxation measurements of water in biological tissues. They showed that such multi-exponential behaviour arises as a consequence of an eigenvalue problem associated with the size and shape of the cell and that this multi-exponential decay can only be observed for samples with a size comparable to that of a biological cell.

### 3.2.5 Summary

In summary we conclude that nuclear relaxation times  $T_1$  and  $T_2$  contain the following information:

- concentration and dynamics of the observed magnetic nuclei
- nature of the environment of the nuclei, in particular the microscopic geometry of their environment.
- influence of the boundaries (e.g. walls) surrounding the homogeneous regions of the sample.

## 3.3 MEASUREMENT OF $T_2$ , DIFFUSION AND FLOW

### 3.3.1 Method of $T_2$ measurement

After the magnetization  $\vec{M}$  is rotated by a  $\frac{1}{2} \pi$  pulse applied along the  $x'$  axis as shown in Fig. 2,  $\vec{M}$  is parallel to the  $y'$  axis, and immediately begins to decay. The nuclear induction signal can be detected with a coil that is part of a circuit tuned at the resonance frequency  $\omega_0$ . The apparatus is arranged in such a way that signals are detected when  $\vec{M}$  has a component perpendicular to  $\vec{B}_0$ , i.e. the receiver coil is parallel to the  $x$  or  $y$  axis. Accordingly, the transverse magnetization rotating in the laboratory frame induces an alternating voltage in the coil, at the Larmor frequency. This oscillating signal can be phase-sensitive detected and decays exponentially if the resonance condition is satisfied. This signal is called the *free induction decay* (FID).

As defined by the Bloch equations (eqns. 3.7a-c),  $T_2$  is the decay time of the transverse magnetization. However, only in favourable cases will the FID decay with the relaxation time  $T_2$ . In particular, the inhomogeneity of the magnetic field  $B_0$  accelerates the decay of the transverse magnetization, because the nuclei in the different parts of the field precess at different frequencies and hence rapidly become out of phase with respect to each other. The FID has an effective transverse relaxation time  $T_2^*$ , given by [2].

$$(T_2^*)^{-1} = T_2^{-1} + \gamma \Delta B_0 / 2 \quad (3.21)$$

where  $\Delta B_0$  is the inhomogeneity of  $B_0$ .

The effect of the magnetic field inhomogeneity of  $B_0$  can be represented by a distribution of the Larmor frequencies  $g(\Delta\omega)$ . Due to this inhomogeneity, the average Larmor frequency  $\omega_0$  in the sample is associated with a range of precession frequencies  $\omega_0 \pm \Delta\omega$ . At a given  $\omega_i$ , a number of nuclei precess, and these are assigned to a *spin isochromatic group* [30]. After a  $\frac{1}{2}\pi$  pulse at  $t=0$  (Fig. 5a) each isochromatic group precesses at a slightly different rate in the  $x',y'$  plane and fans out (Fig. 5b). When, after a time  $\tau$ , a  $\pi$  pulse along the  $y'$  axis is applied (Fig. 5c), a  $180^\circ$  reversal to the isochromatic spin groups is given with respect to the  $y',z'$  plane, the slower and faster moving groups again approach each other. Thus, at time  $2\tau$  phase coherence is restored for a short period of time,

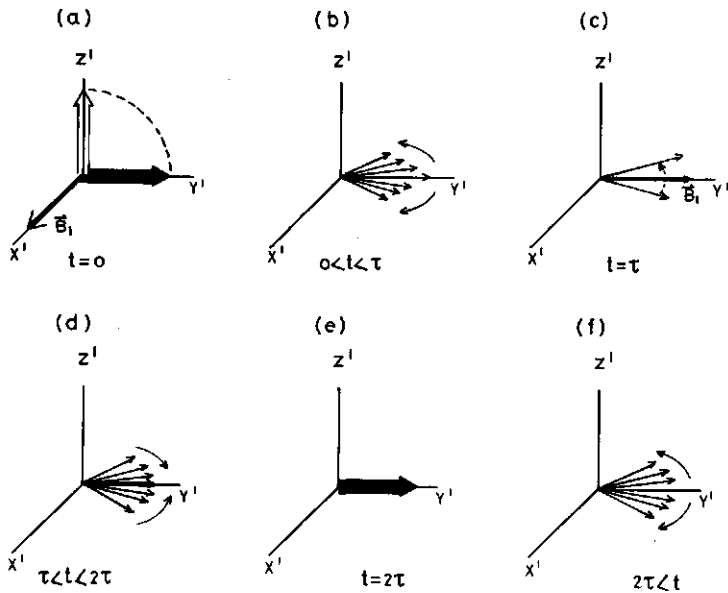


Fig. 5 The production of a spin echo (a)  $t=0$  :  $\frac{1}{2}\pi$  pulse along  $x'$ , (b) free induction decay at  $0 < t < \tau$ , (c) at  $t=\tau$  a  $\pi$  pulse along the  $y'$  axis results in a  $180^\circ$  reversal of the isochromatic spin groups, (d) restoration of phase at  $\tau < t < 2\tau$  yields, (e) a spin-echo at  $t=2\tau$ , (f) phase coherence is again lost.

giving rise to a *spin-echo* (Fig. 5e). Thereafter the spin-groups fan out again (Fig. 5f). The height of the echo at time  $2\tau$  depends on the initial magnetization  $|M_0|$  and on the transverse relaxation time  $T_2$ , which can be obtained from the echo amplitude as a function of  $\tau$ .

However, molecular diffusion also affects the echo height. If between pulses the observed nuclei (attached to the molecules of interest) move from one part of the inhomogeneous field  $B_0$  to another by diffusion, then the compensation for the field inhomogeneity is incomplete and the echo does not reach its full height. Carr and Purcell have shown [23] that for the multiple pulse sequence  $\frac{1}{2}\pi_x, -(\tau - \pi_x, -\tau)_n$  the effect of diffusion can be neglected when  $\tau$  is made small enough. The envelope of the heights of the spin echoes, which occur in between the pulses at times  $2n\tau$ , has the form  $\exp(-2n\tau/T_2)$  and thus yields  $T_2$ . Meiboom and Gill [24] introduced a modification to compensate for off-resonance effects and imperfections in the length of the pulses by the sequence:

$$\frac{1}{2}\pi_x, -(\tau - \pi_y, -\tau)_n$$

This pulse sequence is known as the Carr-Purcell-Meiboom-Gill (CPMG) sequence which is used for the  $T_2$  measurements as reported in this Thesis.

### 3.3.2 Effect of diffusion and flow

As has been stated above, NMR is one of the most versatile techniques for the study of molecular motion through its effect on the Larmor precession frequency. When a molecule moves a distance  $\Delta z$  during a time  $\Delta\tau$  along a field gradient  $G_z$ , the phase shift due to that motion is

$$\Delta\phi = \gamma G_z (\Delta z)(\Delta\tau) \quad (3.22)$$

These motions can be viewed as either incoherent or coherent. Examples of the former are thermal motions of the molecules, e.g. translational and rotational diffusion, and chemical exchange, whereas flow represents coherent motion. Turbulent flow might be considered as having both the properties of coherence (on a short time scale) and randomness (on a longer time scale).



The effects of molecular diffusion and flow in spin-echo experiments has already been recognized by Hahn [30] and Carr and Purcell [23]. In fact the echo amplitude in a CPMG pulse sequence is attenuated by molecular diffusion according to [23]

$$S(t) \propto \exp[-(t/T_2) - \frac{1}{3} \gamma^2 G^2 D \tau^2 t] \quad (3.23)$$

$G$  is a spatial magnetic field gradient,  $D$  the self-diffusion coefficient. As stated before,  $S(t)$  is purely exponential for small  $\tau$ , i.e. if  $\gamma^2 G^2 D \tau^2 \ll T_2^{-1}$ . Stejskal [31] and Stejskal and Tanner [32] noted that the effect of diffusion is to attenuate the echo height whereas the effect of flow is to shift the phase of the echo signal. When the signal is phase sensitive detected, this also attenuates the echo height. Packer [33] showed that in a CPMG pulse sequence only the odd-numbered echoes are affected by flow by a factor  $\cos(\gamma G v \tau^2)$ , where  $v$  is a constant velocity (in m/s) and the linear gradient  $G$  is in the direction of flow.

Several modifications of this basic pulse sequence combined with a linear magnetic field gradient have been proposed and employed for the measurement of self-diffusion or flow. Of these the use of time-dependent field gradients has the advantage of extending the range of  $D$ -values accessible to measurement to smaller values [32], because it permits the use of high field gradients without affecting the effective r.f. pulse length and the shape of the echo. This concept has also been applied to flow measurements [73].

Flow can also affect the echo amplitude in a CPMG pulse sequence without the use of a magnetic field gradient [34,35]. This effect is simply explained by noting that when the liquid is flowing, a fraction of the molecules labelled by a  $\frac{1}{2}\pi$  pulse is replaced by unlabelled molecules. The effect of flow pattern and r.f. field inhomogeneity on the decrease of the echo amplitude has been investigated by Hemminga et al [36].

The next Sections represent a short review of diffusion and flow measurements by NMR, with emphasis on the applicability of this method to biological systems, especially plants.

### 3.4 NMR DIFFUSION MEASUREMENTS IN BIOLOGICAL SAMPLES

Most of the reported self-diffusion coefficients of water in biological samples have been measured using the time-dependent magnetic field gradient method (see Section 3.3) [32]. In plant and animal tissues it was observed that the measured values of  $D$  depend on the pulse spacing  $\tau$  which is indicative of restricted diffusion. This can be explained if the diffusing molecules are not able to travel for an appreciable distance in the time-interval\*  $\tau$  without either meeting a partially reflecting barrier or venturing into a region of decreased mobility. This results in a behaviour that approaches that of a pure liquid for short pulse spacing, while for longer times the measured value of  $D$  decreases [31,37]. Restricted diffusion theory has been developed for a number of differently shaped restrictions. Expressions have been derived for planar [38,39,42], spherical [31,38], and cylindrical [38] impermeable walls and one-, two-, or three dimensional diffusion [40]. Formulae for geometries with an arbitrary diffusion barrier permeability are given by Tanner [41] and Anisimov et al. [43,44]. Tanner's equations contain the distance between the barriers as a parameter, which can be derived from the NMR relaxation data. In plant tissue the tonoplast, in addition to the plasmalemma, were suggested as possible barriers causing restricted diffusion. Thus measurements of  $D$  may yield information about the cell size or the distribution of the size of the cells [41-45].

In tissues containing many components, the observed NMR relaxation-behaviour in time-dependent field gradient spin-echo experiments is dependent on the fraction of each type of spin contributing to the echo. Kärger [46] has presented a theoretical investigation of a two phase system. He derived complicated expressions similar in form to eqns. 3.15 and 3.16, given in Section 3.2 for multisite relaxation including exchange. By a proper choice of the r.f. pulse-sequence and magnetic field gradient pulses [45] together with other experimental variables such as the pulse spacing time  $\tau$ , the magnitude of

---

\* In reality, the use of the parameter  $\tau$  is not completely correct; further details are beyond the scope of this Section, and can be found in ref. [41].

the magnetic field gradient, the duration of this gradient and the time between the gradient pulses [45,47,48] the time-window of the diffusion measurement can be selected, defining the phase or compartment which is under observation.

Data for the self-diffusion coefficient measurements for several plant tissues and cells are listed in Table 3.1. Abetsedarskaya et al. [52] have made corrections for the presence of vacuoles which were suggested to occupy 30-50% of the internal cell volume and to contain bulk water, to obtain the value of D in protoplasm.

Table 3.1. Values of  $T_1$ ,  $T_2$ , D and cell size for various plant tissues and cells at different resonance frequencies and temperatures.

Sample	MHz	Temp °C	Weight % dry matter	$T_2$ ms	$T_1$ ms	$D \times 10^9 \text{m}^2 \text{s}^{-1}$ in cell	$D \times 10^9 \text{m}^2 \text{s}^{-1}$ in proto- plasma	Cell size <sup>d</sup> $\mu\text{m}$	Ref
Water				2500	2500	2.4-2.5			49,50
Maize leaves	20	25	10.5	96	250	2.0	1.82-1.60		52
Bean leaves	20	25	9.5	110	300	1.81	1.56-1.20		52
Bean leaves	20	25				1.59			53
Pea leaves	20	25				1.82			53
Maize roots	20	25	9.1	133	885	1.76	1.49-1.12		52
Apple fruit	20	26				1.84		43	42
Tobacco pith	20	26				2.37 <sup>b</sup>		111	42
Onion scales	20	-10				0.15 <sup>b</sup>			54
Wheat caryopsis embryo	20	-10				0.17 <sup>b</sup>			54
Endosperm tissue of wheat grains	60	22	83 73			0.18 1.2			40
cells of lyo- philically dried yeasts cryptococci	20	20		40		0.25		0.6	44
wheat weevil buds	20	25				0.84 <sup>c</sup>			53
yeast	20	25				0.60 <sup>c</sup>			53
yeast	20	26	35			0.68		5.3	42
Chlorella pyre- noidosa	20	25				1.03 <sup>c</sup>			53

- Corrected for presence of vacuoles
- Nonfreezing water: 0.27 - 0.45 g/g dry matter
- For the higher mobility fraction (85-90%). Less mobile fraction  
D:  $0.2 - 1.0 \times 10^{-6} \text{ cm}^2/\text{s}$  (Hydration water: 0.2 - 0.6 g/g dry matter).
- Inner diameter as measured by NMR diffusion measurements.

The values of  $D$ , as shown in Table 3.1., can be up to a factor of 16 less than the value for pure water, but they are mostly comparable to the values obtained in protein solutions and gels ( $D \sim 1 \text{ à } 2 \times 10^{-9} \text{ m}^2 \cdot \text{s}^{-1}$ ). The smaller  $D$  values of water in protein solutions compared to that in pure water has been proposed [57] to be the result of (a) an obstruction effect, caused by the large and less mobile proteins, impeding the translational motion of the water molecules, (b) the hydration effect, which may either increase or decrease the motion of the hydration water of the proteins, depending on the effect of the protein on the water structure in the vicinity of the protein. Abetsedarskaya et al. [52] considered the obstruction effect to be the predominant cause of the decreased values of  $D$  in leaves of maize and bean and in maize roots.

In the endosperm tissue of wheat grains Callaghan et al. [40] measured the value of  $D$  for water as a function of the tissue water content. Assuming one-dimensional diffusion in a randomly oriented array of capillaries with transverse dimensions  $< 100 \text{ nm}$  these authors find a single diffusion coefficient at each water content, varying from  $0.18 \times 10^{-9}$  at the lowest to  $1.2 \times 10^{-9} \text{ m}^2 \cdot \text{s}^{-1}$  at the highest water content, corresponding to an increase of the hydration water film thickness from  $\sim 0.5$  to  $\sim 2.5 \text{ nm}$ . These values of  $D$  agree fairly well with those of the nonfreezing water fraction in onion scales

Table 3.2 Values of  $T_1$ ,  $T_2$ ,  $D$ ,  $\tau_a$  and  $P_d^c$  for various plant samples.

Sample	Mean cell size ( $\mu\text{m}$ )	MHz	Temp $^{\circ}\text{C}$	$T_2$ ms	$T_1$ ms	$D \times 10^9 \text{ m}^2 \cdot \text{s}^{-1}$ in cell	$\tau_a$ ms	$P_d^c$ $\text{cm} \cdot \text{s}^{-1}$	Ref.
Chlorella vulgaris	3.2 <sup>a</sup>	11	20	54(intra) 14(extra) <sup>d</sup>	205 45	$< 1.7$	19-28	$2.1 \times 10^{-3}$	48
Elodea leaves	$96 \times 27^b$	11	20	$\geq 230$ (intra) <sup>d</sup>		0.76	18.2	$3 \times 10^{-2}$	55
Ivy bark	36 <sup>a</sup>	18.5	20	84(intra) 9(extra)	182 28	1.43	$\sim 40$	$\sim 3 \times 10^{-2}$	56

a diameter

b length x diameter, both in  $\mu\text{m}$

c  $P_d$  = diffusional water permeability of plasmalemma.  $P_d$  is defined by  $P_d = \frac{D}{\delta}$ , ( $\text{cm/s}$ ), where  $D$  is the diffusion constant of water in the plasmalemma, and  $\delta$  is the thickness of the plasmalemma-membrane.

d  $T_2$  of extracellular water not quoted in reference 55.

and wheat caryopsis embryo [54], and with water in lyophilically dried yeast cryptococci [44], but are a factor of 10 higher than the value of  $D$  of the less mobile (hydration) water fraction measured by Miftakhutdinova et al. [53] in wheat weevil buds and yeast.

The self-diffusion of water in the cell and the diffusional water permeability ( $P_d$ , see Table 3.2.) of the plasmalemma has been measured by Stout et al. in an attempt to evaluate the effect of different freezing stresses as well as drought and cold hardiness of plants [48,55,56,58]. These authors have combined the time-dependent magnetic field gradient method with a technique to measure  $P_d$  as applied by Conlon and Outhred [59] and Fabry and Eisenstadt [60] to red blood cells. In this latter NMR technique, intracellular water is distinguished from extracellular water by the difference in  $T_2$  when  $T_2$  of the extracellular water is controlled by added  $MnCl_2$  (see Section 3.2, eqns. 3.14a-b). From such measurements the mean residence time ( $\tau_a$ ) for water molecules within the cell has been determined [48,55,56] since movement through the membrane into the extracellular medium (which has a shorter  $T_2$ ), influences the measured value of  $T_2$  (eqns. 3.15 and 3.16 Section 3.2). Using  $\tau_a$  and the known mean cell radius, the mean value of  $P_d$  can be calculated provided that  $\tau_a$  is limited by  $P_d$  and not by intracellular unstirred layers [61]. The results for three different plant samples are presented in Table 3.2.

In the absence of extracellular  $Mn^{2+}$ ,  $T_2$  in these samples reveals the presence of at least two populations of water, each with different  $T_2$  values. The fast relaxing population was believed to be extracellular water [48,56], whereas the longer  $T_2$  was associated with intracellular water. Intracellular structure was ignored. In *Elodea* leaves, however, diffusion measurements yielded a mean distance of 13.5  $\mu m$  over which the water molecules could freely diffuse. This distance is much shorter than the average geometrical cell size. This indicates internal cell structure, which can explain the low value of  $D$  observed in cells of these leaves: these structures restrict diffusion of the water molecules. The magnitudes of  $D$  in Ivy bark and in *Chlorella vulgaris* are of comparable size with respect to those in other plant cells (Table 3.1).

### 3.5 NMR FLOW MEASUREMENTS IN BIOLOGICAL SAMPLES.

NMR flow measurements include both steady state and pulse NMR methods. Despite the early observations of NMR signals arising from flowing water in a U-tube by Suryan [62], very little additional information was published until 1960. The earlier work was reviewed by Zhernovoi and Latyshev [63], who also derived theoretical expressions relating signal amplitude and width to experimental factors involved in NMR experiments in flowing fluids, and who developed several devices of practical interest. In a more recent review Jones and Child [64] have discussed the application of NMR flow measurements in industrial, chemical, and physiological situations.

#### 3.5.1 History of *in vivo* blood flow measurements

For biological samples, the recognition of the potential of NMR in biological and physiological flow measurements has stimulated the study of blood flow *in vitro* and *in vivo*. The earliest work directed toward the application of the NMR principles to noninvasive *in vivo* measurement of blood flow was carried out in 1956 by Bowman [65] (using the method reported by Suryan [62]), who observed a linear relation due to saturation effects between signal amplitude and flow rate, in a continuous  $B_1$  field.

Absolute flow rates have been measured using magnetic labelling of nuclei by determining the "time-of-flight" of tagged nuclei travelling the distance between two coils, placed in a static magnetic field [66]. Many improvements and variations on this technique have been reported [63,65], yielding various tagging techniques for non-invasive measurement of blood flow in humans [65].

The first measurement of blood flow *in vivo* was reported by Singer in 1959 [67]. He measured the NMR signal amplitudes  $A_f$  and  $A$  in the presence and absence of flow, respectively, using Suryan's expression [62] to obtain the average linear velocity of flow [68]

$$\bar{v} = (L_0/T_1)[(A_f - A)/A] \quad (3.24)$$

where  $L_0$  is the effective length of tube in the r.f. field. Due to the contribution of tissue signal to the total NMR signal, however, the method only yields relative blood flow rates. Recently, Radda et al [99] described a pulsed version of Suryan's original experiment which satisfies the requirement that the flow measurement must be independent on  $T_2$ . This requirement is due to the fact that  $T_2$  of blood is determined by the oxygenation of the blood [100]. Singer also presented the theory of the "time-of-flight" method. Measurements of blood flow velocity in the median veins of human subjects by this tagging technique have been reported in 1970 by Morse and Singer [69]. NMR blood flow measurements are reviewed by Battocletti et al. [65,70]. It has been observed that the measurement of NMR signal amplitude in time-of-flight measurements leads to knowledge of volume flowrate [65].

### 3.5.2 Pulsed NMR flow measurements

As stated in Section 3.3, pulsed NMR methods with and without steady state or time-dependent magnetic field gradients, can be used to measure flow velocities. Hahn [71] was the first to employ a spin-echo technique in combination with a magnetic field gradient to measure the motion of sea water and derived the important result

$$\Delta\phi = \gamma G \bar{v} \tau^2 \quad (3.25)$$

where  $\Delta\phi$  is the average phase shift of the fluid signal due to an average linear velocity  $\bar{v}$ ,  $G$  is the magnetic field gradient and  $\tau$  is the time between the r.f. pulses. Grover and Singer [72] have used a similar two-pulse method to determine the velocity distribution function, defined as the density of flowing protons per velocity interval, characterizing the blood flow in a finger. Following  $\frac{1}{2}\pi$  and  $\pi$  pulses separated in time by  $\tau$ , the echo amplitude  $A(2\tau)$  was measured as a function of  $2\tau$ . Until now, no other spin-echo NMR blood flow measurements have been reported in the literature. This may be due to the pulse sequences used in these experiments, all consisting of one or more  $\frac{1}{2}\pi$  pulses, creating a contribution of stationary tissue water to the NMR signal (see also Section 3.5.3).

Several CPMG type multiple spin-echo sequences have been recommended for examining the influence of flow patterns on the spin-echo decays. Packer and his group have made a series of careful experimental and theoretical studies in this area, using both static and time-dependent magnetic field gradients [33,73,74]. The CPMG pulse sequence (Section 3.3) has been replaced by the sequence  $\frac{1}{2}\pi - \tau - \pi(-\tau' - \pi)_n$ , with  $\tau'$  slightly larger than  $\tau$ , or by  $\frac{1}{2}\pi(-\tau - \pi)_n$ , both of these pulse sequences minimize the effect of diffusion on the time dependent NMR signal, whereas the effect of flow on this signal can be more easily determined, as compared to that in the CPMG method [33]. In the latter pulse sequence, plug flow for example produces a cosine modulation of the spin-echo amplitude, whereas the effect of diffusion is the same as in the CPMG sequence (Section 3.3). It has been shown that laminar flow results in a  $(\sin x)/x$  modulation [73,74]. Garroway [75] has used a  $\frac{1}{2}\pi - \tau - \frac{1}{2}\pi$  sequence in combination with a linear magnetic field gradient to determine the spatial profile of the velocity distribution for the laminar flow of water in circular and rectangular pipes, from the shape of the FID (Section 3.3) following the second  $\frac{1}{2}\pi$  pulse. An improved method, using the  $\frac{1}{2}\pi_x[-\tau - \frac{1}{2}\pi_y]_n$  pulse sequence [75] allowed direct measurement of the velocity distribution. This author has also suggested the use of multiple-pulse line-narrowing techniques [76,77] (yielding an effective  $T_{2e}$  of 10-40 ms) in order to measure flow of solids e.g. in slurries.

Using a  $\frac{1}{2}\pi - \tau - \pi$  pulse sequence, Lucas et al. [78] have measured flow profiles of pressure-driven flow in a rectangular flow channel, and of convective flow, driven by the transverse density gradient due to a temperature gradient between two flat plates. Because of the large value of  $T_2$  of the fluid which these authors studied - superfluid  $^3\text{He}/^4\text{He}$  mixtures - they were able to detect flow velocities as small as 10  $\mu\text{m/s}$ . Using a CPMG sequence in combination with a linear magnetic field gradient, Fukuda and Hirai [79] were able to obtain the velocity profiles and distributions of Poiseuille (laminar) and turbulent flow. These authors measured the magnetic field gradient dependence of the first and the second spin-echo amplitude, demonstrating that information on the velocity profile can be obtained from the first spin-echo amplitude, whereas the amplitude of the second echo depends on the velocity fluctuations [79]. A more detailed discussion on flow profiles is given in Chapter 4 and 5.



Hemminga et al. [36,80,96,98] have described two NMR spin-echo methods to detect flow velocities and profiles of flowing fluids in the presence of stationary fluid. These methods are described in the following Section (3.5.3)

### 3.5.3 NMR flow measurements in plants

In order to measure water flow rates in biological objects such as plant stems, the method must be sensitive to small flow rates (1-30 mm/s), and to be able to discriminate between a small fraction of flowing water (about 2-10%) of the total amount of water in the sample volume and a large amount of stationary water. Both NMR methods described by Hemminga et al. [36,80,96,98] can discriminate between flowing and stationary water. The first is a difference method based on the CPMG pulse sequence and does not require a magnetic field gradient [36]. In the case of stationary water, the echo decay in the CPMG sequence is given by

$$S(t) = S_0 \exp(-t/T_2) \quad (3.26)$$

where  $S_0$  is the amplitude of the signal at time  $t=0$ , which is proportional to the equilibrium magnitude of the magnetization (eqn. 3.3). When the liquid moves with a uniform velocity  $v = \bar{v}$  (plug flow), eqn. 3.26 is multiplied by a factor  $1-fvt/l$  [35], giving

$$S(t) = S_0 (1-fvt/l) \exp(-t/T_2) \quad \text{for } t \leq l/v \quad (3.27a)$$

and

$$S(t) = S_0 (1-f) \exp(-t/T_2) \quad \text{for } t > l/v \quad (3.27b)$$

for a rectangularly shaped  $B_1$  r.f. field, where  $f$  represents the fraction of flowing water w.r.t. the total and  $l$  the length of the r.f. coil. After  $t > l/v$ , the volume of flowing water in the r.f. coil has been completely replaced and the echo decay is determined only by the stationary water fraction. The contribution of the stationary water to the echo decay  $S(t)$  in eqn. 3.27a and 3.27b can be removed by subtracting two echo decays, one with  $v \neq 0$ , the other with  $v = 0$ ; the difference signal is given by

$$\Delta S(t) = fS_0 (vt/l) \exp(-t/T_2) \quad \text{for } t \leq l/v \quad (3.28a)$$

and

$$\Delta S(t) = fS_0 \exp(-t/T_2) \quad \text{for } t > l/v \quad (3.28b)$$

Difference decay curves have also been derived for laminar flow and for a Gaussian  $B_1$  r.f. field.

The application of this spin-echo difference method for measurements of flow rates in the plant stem is of course limited by the fact that an echo-decay at  $\bar{v} = 0$  must be available as a reference. The authors [36] have suggested that in the dark the sap stream has almost stopped and thus the decay curve at  $\bar{v} = 0$  can be determined and stored in some form. However, in Chapter 5 it is shown that the

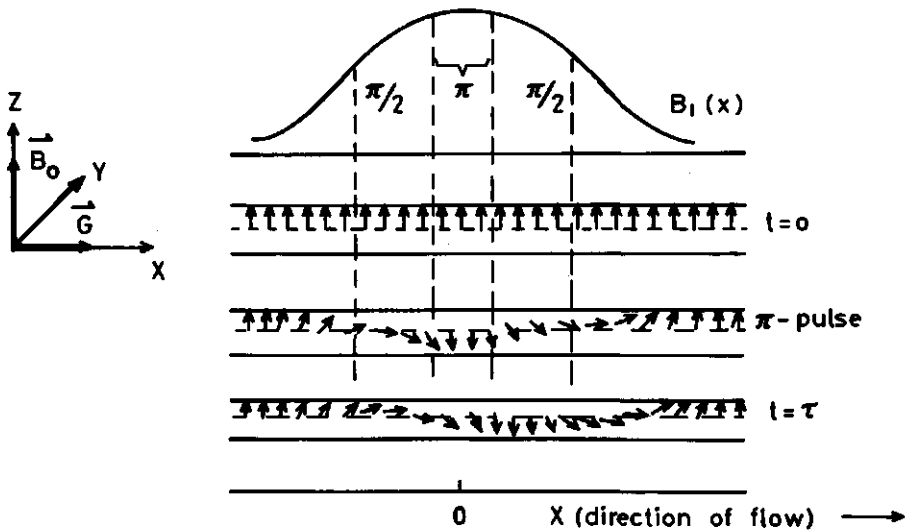


Fig. 6 Basic principles of the  $\pi$ -( $\tau$ )- $\pi$  pulse method for flow measurements: water molecules receive r.f. pulses with a pulse angle gradually increasing from 0 to  $\pi$ , as the distance from the center of the r.f. coil increases from infinity to zero, and simultaneously move along the magnetic field gradient  $\vec{G}$ .

situation  $\bar{v} = 0$  cannot be easily realized - even in the dark - and in Chapter 7 that  $T_2$  of stationary water changes with water content and with flow velocity. This renders the difference method impractical for flow measurements in stems of intact plants.

The second method reported by Hemminga et al. [80] is a pulsed NMR method, based on a sequence of equidistant  $\pi$  pulses in combination with a linear magnetic field gradient. As shown in Chapter 4, the NMR signals of flowing water are the result of the movement of water into the r.f. coil from a region outside it. Thus the water molecules receive r.f. pulses with a pulse angle gradually increasing from 0 to  $\pi$ , as the distance from the center of the r.f. coil increases from infinity to zero. This occurs in reverse at the other side of the coil (Fig. 6). Simultaneously, movement of the water molecules along the magnetic field gradient  $\vec{G}$  produces a phase shift  $\Delta\phi$  of the echoes with respect to the rotating frame of reference [31,33, see also Section 3.3]. Using eqn. 3.25 and noting that  $v\tau = \Delta x$ , where  $\Delta x$  is the distance travelled during time  $\tau$  in the direction of  $\vec{G}$  (Fig. 6), we obtain for the phase shift  $\Delta\phi$ :

$$\Delta\phi = \gamma G \Delta x \tau \quad (3.29)$$

For flowing water both effects yield a signal  $S(t)$  that is increasing in time, and is modulated by a periodical function with a frequency directly proportional to the mean flow velocity  $\bar{v}$ . At resonance, stationary water yields zero signal (base-line), and the method therefore discriminates flowing water from stationary water (see Chapter 4).

In addition, the method allows determination of flow in a single experiment. These features make the method attractive for study of biological samples, as shown for plant stems (Chapter 5 and 6). Linear flow velocity as well as volume flowrate can be determined simultaneously by this method (Chapter 4), yielding an estimate of the effective area of the transport vessels and of the spin-spin relaxation time  $T_2$  of water contained by these vessels (Chapters 4, 5 and 6). The limitations of this method as applied to measurement of water flow in plant stems are discussed in Chapter 5.

### 3.6 T<sub>2</sub> AND WATER CONTENT

Although there is no straightforward theoretical model for the interpretation of the observed NMR relaxation behaviour (Section 3.2), many authors have demonstrated a relationship between T<sub>1</sub>, T<sub>2</sub> and water content in biological objects. Daszkiewicz et al. [81] were the first to show that the NMR relaxation rates depend on protein concentration in protein solutions, and derived the relation

$$T_1^{-1} = T_{1_w}^{-1} + k_1 C \quad (3.30)$$

for protein concentrations less than 100 mg/ml, where T<sub>1<sub>w</sub></sub> is the spin-lattice relaxation time of pure water, k<sub>1</sub> an experimental constant and C the concentration of protein in g/g H<sub>2</sub>O. A similar relationship has been shown for T<sub>2</sub> [81]. Cooke and Wien [82] have shown that the same result is obtained for muscle tissue and solutions of muscle proteins. They interpreted their results in terms of a *fast-exchange-two-state* (FETS) model, including fast exchange between a bulk water fraction and a - minor - water fraction bound to macromolecules. This results in a single experimental relaxation time which is the weighted average of the two separate times T<sub>1<sub>f</sub></sub> (free water) and T<sub>1<sub>b</sub></sub> (bound water) as given in eqn. 3.15. The relationship between T<sub>1</sub>, T<sub>2</sub> and water content has been demonstrated in several biological objects, e.g., muscle and brain tissue [83-85], mammalian tissue and cells [86,87], normal and cryolesion rat liver tissue [88], and in normal and malignant tissues [e.g. 89,90]. These authors have also explained this relationship in terms of the FETS-model.

A more general expression for the weighted average relaxation rate should include the residence time τ<sub>b</sub> of a proton of the water molecule, or the residence time of the whole water-molecule, whichever is shorter, in the hydration layer of the macromolecule, resulting in the expression (see also eqn. 3.16):

$$T_1^{-1} = P_f T_{1_f}^{-1} + P_b (T_{1_b} + \tau_b)^{-1} \quad (3.31)$$

where the symbols have the same meaning as in eqn. 3.15, and τ<sub>b</sub> > T<sub>1<sub>b</sub></sub>.

Under physiological conditions, the mean time between proton jumps is shorter than  $\sim 2 \times 10^{-3} \text{ s}$  [91]. This value of  $\tau_b$  is less than that found for  $T_{1b}$  in albino mouse muscle and liver [83] and in solutions of hen egg albumin [83], in which  $T_{1b} \sim 7 \times 10^{-2} \text{ s}$ , illustrating that  $\tau_b$  may be neglected in eqn. 3.31. In skeletal muscle Hazlewood et al. [19] estimated the value of  $T_{1b}$  to be  $\sim 0.42 \text{ ms}$ , comparable to or less than that of  $\tau_b$ .

In those cases where the role of intermolecular dipolar relaxation cannot be neglected in the proton relaxation of the bound water molecules, the total proton relaxation rate of the bound water is the sum of the intra- and intermolecular dipolar relaxation rates [8].

Beall et al. [92], studying  $T_1$  and water content as a function of the growth cycle of Hela cells, demonstrated that during the mitosis and synthesis period of DNA  $T_1$  is related to the water content of the cell. During the transition from the DNA synthesis period to the post-DNA synthesis period, however, significant changes in  $T_1$  were observed, which were independent of changes in the water content. Samuilov et al [93] observed that in germinating Russian bean seeds  $T_1$  increases with increasing water content in the course of water-uptake by the seeds. From the dependence of  $T_1$  on the ratio of weight dry matter per weight water these authors demonstrated the existence of three sudden changes in the relationship between  $T_1$  and this ratio enabling them to discriminate not less than four water fractions in the seeds, differing with respect to their physical properties (e.g. relaxation rates) and, accordingly, with respect to the nature of their interaction with different surfaces and components of the cell-structure [93].

In the crown of winter wheat cereals Gusta et al. [94,95] demonstrated a linear relationship between the long component of the transverse relaxation rate  $T_2^{-1}$  and the water content. From this relationship these authors calculated  $T_{1f}$  values for the bulk water, which were lower for cold acclimatised wheat genotypes than for less hardy genotypes.

The relationship between  $T_1^{-1}$  and water content (eqn. 3.15), and the effect of  $\text{Li}^+$ ,  $\text{K}^+$  and  $\text{Cl}^-$  ions on this relationship, in roots of *Zea mays* has been studied by Bacić et al [16]. It was found that a minimum in the magnitude of  $T_1$  versus external salt concentration exists at  $\sim 10^{-3} \text{ M}$ , which corresponds with a minimum in water content

The changes in  $T_1$  reflect a) the osmotic effect of ions on  $P_f$ , the free water fraction, and b) the direct effect of ions on macromolecular hydration shells and the disordering of the free water structure ([16], see also [17]).

Hsi et al. [97] studied  $T_2$  in milled Northern white-cedar wood chips (*Thuja occidentalis L*). At water contents below 0.38 g of water per gram of dry wood, no freezing effect on  $T_2$  is detected. At larger water contents the spin-spin relaxation is found to be non-exponential. This was explained by assuming that at water contents above 0.38 g of water per gram of dry wood, additional water only increases a second slowly relaxing water molecule population, which was associated with bulk water, the protons of which exhibit rapid exchange with a few surface-sites with very efficient relaxation [97]. Using a different approach by employing a diffusion model, including magnetic sinks, Brownstein [26] was able to explain the measurements of Hsi et al. [97]. This model essentially involves two regions of water, a surface layer of macromolecules  $\leq 0.26 \mu\text{m}$  thick, with a severely reduced diffusion constant for water ( $D < 2.7 \times 10^{-12} \text{ m}^2 \cdot \text{s}^{-1}$ ), and the additional water outside this layer.

In Chapter 7 of this Thesis the results of the study of the effect of  $\text{Mn}^{2+}$  (a paramagnetic ion) on the relationship between  $T_2^{-1}$  and water content in wheat leaves are presented.

## REFERENCES

1. T.C. Farrar, E.D. Becker, "Pulse and Fourier Transform NMR" (Academic Press, New York, 1971).
2. A. Abragam, "The Principles of Nuclear Magnetism" (Oxford University Press, Oxford, 1961).
3. C.P. Slichter, "Principles of Magnetic Resonance" (Springer-Verlag, Berlin, 1978).
4. C.P. Poole, jr. and H.A. Farrar, "Relaxation in Magnetic Resonance" (Academic Press, New York, 1971).
5. F. Bloch, Phys. Rev. 70 (1946), 460; F. Bloch, W.W. Hansen, and M. Packard, Phys. Rev. 70 (1946), 474.
6. A. Carrington and A.D. McLachlan, "Introduction to Magnetic Resonance", Chapter 11 (Harper and Row, New York, 1967).
7. B.M. Fung, Biophys. J. 18 (1977), 235.
8. H.T. Edzes, E.T. Samulski, J. Magn. Reson. 31 (1978), 207.
9. H.T. Edzes, Thesis, Groningen, The Netherlands, 1976.
10. J.A. Glasel, K.H. Lee, J. Am. Chem. Soc. 96 (1974), 970.
11. I. Solomon, Phys. Rev. 99 (1955), 559.
12. N. Bloembergen, J. Chem. Phys. 27 (1957), 572.
13. R.A. Dwek, "Nuclear Magnetic Resonance in Biochemistry: applications to enzyme systems" Chapter 9 (Clarendon Press, Oxford, 1973).
14. G. Engel, H.G. Hertz, Ber. Bunsenges. Phys. Chem. 72 (1968), 808.
15. G.J. Béné, Adv. Electronics Electron Physics 49 (1979), 85.
16. G. Bacić, B. Bozović, S. Ratković, Studia Biophysica 70 (1978), 31.
17. G.P. Raaphorst, P. Law. J. Kruuv, Physiol. Chem. & Physics 10 (1978), 177.
18. K.J. Packer, Phil. Trans. R. Soc. London B. 278 (1977), 59.
19. J.R. Zimmerman, W.E. Brittin, J. Phys. Chem. 61 (1957), 1328.
20. C.F. Hazlewood, D.C. Chang, B.L. Nichols, D.E. Woessner, Biophys. J. 14 (1974), 583.
21. J. Jen, Adv. Mol. Relaxation Processes 6 (1974), 171.
22. J. Jen, J. Magn. Reson. 30 (1978), 111.
23. H.Y. Carr, E.M. Purcell, Phys. Rev. 94 (1954), 630.
24. S. Meiboom, D. Gill, Rev. Sci. Instrum. 29 (1958), 688.
25. V.D. Fedotov, F.G. Miftakhutdinova, Sh.F. Murtazin, Biofizika 14 (1969), 873.
26. K.R. Brownstein, J. Magn. Reson. 40 (1980), 505.
27. K.R. Brownstein, C.E. Tarr, Phys. Rev. A. 19 (1979), 2446.
28. K.R. Brownstein, C.E. Tarr, J. Magn. Reson. 26 (1977), 17.
29. D.L. Weaver, J. Magn. Reson. 37 (1980), 543.
30. E.L. Hahn, Phys. Rev. 80 (1950), 580.
31. E.O. Stejskal, J. Chem. Phys. 43 (1965), 3597.
32. E.O. Stejskal, J.E. Tanner, J. Chem. Phys. 42 (1965), 288.
33. K.J. Packer, Molec. Phys. 17 (1969), 355.
34. L.R. Hirschel, L.F. Libelo, J. Appl. Phys. 32 (1961), 1404.
35. D.W. Arnold, L.E. Burkhart, J. Appl. Phys. 36 (1965), 870.
36. M.A. Hemminga, P.A. de Jager, A. Sonneveld, J. Magn. Reson. 27 (1977), 359.
37. D.E. Woessner, J. Phys. Chem. 67 (1963), 1365.
38. C.H. Neuman, J. Chem. Phys. 60 (1974), 4508.
39. B. Robertson, Phys. Rev. 151 (1966), 273.
40. P.T. Callaghan, K.W. Jolley, J. Lelievre, Biophys. J. 28 (1979), 133.
41. J.E. Tanner, J. Chem. Phys. 69 (1978), 1748.
42. J.E. Tanner, E.O. Stejskal, J. Chem. Phys. 49 (1968), 1768.

43. A.V. Anisimov, F.G. Miftakhutdinova, *Biofizika* 22 (1977), 866 (Biophysics (USSR) 22 (1977), 898).
44. A.V. Anisimov, F.G. Miftakhutdinova, S.I. Aksenov, *Biofizika* 23 (1978), 479 (Biophysics (USSR) 23 (1978), 485).
45. J.E. Tanner, *Biophys. J.* 28 (1979), 107.
46. J. Kärger, *Ann. Phys.* 27 (1971), 107.
47. K.J. Packer, T.C. Sellwood, *J. Chem. Soc. Faraday II*, 74 (1978), 1592.
48. D.G. Stout, P.L. Steponkus, L.D. Bustard, R.M. Cotts, *Plant Physiol.* 62 (1978), 146
49. D.M. Cantor, J. Jonas, *J. Magn. Reson.* 28 (1977), 157.
50. L.A. Woolf, *J. Chem. Soc. London I.* 71 (1975), 784.
51. N.J. Trappeniers, C.J. Gerritsma, P.J. Oosting, *Phys. Lett.* 18 (1965), 256.
52. L.A. Abetsedarskaya, F.G. Miftakhutdinova, V.D. Fedotov, *Biofizika* 13 (1968), 630 (Biophysics (USSR) 13 (1968), 750).
53. F.G. Miftakhutdinova, A.V. Anisimov, G.A. Velikanov, *Dokl. Akad. Nauk SSSR* 224 (1975), 487 (*Dokl. Botanical Sciences* 224 (1975), 74).
54. F.G. Miftakhutdinova, A.V. Anisimov, *Fiziol. Rast.* 23 (1976), 799 (*Sov. Plant. Physiol.* 23 (1976), 671).
55. D.G. Stout, R.M. Cotts, P.L. Steponkus, *Can. J. Bot.* 55 (1977), 1623.
56. D.G. Stout, P.L. Steponkus, R.M. Cotts, *Plant. Physiol.* 62 (1978), 636.
57. J.H. Wang, *J. Amer. Chem. Soc.* 76 (1954), 4755.
58. P.M. Chen, L.V. Gusta, D.G. Stout, *Plant Physiol.* 61 (1978), 878.
59. T. Conlon, R. Outhred, *Biochim. Biophys. Acta* 288 (1972), 354.
60. N.E. Fabry, M. Eisenstadt, *Biophys. J.* 15 (1975), 1101.
61. J. Dainty, In "The Physiology of Plant Growth and Development" (M.B. Wilkins, ed) p.p. 421-452 (McGraw-Hill, New York, 1969).
62. G. Suryan, *Proc. Indian Acad. Sci., Sect. A* 33 (1951), 107.
63. A.I. Zhernovoi, G.D. Latyshev, "Nuclear Magnetic Resonance in a Flowing Liquid" (Consultants Bureau, New York, 1965).
64. D.W. Jones, T.C. Child, in "Advances in Magnetic Resonance" (J.S. Waugh, ed.), vol 8 (Academic Press, New York, 1976).
65. J.H. Battocletti, R.E. Halbach, S.X. Salles-Cunha, A. Sances, *Medical Phys.*, in press.
66. V. Kudravcev, R.L. Bowman, *Digest of Technical Papers*, 13th Ann. Conf. Eng. in Med. & Biol, pp. 21 and 25 (Washington D.C., 1960).
67. J.R. Singer, *Science* 130 (1959), 1652.
68. J.R. Singer, *J. Appl. Phys.* 31 (1960), 125.
69. O.C. Morse, J.R. Singer, *Science* 170 (1970), 440.
70. J.H. Battocletti, S.M. Evans, S.J. Larson, F.J. Antonich, R.L. Bowman, V. Kudravcev, A. Sances, J.H. Linehan, R.E. Halbach, W.K. Genthe, in "Flow: its Measurement and Control in Science and Industry", (R.B. Dowdall, ed.), Vol. 1, Part 3, p. 1401 (*Instrum. Soc. Amer.*, Pittsburgh, Pennsylvania, 1974).
71. E.L. Hahn, *J. Geophys. Res.* 65 (1960), 776.
72. T. Grover, J.R. Singer, *J. Appl. Phys.* 42 (1971), 938.
73. K.J. Packer, C. Rees, D.J. Tomlinson, *Advan. Mol. Relaxation Processes* 3 (1972), 119.
74. H.J. Hayward, K.J. Packer, D.J. Tomlinson, *Mol. Phys.* 23 (1972), 1083.
75. A.N. Garroway, *J. Phys. D: Appl. Phys.* 7 (1974), L. 159.
76. J.S. Waugh, L.M. Huber, U. Haeberlen, *Phys. Rev. Lett.* 20 (1968), 180.
77. W.K. Rhin, D.D. Elleman, R.W. Vaughan, *J. Chem. Phys.* 59 (1973), 3740.
78. P.G.J. Lucas, D.A. Penman, A. Tyler, E. Vavasour, *J. Phys. E: Sci. Instrum.* 10 (1977), 1150.
79. K. Fukuda, A. Hirai, *J. Chem. Soc. Japan* 47 (1979), 1999.
80. M.A. Hemminga, P.A. de Jager, *J. Magn. Reson.* 37 (1980), 1.
81. O.K. Daszkiewicz, J.W. Hennel, B. Lubas, T.W. Szczepkowski, *Nature* 200 (1963), 1006.



82. R. Cooke, R. Wien, *Biophys. J.* 11 (1971), 1002.
83. B.M. Fung, D.L. Durham, D.A. Wassil, *Biochem. Biophys. Acta* 339 (1975), 191.
84. B.M. Fung, *Biochem. Biophys. Acta* 497 (1977), 317.
85. J. Sidanović, S. Ratković, M. Kraincanić, M. Jovanović, *Endokrinologie* 69 (1977), 55.
86. H.S. Sandhu, G.B. Friedmann, *Med. Phys.* 5 (1978), 514.
87. R. Ader, J.S. Cohen, *J. Magn. Reson.* 34 (1979), 349.
88. M. Schara, M. Sentjurc, R. Golouk, M. Rozmarin, *Cryobiology* 15 (1978), 333.
89. I.C. Kiricuta, V. Simplaceanu, *Cancer Res.* 35 (1974), 1164.
90. R.E. Block, G.P. Maxwell, D.L. Branam, *J. Natl. Cancer Inst.* 59 (1977), 1731.
91. S. Meiboom, *J. Chem. Phys.* 34 (1969), 375.
92. P.T. Beall, D.C. Chang, C.F. Hazelwood, in "Biomolecular Structure and Function" (P.F. Agris, ed.), p. 233 (Academic Press, New York, 1978).
93. F.D. Samuilov, V.I. Nikiforova, E.A. Nikiforov, *Fiziol. Rast.* 23 (1976), 567 (Sov. Plant Physiol. 23 (1976), 480).
94. L.V. Gusta, M.J. Burke, A.C. Kapoor, *Plant. Physiol.* 56 (1975), 707.
95. L.V. Gusta, D.B. Fowler, P. Chen, D.B. Russell, D.G. Stout, *Plant Physiol.* 63 (1979), 627.
96. P.A. de Jager, M.A. Hemminga, A. Sonneveld, *Rev. Sci. Instrum.* 49 (1978), 1217.
97. E. Hsi. R. Hossfeld, R.G. Bryant, *J. Colloid Interface Sci.* 62 (1977), 389.
98. A preliminary note has been given by A. Sonneveld, M.A. Hemminga, P.A. de Jager, T.J. Schaafsma at the conference "The Less Receptive Nuclei" (Advanced Study Institute on Advances in NMR), held 5-16 September 1976, Sicily.
99. G.K. Radda, P. Styles, K.R. Thulborn, J.C. Waterton, *J. Magn. Reson.* 42 (1981), 488.
100. K.R. Thulborn, J.C. Waterton, P. Styles, G.K. Radda, *Biochem. Soc. Trans.* 9 (1981), 233.

## 4 FLOW MEASUREMENTS IN MODEL SYSTEMS

### 4.1 INTRODUCTION

Several indirect methods have been used to study water transport in plants by measuring the mean linear flow velocity or the volume flowrate of water in the vascular system of plant stems [1]. None of these methods detects the movement of water itself, however, and many are invasive.

Nuclear magnetic resonance (NMR) is a suitable technique to study liquid flow [2-7]. In most of these NMR methods, stationary liquid - such as non-flowing water in the tissue of the plant stem - gives rise to a large NMR signal in addition to the signal due to flowing liquid. A recent paper [8] describes a spin-echo NMR method, based on a pulse sequence of equidistant  $\pi$  pulses and a linear magnetic field gradient in the direction of flow. This method permits the detection of flow velocities of flowing fluid in the presence of stationary fluid, and NMR signals are generated, the shape of which is correlated to the flow velocity and flow profile.

This Chapter presents a semi-empirical formalism of this pulse NMR method, resulting in an analytical expression for the shape of the time dependence of the NMR signal-amplitude, allowing a straightforward simulation of the experimental signals of plug flow and laminar flow. In this way insight is gained in the effect of the experimental parameters on the signal shape. This has not been possible using the formalism given by Hemminga and de Jager [8]. In addition, we present a detailed discussion of this pulse method as applied to flow in plant stems and based on measurements in capillary model systems, simulating the plant stem. It is shown that from these flow measurements the mean linear flow velocity  $\bar{v}$ , the volume flowrate  $Q$ , the effective cross-section of the capillary  $A$ , and the spin-spin relaxation time  $T_2$  of the flowing water can be determined.

### 4.2 THEORY

The response of a spin system, flowing in a r.f.  $B_1$ -field and along a linear magnetic field gradient, to a sequence of equidistant,

identical pulses has been treated by Hemminga and de Jager [8]. Because of the complexity of the theory the shape of the NMR signals could not be expressed in a closed analytical form and this has been obtained by these authors using computer simulations. With this approach determination of the effect of the parameters of the method on the size and shape of the signal and the presence of additional information hidden in the signals is a tedious matter.

After a brief outline of their results, we present here a semi-empirical approach, resulting in an analytical expression, which can be straightforwardly applied to experimental NMR signals of flowing fluids.

#### 4.2.1 System description

Consider a system of nuclei ( $I = \frac{1}{2}$ ) in a magnetic field  $\vec{B}_0$  directed along the z axis of a laboratory coordinate system  $\{x, y, z\}$ ;

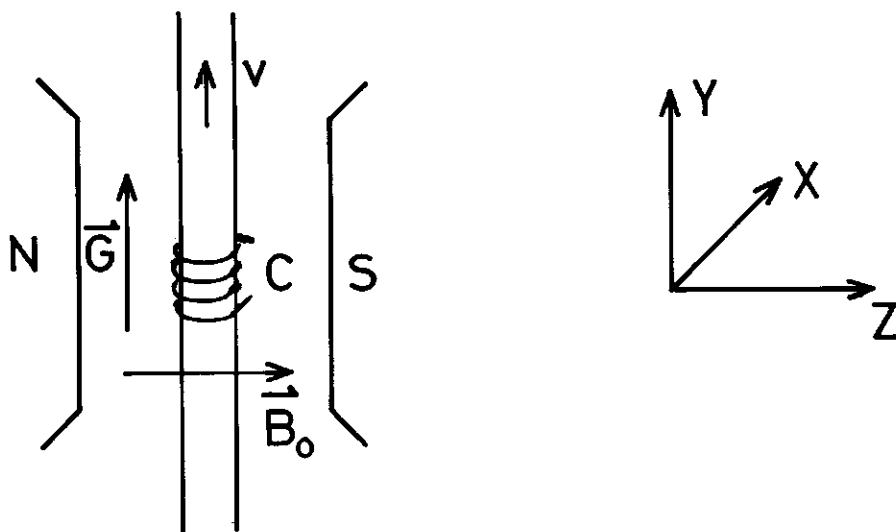


Fig. 1 A schematic representation of a capillary system and sample coil within the magnetic field. The fluid in the inner tube is flowing with flow velocity  $v$ . The r.f. coil is indicated by  $C$ ,  $x, y$  and  $z$  are the axes of a right-handed laboratory coordinate system.

a linear magnetic gradient  $\vec{G}$  (gauss/m) is imposed on  $\vec{B}_0$ , along  $y$ , so that  $B_z(y) = B_0 + yG$  (Fig. 1). Let the nuclei move in the  $+y$  direction with a uniform velocity  $v$  (mm/s), which is the situation for plug flow.

The sample is contained in a tube that extends along the  $y$  axis through the transmitter/receiver coil of a pulsed NMR spectrometer (Fig. 1). The axis of this coil coincides with the  $y$  axis.

The motion of the spin magnetization is considered in a frame  $\{x', y', z'\}$  rotating about the  $B_0(z)$  direction with the Larmor frequency  $\vec{\omega}_0$ . It is assumed that off-resonance effects on the effective r.f. field can be ignored, so that it is equal to  $B_1$  and directed along the  $x'$  axis (see Section 4.3.1). Let the mean Larmor frequency of all nuclei be  $\vec{\omega}_0 = -\gamma\vec{B}_0$ , where  $\vec{B}_0 = \vec{B}_z(y=0)$ .

A sequence of equidistant r.f. pulses (time duration  $t_p$ , period  $\tau$ ,  $\tau \gg t_p$ ) is applied to the sample. During the pulse sequence the nuclei move through the  $B_1$  field and along the linear field gradient  $\vec{G}$ .

To describe the effect of flow, the nuclei in the fluid sample are considered to be divided into small equal groups along the  $y$  axis. The position of such a group of nuclei at the  $n$ th pulse (at time  $t = n\tau$ ) is then given by

$$y_n = y_0 + vnt \quad (4.1)$$

where  $y_0$  is the position of the group at the start of the pulse sequence at  $t = 0$ . In the rotating frame, the precession frequency of the magnetization vector  $\vec{M}$  of such a group is then given by

$$\omega_n = \gamma G y_n \quad (4.2)$$

$\gamma$  is the gyromagnetic ratio. The precession angle in a time  $dt$  between the pulses is  $d\phi = \omega_n dt$ . This is illustrated in Fig. 2.

Between the  $(n-1)$ th and  $n$ th pulse the precession angle  $\Delta\phi_n$  becomes

$$\Delta\phi_{n\tau} = \int_{(n-1)\tau}^{n\tau} \omega(t) dt = \gamma G y_0 \tau + \frac{1}{2}(2n-1)\gamma G v \tau^2 \quad (4.3)$$

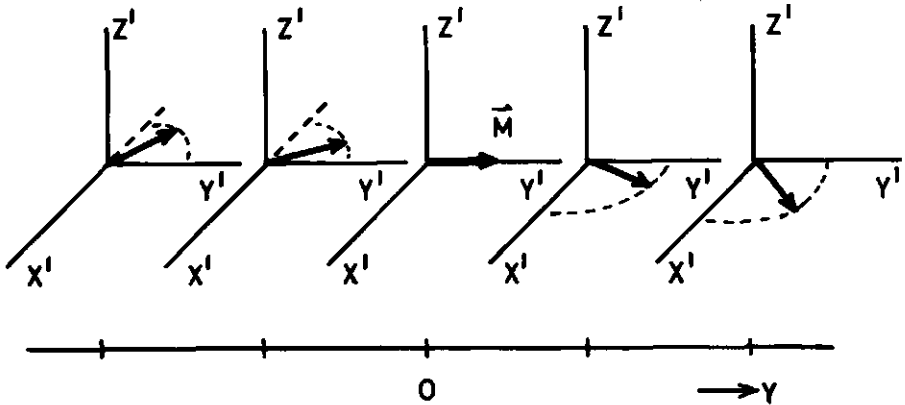


Fig. 2 Schematic representation of the magnetization  $\vec{M}$  of a group of nuclei at time  $dt$  after a  $(\frac{1}{2}\pi)_x$  pulse, as viewed along the  $y$  axis. Each group has a precession frequency, which is a function of the position on the  $y$  axis, due to the magnetic field gradient  $G = dB_0/dy$ . The rotating frame  $\{x', y', z'\}$  rotates with Larmor frequency  $\vec{\omega}_0 = -\gamma\vec{B}_0$ .

(Note that to reach eqn. 4.3 we have replaced  $n\tau$  by  $t$  in eqn. 4.1 and made use of eqn. 4.2, whereas in eqn. 4.1 we have used the model of spin isochromatic groups with finite thickness ( $v\tau$ ), assuming that the field gradient can be considered to vary stepwise, resulting in  $\Delta\phi_n = \omega_n\tau$ . However, the difference between these two approaches is  $\frac{1}{2}\gamma Gv\tau^2$ , which is negligible with respect to  $n\gamma Gv\tau^2$  for  $n \gg 1$ . Throughout this Chapter we will use eqn. 4.3. In view of this approximation, we may also use the model of spin isochromatic groups).

Before we can apply these concepts to the case in hand, we have to make an additional assumption. It is assumed that the nuclei of the flowing fluid have experienced the static field  $B_0$  long enough

to have attained Boltzmann equilibrium before entering the transmitter/receiver coil, so that at the beginning of the pulse sequence the total magnetization vector of all groups of nuclei is  $\vec{M}_0$ , directed along the  $z'$  axis.

#### 4.2.2 Motion of the magnetization in the rotating frame.

Hemminga and de Jager [8] noted that the  $n$ th pulse of the sequence rotates the magnetization of an isochromatic group ( $\vec{M}$ ) about the  $x'$  axis by an angle  $\alpha_n$ , defined as

$$\alpha_n = \gamma B_1(y_n) t_p \quad (4.4)$$

where  $B_1(y_n)$  is the spatial distribution of the  $B_1$  field in the  $y$  direction. The magnetization immediately after the  $n$ th pulse  $\vec{M}_n^+$  is related to the magnetization before the pulse  $\vec{M}_n^-$  by the rotation matrix  $\bar{R}_x(\alpha_n)$ :

$$\vec{M}_n^+ = \bar{R}_x(\alpha_n) \vec{M}_n^- \quad (4.5)$$

Between pulses, the magnetization freely precesses about the  $z$  axis and the magnetization at the beginning of the  $(n+1)$ th pulse is given by

$$\vec{M}_{n+1}^- = \{1 - \exp(-\tau/T_1)\} \vec{M}_0 + \bar{R}_z(\Delta\phi_n) \bar{S}(\tau, T_1, T_2) \vec{M}_n^+ \quad (4.6)$$

$\bar{R}_z$ , represents a rotation about the  $z'$  axis and  $\bar{S}(\tau, T_1, T_2)$  is a diagonal matrix with elements

$$S_{x'x'} = S_{y'y'} = \exp(-\tau/T_2) \text{ and } S_{z'z'} = \exp(-\tau/T_1),$$

where  $T_1$  and  $T_2$  are the spin-lattice and spin-spin relaxation times respectively.

When  $\tau \ll T_2$ , only the integral  $A_{x',n}$  of the x' component of the magnetization between the nth and (n+1)th pulses is relevant and this is given by

$$A_{x',n} = \sin \Delta \phi_n M_{x',n}^+ / \Delta \phi_n + (1 - \cos \Delta \phi_n) M_{y',n}^+ / \Delta \phi_n \quad (\tau \ll T_2) \quad (4.7)$$

$A_{y',n}$  is negligible with respect to  $A_{x',n}$  when  $\tau \ll T_2$ . The actual NMR signal  $S_n$  is derived by multiplying eqn. 4.7 by the sensitivity of the r.f. coil, which is given by  $B_1(y_n)$ , and then summing over all groups of nuclei along the y axis:

$$S_n = \int_{-\infty}^{+\infty} B_1(y_n) A_{x',n} dy_0, \quad (4.8)$$

where  $y_n$  is a function of  $t = n\tau$  as defined in eqn. 4.1.

It is not possible to obtain eqns. 4.1 to 4.8 in a closed form and thus  $S_n$  has been calculated numerically for different r.f. field distributions and flow profiles [8]. These calculations are very timeconsuming, however.

#### 4.2.3 $\pi$ pulses

Until now the rotation angle of the pulses in the pulse sequence was of minor importance for the theoretical description. From now on we restrict our treatment to the case of a pulse sequence of equidistant  $\pi$  pulses, also assuming  $\tau \ll T_2$ . This assumption is very reasonable, since for our measurements  $\tau = 1.6$  ms and curve fitting has been carried out for  $T_2 \geq 200$  ms.

Assuming that we have a Gaussian shaped distribution of the  $B_1$  field,  $B_1(y)$  is then given by  $B_1(y) = B_1(0) \exp(-2y^2/L^2)$ , where  $L$  is the distance between the inflection points of the distribution and  $B_1(0) = \pi/\gamma t_p$ .

At  $t=0$  the first pulse rotates the magnetization  $\vec{M}$  of an isochromatic group at position  $y_0$  by an angle  $\alpha = \pi \cdot \exp(-2y_0^2/L^2)$ . This results in a component  $A$  in the  $x',y'$ -plane given by  $A = M \sin\{\pi \cdot \exp(-2y_0^2/L^2)\}$ , directed along the  $y'$  axis.

During the period  $t=0 \rightarrow t=\tau$  this group of nuclei gains a phase angle  $\Delta\phi_\tau$  with respect to the  $y'$  axis as given by eqn. 4.3 with  $n=1$ :

$$\Delta\phi_\tau = \gamma Gy_0 \tau + \frac{1}{2} \gamma G v \tau^2 \quad (4.9)$$

At  $t=\tau$  the component of the magnetization of this group of nuclei along the  $x'$  axis  $A_{x'}(\tau)$  is

$$A_{x'}(\tau) = M \sin\{\pi \cdot \exp(-2y_0^2/L^2)\} \sin(\Delta\phi_\tau) \quad (4.10)$$

The total  $x'$  component of the magnetization is found by summing the  $A_{x'}$  of two isochromatic groups which are positioned at  $t=0$  symmetrically around  $y=0$ , and integrating over  $y_0$  from 0 to  $\infty$ , yielding

$$S_{x'}(\tau) \propto \int_0^\infty \sin\{\pi \cdot \exp(-2y_0^2/L^2)\} \sin(\frac{1}{2} \gamma G v \tau^2) \cos(\gamma Gy_0 \tau) dy_0 \quad (4.11)$$

At time  $t=\tau$  the isochromatic group of spins receives a second pulse, which now equals  $\alpha = \pi \cdot \exp[-2(y_0 + v\tau)^2/L^2]$ . This pulse rotates the magnetization of the isochromatic group by  $\alpha$  around the  $x'$  axis, leaving  $A_{x'}$  unaffected but changing the total magnetization in the  $x', y'$ -plane by rotating the  $z'$  and  $y'$  components. Attempts to evaluate this process completely in order to obtain a closed expression have been unsuccessful. By making some plausible assumptions on the shape of the r.f. field  $B_1(y)$ , we may obtain an approximate closed expression for  $S_{x'}$ .

#### 4.2.4 A semi-empirical approach

It has been stated by Hemminga and de Jager [8] that the NMR signal of flowing fluid will mainly arise from the region of  $y$  values where  $B_1(y)$  corresponds to  $\frac{1}{4}\pi$  to  $\frac{3}{4}\pi$  pulses. Let us therefore assume that we can represent the distribution  $B_1(y)$  as a rectangle with length  $l$ , corresponding to  $\pi$  pulses for  $|y| < \frac{1}{2}l$ ; at the falling and rising edges of this r.f. field at  $|y| = \frac{1}{2}l$   $\alpha = \frac{1}{2}\pi$  ( $B_1 = \frac{1}{2}B_1(0)$ ); outside the coil  $B_1$  vanishes. This is shown in Fig. 3.



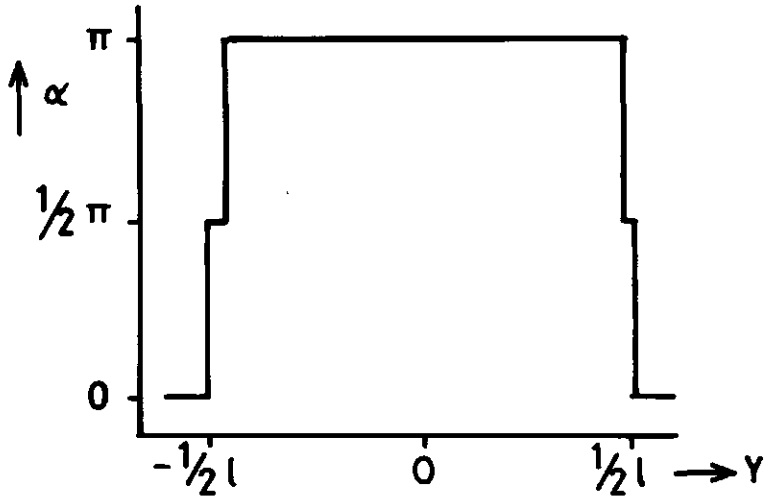


Fig. 3 Distribution of the r.f. field of the transmitter/receiver coil along the  $y$  axis: for  $-\frac{1}{2}l < y < \frac{1}{2}l$ ,  $\alpha (= \gamma B_1 t_p) = \pi$ , for  $|y| = \frac{1}{2}l$ ,  $\alpha = \frac{1}{2}\pi$  and for  $|y| > \frac{1}{2}l$ ,  $\alpha = 0$ .

We define the magnetization of an isochromatic group by

$$M = M_0 \cdot v\tau/l \quad (4.12)$$

assuming that after  $n = l/v\tau$  pulses the flowing fluid in the coil (magnetization  $M_0$ ) has been completely refreshed. This also implies that there are  $n = l/v\tau$  different isochromatic groups in the coil.

Now we can follow the signal that is generated by the pulse sequence while fluid moves into the inside of the r.f. coil, along the magnetic field gradient. At the first pulse ( $t=0$ ) the  $\frac{1}{2}\pi$  pulses at the edges of the  $B_1$  field rotate the magnetization of the isochromatic groups  $\vec{M}$  at  $|y| = \frac{1}{2}l$ .

The isochromatic group at  $y = \frac{1}{2}l$  moves out of the r.f. coil and its magnetization is not observed. The isochromatic group at  $y = -\frac{1}{2}l$  moves into the coil and during the period  $t=0 \rightarrow t=\tau$  it gains a phase angle  $\Delta\phi_\tau$  with respect to the  $y'$  axis as given by eqn. 4.10 with  $y_0 = -\frac{1}{2}l$ , resulting in an  $x'$  component at time  $t=\tau$ :  $A_{x'}(\tau) = M \sin \Delta\phi_\tau$ . At time  $t=\tau$  this isochromatic group of spins receives a second pulse, which now equals a  $\pi$  pulse, rotating the magnetization of this group by  $\pi$  around the  $x'$  axis, i.e.

$$\phi_{\tau^+} = \pi - \Delta\phi_{\tau} \quad (4.13)$$

where  $\phi_{\tau}$  is the total phase angle at a given time  $t$  and  $\tau^+$  the time immediately following the second pulse. (All pulses are assumed to be of negligible duration). During the period  $\tau \rightarrow 2\tau$  the isochromatic group of nuclei gains a phase angle  $\Delta\phi_{2\tau}$  which is given by eqn. 4.3 with  $n=2$ :  $\Delta\phi_{2\tau} = \gamma Gy_0 \tau + \frac{3}{2} \gamma Gv \tau^2$ . This results in a net gain of phase at  $t=2\tau$  of  $\phi_{2\tau} = \Delta\phi_{2\tau} + \phi_{\tau^+} = \pi + \gamma Gv \tau^2$ . The third pulse at  $t=2\tau$  also rotates the magnetization of the spin isochromatic group by  $\pi$  around the  $x'$  axis, resulting in

$$\phi_{2\tau^+} = \pi - \phi_{2\tau} = -\gamma Gv \tau^2 \quad (4.14)$$

In general it can be shown that

$$\phi_{n\tau} = \pi + \frac{n}{2} \gamma Gv \tau^2 \quad (n \text{ even}) \quad (4.15a)$$

and

$$\phi_{(n+1)\tau} = \frac{(n+1)}{2} \gamma Gv \tau^2 + \frac{1}{2} \gamma Gy_0 \tau \quad (4.15b)$$

Now, if phase sensitive detection is used and the detector is adjusted for maximum signal along the  $x'$  axis the  $x'$ -component of the magnetization of this isochromatic group of nuclei at  $t=n\tau$  is proportional to

$$A_{x'}(n\tau) = M \sin\phi_{n\tau} \quad (n \text{ even or odd}) \quad (4.16)$$

Alas, at time  $t=\tau$  a second isochromatic group arrives at  $y_0 = -\frac{1}{2}l$  and receives the  $\frac{1}{2}\pi$  part of the pulse. In addition, the magnetization in the  $x', y'$  plane is attenuated by the spin-spin relaxation characterized by  $T_2$ . So the total signal detected at  $t=2\tau$ ,  $S(2\tau)$ , is given by

$$S(2\tau) = M [\sin\phi_{\tau} e^{-\tau/T_2} + \sin\phi_{2\tau} e^{-2\tau/T_2}] \quad (4.17)$$

Continuing this process, at time  $t=2\tau$  a third isochromatic group arrives at  $y_0 = -\frac{1}{2}l$ , receives the  $\frac{1}{2}\pi$  part of the pulse and starts relaxation in the  $x', y'$  plane, and so on, resulting in

$$S(n\tau) = \sum_{m=1}^n A_{x'}(n\tau) \cdot e^{-n\tau/T_2}, \text{ for } n \leq \frac{1}{v\tau} \quad (4.18)$$

After  $n > 1/v\tau$  the signal reaches a steady state. The sum in eqn. 4.18 can be given by a closed expression using eqns. 4.15 and 4.16, by replacing  $n\tau$  by  $t'$ , integrating over  $t'$  from 0 to  $t$  for the even and uneven phase angles and dividing by  $\tau$ , resulting for  $t \leq 1/v$  in

$$S(t) = \frac{S_0 \cdot v}{I \cdot C} \left[ \{\cos\phi_0 - 1\} \{e^{-t/T_2} \left( -\frac{1}{T_2} \sin\phi(t) - \frac{1}{2}\gamma G v t \cos\phi(t) \right) + \frac{1}{2}\gamma G v t \right. \right. \\ \left. \left. - \sin\phi_0 \{e^{-t/T_2} \left( -\frac{1}{T_2} \cos\phi(t) + \frac{1}{2}\gamma G v t \sin\phi(t) \right) + \frac{1}{T_2} \} \right] \quad (4.19a)$$

where  $S_0$  is the signal detected from the magnetization  $M_0$ ,  $C=2\{(1/T_2)^2 + (\frac{1}{2}\gamma G v t)^2\}$ ,  $\phi_0 = \frac{1}{2}\gamma G v t^2 + \frac{1}{2}\gamma G t l$  and  $\phi(t) = \frac{1}{2}\gamma G v t$ . At  $t > 1/v$  the flowing fluid has been refreshed in the coil and the signal reaches a steady state, which is given by

$$S_E = \frac{S_0 \cdot v}{I \cdot C} \left[ \{\cos\phi_0 - 1\} \{e^{-1/vT_2} \left( -\frac{1}{T_2} \sin\phi_E - \frac{1}{2}\gamma G v t \cos\phi_E \right) + \frac{1}{2}\gamma G v t \right. \right. \\ \left. \left. - \sin\phi_0 \{e^{-1/vT_2} \left( -\frac{1}{T_2} \cos\phi_E + \frac{1}{2}\gamma G v t \sin\phi_E \right) + \frac{1}{T_2} \} \right] \quad (4.19b)$$

with  $\phi_E = \frac{1}{2}\gamma G l \tau$ . For  $T_2 = \infty$  eqns. 4.19 reduce to

$$S(t) = S_0 (\gamma G t l)^{-1} [\cos\phi_0 + \cos\phi(t) - \cos\{\phi_0 - \phi(t)\} - 1], \quad t \leq \frac{1}{v} \quad (4.20a)$$

$$S_E = S_0 (\gamma G t l)^{-1} [\cos\phi_0 + \cos\phi_E - \cos\{\phi_0 - \phi_E\} - 1], \quad t > \frac{1}{v} \quad (4.20b)$$

So far we have considered the signal generated by a pulse sequence of equidistant  $\pi$  pulses from fluid that moves into a rectangular r.f. field along a linear magnetic field. By doing so no signal is observed from the fluid already in the coil at  $t=0$ .

However, as can be shown from eqn. 4.11, this does not correspond to the experimental situation, where the  $B_1$ -field distribution is non-rectangular. Then fluid present in the coil at  $t=0$  gives rise to a signal. This is equivalent to assuming that the sample contains a magnetization  $P_0(//y')$  at  $t=0$  of the isochromatic groups at  $-\frac{1}{2}l < y < \frac{1}{2}l$ , in the presence of a rectangular  $B_1$ -field, as used before. Following the above description for the fluid that moves into the  $B_1$ -field it can be easily shown that the signal generated by the isochromatic groups situated in the coil at  $t=0$  just before an odd numbered pulse, is given by

$$E\{(2n+1)\tau\} = -E_0 \left(1 - \frac{2nv\tau}{l}\right) \sin(n\gamma Gv\tau^2) e^{-2n\tau/T_2}, \text{ for } (2n+1) \leq \frac{l}{v\tau} \quad (4.21a)$$

and

$$E\{(2n+1)\tau\} = 0, \text{ for } (2n+1) > \frac{l}{v\tau} \quad (4.21b)$$

where  $E_0$  is the signal due to  $P_0$ . Noting that the signal due to the even numbered pulses ( $E(2n\tau)$ ) has a similar shape to the signal  $E\{(2n+1)\tau\}$ , we can replace  $(2n+1)\tau$  by  $t$  in eqn. 4.21 and obtain an approximate expression for the total signal generated by plug flow:

$$S_{\text{plug}}(t) = S(t) + E(t) \quad (4.22)$$

where  $S(t)$  is given by eqn. 4.19 and  $E(t)$  by eqn. 4.21. The amplitude-ratio of  $E(t)$  and  $S(t)$ ,  $E_0/S_0$  is an adjustable parameter between 0 and 1. We will use this parameter for curve-fitting.

Fig. 4A and 4B shows calculated  $S(t)$  and  $E(t)$  signals, resp., for a particular set of  $G$ ,  $\tau$ ,  $T_2$  and  $l$  and various values of  $v$ , using 4.22.

#### 4.2.5 Laminar flow

For laminar flow, the liquid velocity  $v$  varies with the distance  $r$  from the tube axis as given by

$$v(r) = 2\bar{v}(1 - r^2/R^2), \quad (4.23)$$

where  $\bar{v}$  is the mean liquid velocity and  $R$  is the tube radius. The amount of fluid with velocity  $v(r)$  lying between  $r$  and  $r+dr$  is  $2\pi r dr$ .

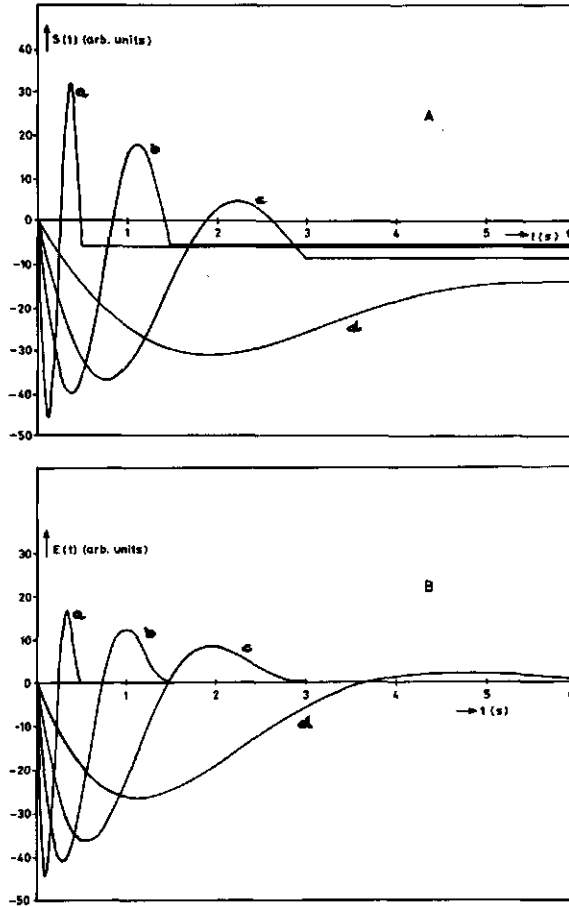


Fig. 4 Calculated NMR signals  $S(t)$  (A) and  $E(t)$  (B) of plug flow in a rectangular  $B_1$ -field distribution, calculated with eqns. 4.19a,b and 4.21a,b, resp.  $l = 15$  mm,  $G = 20$  G/m,  $T_2 = 2.4$  s and  $\tau = 1.6$  ms. The values of  $v$  (in mm/s) are: 30 (a), 10 (b), 5 (c) and 2 (d).

The signal for laminar flow can now be calculated from eqn. 4.22 using

$$S_{\text{lam}}(t) = 2(R)^{-2} \int_0^R S_{\text{plug}}\{t, v(r)\} r dr = (2\bar{v})^{-1} \int_0^{2\bar{v}} S_{\text{plug}}(t, v) dv, \text{ for } t \leq \frac{1}{2\bar{v}} \quad (4.24a)$$

At  $t \geq 1/2\bar{v}$  the flowing fluid with higher velocity components has been refreshed in the coil and the signal from this fluid reaches the steady state as given by eqns. 4.19b and 4.21b. At time  $t$  this holds for  $v$  between  $2\bar{v}$  and  $1/t$ . Therefore at  $t > 1/2\bar{v}$  the signal for laminar flow must be calculated using

$$S_{lam}(t) = (2\bar{v})^{-1} \left[ \int_0^{1/t} S_{plug}(t,v) dv + \int_{1/t}^{2\bar{v}} S_E(v) dv \right] \quad \text{for } t > \frac{1}{2\bar{v}} \quad (4.24b)$$

For  $T_2 = \infty$  and  $P_0 = 0$  eqn. 4.24a becomes

$$S_{lam}(t) = S_0(\gamma G \tau l)^{-1} [(\cos\phi_0 - 1)(1 - \sin\bar{\phi}(t)/\bar{\phi}(t)) - \sin\phi_0 \sin^2 \frac{1}{2}\bar{\phi}(t)/\frac{1}{2}\bar{\phi}(t)],$$

for  $t \leq \frac{1}{2\bar{v}}$  (4.25)

where  $\bar{\phi}(t) = \gamma G \bar{v} \tau t$ . A comparison between eqns. 4.19a and 4.25 shows that for plug flow we have sine and cosine terms, whereas laminar flow gives  $1 - \sin x/x$  and  $\sin^2 x/x$  terms. The same conclusion holds for  $T_2 = \infty$  and  $P_0 \neq 0$ . Thus, in general, we expect  $S_{plug}(t)$  and  $S_{lam}(t)$  to have different shapes.

#### 4.2.6 Determination of the flow velocity

To obtain the flow velocity from the signals of flowing liquid using a sequence of  $\pi$  pulses two methods have been suggested by Hemminga and de Jager [8]: (i) from an analysis of the initial slope of the  $(\frac{\partial S}{\partial t})_0$ , which has been shown experimentally to be proportional to  $v$  (or  $\bar{v}$  in the case of laminar flow); (ii) if the signal reaches a maximum or minimum, the position  $t_{max}$  of that extremum has empirically been shown to be inversely proportional to  $v$  (or  $\bar{v}$ ).

For plug flow the relationship between  $v$  and  $(\frac{\partial S}{\partial t})_0$  and between  $v$  and  $t_{max}^{-1}$  can be easily obtained for the case where the contribution of  $E(t)$  to the total signal is small (as for a  $\pi$  pulse sequence) using eqn. 4.19a, yielding

$$\left(\frac{\partial S}{\partial t}\right)_0 = -\frac{1}{2} S_0 \sin\phi_0 v/l \quad (4.26)$$

for the initial slope,

and, via  $\frac{\partial S}{\partial t} = 0$  for  $t_{\max}$ ,

$$v = (\gamma G t)^{-1} (\phi_0 \pm \pi) t_{\max}^{-1} \quad (4.27)$$

To obtain eqn. 4.26 it has been assumed that  $T_2$  has no effect on  $(\frac{\partial S}{\partial t})_0$ . Eqn. 4.27 shows that the position of the extremum does not depend on  $T_2$ . The small contribution of  $E(t)$  to the total signal however introduces a  $T_2$  dependence on the position of the extremum of the signal (see Section 4.2.7). Whether this extremum is a maximum or a minimum depends on the direction of  $\vec{G}$  and  $\vec{v}$ . As can be verified from eqns. 4.19 and 4.21 the signal alters sign when  $\vec{v}$  or  $\vec{G}$  reverses direction. (Note that  $\phi_0$  is  $G$  dependent and  $\sin\phi_0$  becomes  $-\sin\phi_0$  when  $G$  alters sign). This illustrates that the method can also be used to reveal the *direction* of flow.

For laminar flow  $(\frac{\partial S}{\partial t})_{0,\text{lam}}$  can be found using eqns. 4.24a and 4.19, resulting in

$$(\frac{\partial S}{\partial t})_{0,\text{lam}} = -\frac{1}{2} S_0 \sin\phi_0 \bar{v}/l \quad (4.28)$$

whereas the relationship between  $\bar{v}$  and  $t_{\max}^{-1}$  can only be obtained numerically. Comparison of eqns. 4.26 and 4.28 shows that for a system undergoing laminar flow with an average velocity equal to that of plug flow, the initial slope of the signal is equal to that observed with plug flow.

#### 4.2.7 Determination of $T_2$ and volume flowrate

The effect of spin-spin relaxation on the signal from flowing liquid can be explained by considering the two separate contributions to the signal, i.e.  $S(t)$  and  $E(t)$ . As has been pointed out in Section 4.2.4 the magnetization of the isochromatic groups flowing into the r.f. coil starts relaxation in the  $x',y'$  plane at the moment that such a spin group reaches  $y = -\frac{1}{2}l$ . Owing to this mechanism  $S(t)$  decays not as a simple exponential in time, but as a sum of exponentials (see eqn. 4.18) which start at different times, resulting in an

effective decay time that is longer than  $T_2$ . The second contribution to the signal, from the liquid that was already situated in the coil at  $t=0$ , has been assumed to be generated at  $t=0$  and to decay exponentially with  $T_2$ .

Assuming again that the contribution of  $E(t)$  to the total signal is small for plug flow it can be shown from eqns. 4.19 and 4.27 that the spin-spin relaxation time  $T_2$  can be found from

$$\ln[\partial(S(t_{\max})t_{\max})/\partial t_{\max}] = \ln D_1 - t_{\max}/T_2, \quad (4.29)$$

where  $D_1 = S_0(\gamma G \tau) {}^1D_0 \{(\cos\phi_0 - 1)\sin D_0 - \sin\phi_0 \cos D_0\}$ ,  $D_0 = \frac{1}{2}(\phi_0 \pm \pi)$  and  $S(t_{\max})$  is the height of the signal at  $t_{\max}$ . This is the basis of the determination of the spin-spin relaxation time  $T_2$  from the NMR signals of flowing water.

The signal  $S_0$  detected from the total magnetization  $M_0$  in the r.f. coil is directly proportional to the amount of flowing water in the coil  $V$ . This amount can be determined by extrapolating the  $\ln[\partial(S(t_{\max})t_{\max})/\partial t_{\max}]$  vs.  $t_{\max}$  curve to  $t_{\max} = 0$  (eqn. 4.29).  $V$  must be calibrated for given values of  $G$  and  $\tau$  (see  $D_1$  in eqn. 4.29).

The volume flowrate  $Q$  can now be calculated from

$$Q = v \cdot V/L_{\text{eff}}, \quad (4.30)$$

where  $L_{\text{eff}}$  is the effective r.f. coil length.  $L_{\text{eff}}$  does not necessarily equal  $l$ , owing to the difference in the shape of the r.f. field distribution in theory and practice. It is noticeable that  $V/L_{\text{eff}}$  equals the cross-sectional area  $A$  of the capillary.

For laminar flow it is impossible to obtain from eqns. 4.24 expressions similar to eqns. 4.29 and 4.30. However, empirically,  $T_2$  can be obtained using the same procedure as for plug flow.

### 4.3 SOME COMMENTS ON THE SEMI-EMPIRICAL APPROACH

#### 4.3.1 Approximations

In the semi-empirical formalism developed in Section 4.2.4 we have made the following approximations: (i) the r.f. field distri-



bution is assumed to be rectangular (see Fig. 3); (ii) off-resonance effects on the effective r.f. field  $B_{\text{eff}}$  have been neglected; (iii) the variation of the magnetization during the pulse sequence has been followed by sampling the signal at time  $t = n\tau$ , just before a pulse; (iiii) the effects of spin-lattice relaxation and diffusion have been neglected.

#### 4.3.1.1 Distribution of the r.f. field

The actual r.f. field distribution depends on the geometry of the transmitter/receiver coil in use: a solenoid type coil does not produce the same distribution as a Helmholtz type. Their  $B_1$ -field distributions will differ, in particular with respect to the full width at half maximum ( $L$ ). In our model this is accounted for by the length of the rectangular r.f. field distribution  $l$  (to be distinguished from  $L_{\text{eff}}$ , used in Section 4.2.7). Varying  $l$  results in two effects (eqns. 4.19): (i) the time at which the steady state is reached is affected:  $t = l/v$ , (ii) the value of  $\phi_0$  changes. The effective length of the r.f. coil as experimentally found from the time at which the signal reaches its steady state, is used in simulations of the signal, taking (i) into account.

However, we have stated above (Section 4.2.4) that the NMR signal of flowing water will mainly arise from the region of  $y$  values where  $B_1(y)$  corresponds to  $\frac{1}{2}\pi$  to  $\frac{3}{2}\pi$  pulses. In general, this region will not coincide with  $|y| = \frac{1}{2}l$ , as in the model for the rectangular  $B_1$ -field distribution. Actually, by taking  $l$  equal to the effective length of the r.f. coil, the off-resonance frequency of the region where the signal is generated, i.e.  $\sim \phi_0$ , is too high. Therefore in fitting procedures we have used  $\phi_0 < (\frac{1}{2}\gamma G l + \frac{1}{2}\gamma G v \tau^2)$ . Thus,  $\phi_0$  is the only adjustable parameter which does not follow from experiment, and which is used for curve-fitting.

#### 4.3.1.2 Off-resonance effects on the effective r.f. field

The off-resonance effects on the effective r.f. field are dependent on the duration of the  $\pi$  pulse (the quality factor of the r.f. coil) and the magnitude of the magnetic field gradient. Experimentally we have used a solenoid as well as a Helmholtz type r.f. coil (see

Section 4.4), with  $\pi$  pulses of 15  $\mu$ s and 30  $\mu$ s, respectively. The values of G are in the order of 10 G/m.

For the solenoid the width of  $B_1(y)$  at half maximum is  $\sim 10$  mm. Assume we have a Gaussian shaped  $B_1$ -field distribution. If  $B_1(y)=10^\circ$ ,  $B_{\text{eff}}=10.5^\circ$  and  $B_{\text{eff}}$  is tilted towards the  $z'$  axis by  $15^\circ$  with respect to the  $x'$  axis. For  $B_1(y)=45^\circ$   $B_{\text{eff}}$  becomes  $45^\circ$  and has only a  $2.5^\circ$  deviation from the  $x'$  axis.

The  $B_1$  distribution of the Helmholtz coil has a full width at half maximum of about 7 mm. Then, for  $B_1(y)=10^\circ$ ,  $B_{\text{eff}}=10.8^\circ$  and is tipped away from the  $x'$  axis by  $21^\circ$ , whereas for  $B_1(y)=45^\circ$   $B_{\text{eff}}$  becomes  $45^\circ$  and the deviation from the  $x'$  axis is  $3.4^\circ$ .

These calculations demonstrate that the off-resonance effects on the effective r.f. field at the values of G used are of minor importance, but they become more serious for higher values of G and for less sensitive r.f. coils.

Calculations performed by Hemminga and de Jager on the effect of  $B_{\text{eff}}$  on the NMR signal shape of flowing fluid have shown little variations for values of G below about 25 G/m for the solenoid r.f. coil [8]. Extrapolating this finding with the aid of the above calculations, the signal shape measured with the Helmholtz coil is not expected to be affected by off-resonance effects for  $G < 18$  G/m. Experimentally we have used  $G \leq 15$  G/m.

#### 4.3.1.3 Sampling time

Experimentally the signal of flowing fluid has been obtained by integrating the  $x'$  component of the magnetization between the pulses (see Section 4.4.). To derive eqns. 4.19 and 4.20 we have followed the variation of the magnetization by sampling the signal at time  $t=n\tau$ , just before a r.f. pulse. In these equations integration has been omitted.

Sampling on  $t=(n+\frac{1}{2})\tau$ , just between two pulses, for the phase angle  $\phi$  we obtain the result:

$$\phi_{(n+\frac{1}{2})\tau} = \frac{1}{8}\gamma G v \tau^2 - \frac{1}{4}\gamma G l \tau \quad (n \text{ even}) \quad (4.31a)$$

and

$$\phi_{(n+\frac{1}{2})\tau} = \pi + \frac{1}{8}\gamma G v \tau^2 + \frac{1}{4}\gamma G l \tau \quad (n \text{ odd}) \quad (4.31b)$$

Comparing eqns. 4.31 and 4.15 shows that in the latter  $\phi_{n\tau}$  is dependent on  $n$ , whereas in the former  $\phi_{(n+\frac{1}{2})\tau}$  does not depend on  $n$ . In view of 4.31a,b  $M_x, \{(n+\frac{1}{2})\tau\}$  becomes stationary in time for  $n$  even as well as odd. Clearly this is due to (i) the use of a rectangular r.f. field distribution with the property that we have effectively  $\pi$  pulses for  $|y| < \frac{1}{2}$  (Fig. 3), and (ii) sampling on  $t = (n+\frac{1}{2})\tau$ . For every other sampling time  $t = (n+x)\tau$ ,  $0 < x < 1$ , the value of  $M_x, \{(n+x)\tau\}$  depends on  $n$ . Thus, simplifying the actual r.f. field by a rectangular distribution, results in a predicted dependence of the signal shape on sampling time.

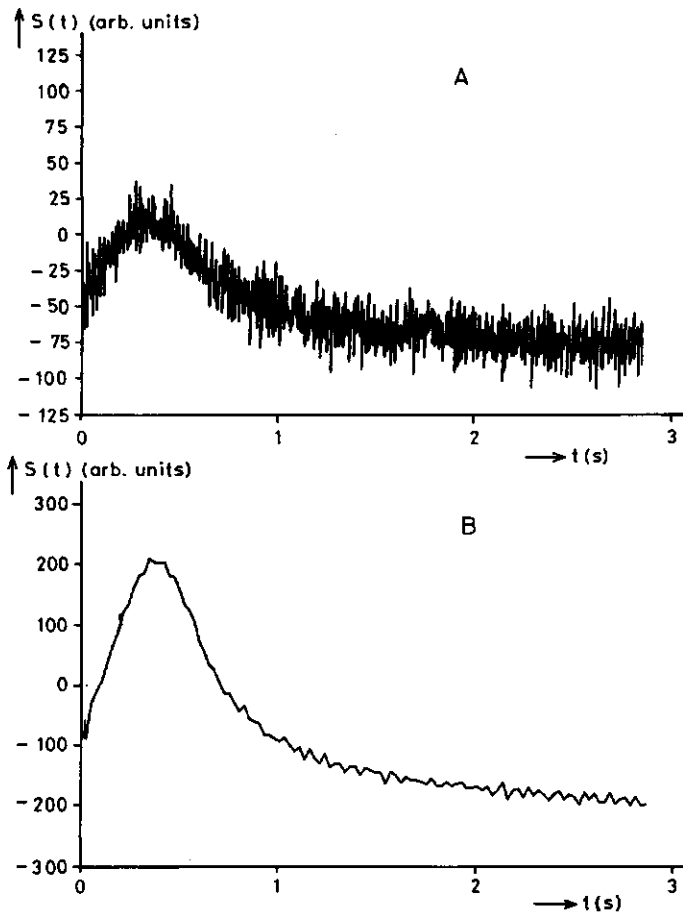


Fig. 5 Experimental NMR signals  $S(t)$  of flowing water vs. time, generated by a sequence of equidistant  $\pi$  pulses. (A) Signal obtained by sampling at time  $t = (n+\frac{1}{2})\tau$ , just between the two pulses, (B) signal obtained by integrating the magnetization between the pulses. Further experimental conditions are identical for (A) and (B).

Experimentally we have sampled the magnetization of the flowing fluid at times  $t=(n+\frac{1}{2})\tau$  (Fig. 5A). Under identical experimental conditions, but now integrating the signal between the pulses, signals were obtained with identical shape, but with a much higher signal-to-noise ratio (see Fig. 5B). No other sampling times have been used, so we have no further information on the dependence of the signal shape on sampling time.

By sampling at  $t=n\tau$ , the off-resonance contribution  $\phi_0$  of the region where the signal is generated becomes too large (Compare the  $\frac{1}{2}\gamma G\tau$  part in eqns. 4.31 and  $\frac{1}{2}\gamma G\tau$  in eqns. 4.15). This is an additional argument to use  $\phi_0 < \frac{1}{2}\gamma G\tau + \frac{1}{2}\gamma Gv\tau^2$  in fitting procedures (see also Section 4.3.1.1).

#### 4.3.1.4 Effect of $T_1$ relaxation and diffusion.

The neglect of spin-lattice relaxation in our model is justified since the fluid in the r.f. coil only experiences  $\pi$  pulses. Any change in magnetization along the  $z'$  axis, therefore, is not rotated to the  $x',y'$  plane. In reality, the spin-lattice relaxation mechanism causes the magnetization to return to the equilibrium position along the  $z'$  axis. Besides, we have a pulse angle distribution over the r.f. coil (eqn. 4.4), so that part of the  $z'$  magnetization can be rotated to the  $x',y'$  plane. However, as long as  $T_2 \ll T_1$  the signal shape is mostly influenced by the spin-spin relaxation mechanism. This condition is commonly met in biological systems.

The effect of diffusion can be incorporated into the theory by replacing  $n\tau/T_2$  in eqns. 4.18 and 4.21a by  $n\tau/T_2 + \frac{1}{3}\gamma^2 G^2 D\tau^2 n\tau$  [3], where  $D$  is the translational diffusion constant. However, if  $T_2 \ll (\frac{1}{3}\gamma^2 G^2 D\tau^2)^{-1}$  the diffusion term can be neglected. Using  $G \leq 15$  G/m,  $\gamma \approx 2.7 \times 10^4$  rad/G·s (for protons),  $\tau = 1.6$  ms, and assuming  $D \approx 2 \times 10^{-9}$  m<sup>2</sup>/s for water this condition is easily met.

#### 4.3.2 Comparison between theoretical approaches.

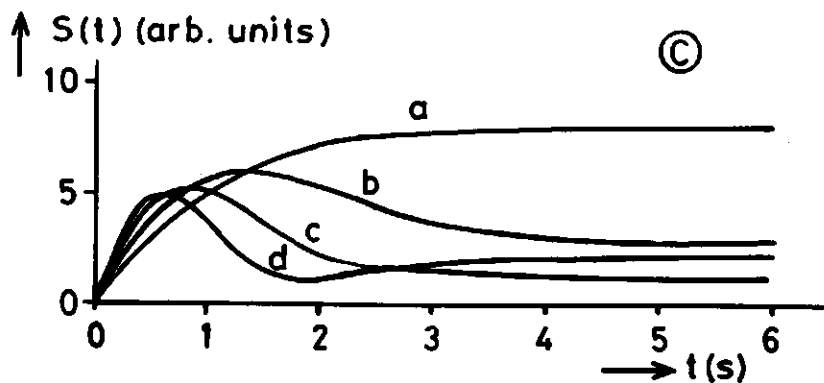
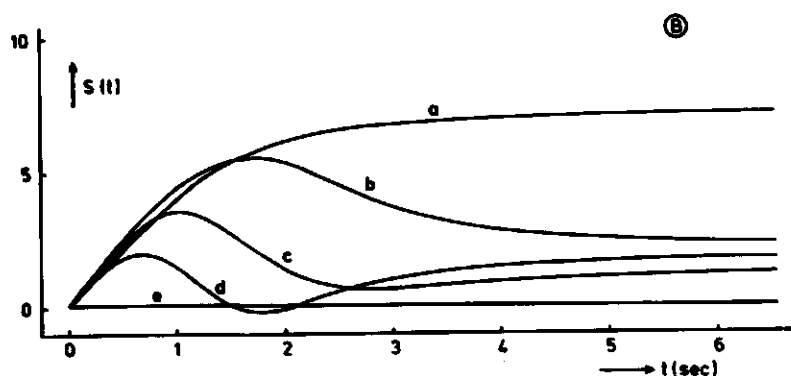
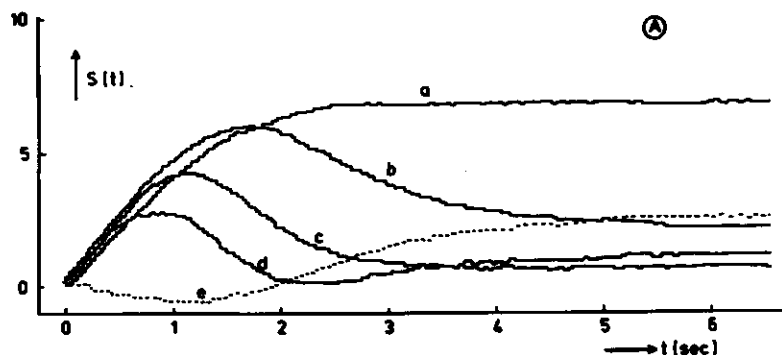
In Figures 6, 7 and 8 a comparison is presented between experimental NMR signals of flowing fluid as obtained with the  $\pi$  pulse sequence with computer simulations based on the formalism developed by Hemminga and de Jager [8] (eqns. 4.1 through 4.8) and computer

simulations based on our treatment (eqns. 4.19a,b and 4.21a,b) for laminar flow. In these Figures A and B are respectively the experimental NMR signals and the computer simulations as given by Hemminga and de Jager [8], whereas C shows our computer simulations. Fig. 6 shows the effect of the field gradient  $G$  on the NMR signals. Fig. 7 and 8 represent NMR signals  $S_{1\text{lam}}(t)$  obtained with various values of the mean liquid velocity  $\bar{v}$ . In Fig. 7  $G$  has been chosen in such a way that the signals do not have a maximum, whereas in Fig. 8 a higher value of  $G$  is employed.

Within the limitations of the theoretical model the agreement is very good between our simulations and the experimental NMR signals, as well as the curves calculated by Hemminga and de Jager. In order to obtain our simulations we have used the experimental values of  $\tau$ ,  $T_2$ ,  $G$  and  $\bar{v}$  as given in [8]. The value of  $l$  has been determined from plug flow curves as calculated with the computer program used by Hemminga and de Jager [8]. The time at which the plug flow signal reaches its steady state has been taken as  $t=l/v$ . For all velocities  $l$  has been calculated to be 27 mm for the dimensions of the r.f. coil used by Hemminga and de Jager [8]. The value of  $\phi_0$  (see eqn. 4.19 and Section 4.3.1.1) has been adjusted to give the best fit for the shape of the signals. It is rather surprising that in all simulations  $\phi_0$  was found to equal 0.5, whereas in theory  $\phi_0$  is proportional to  $G$ . The amplitude-ratio  $E_0/S_0$  in eqn. 4.22 has been chosen to yield the best agreement between the experimental and calculated  $S(t_{\text{max}})$  vs  $t_{\text{max}}$  curve. This ratio was found to be  $0.03 \leq E_0/S_0 \leq 0.05$ . The vertical scaling factor is the same for all simulations in Figs. 6C, 7C and 8C.

The simulations given in Figs. 6C, 7C and 8C have been calculated on a MINC-11/03 microcomputer, using a BASIC program. The calculation time of a theoretical NMR signal is about 5 min. The calculation time (CPU-time) of the curves in Figs. 6B, 7B and 8B, which have been performed on a DEC SYSTEM-1090, using a FORTRAN program, is about 30 min. So, our treatment yields an enormous gain in computing-time.

Fig. 6 (A) Effect of the field gradient  $G$  on the experimental NMR signals  $S(t)$  of flowing water in a capillary, generated by a sequence of equidistant  $\pi$  pulses, as given by Hemminga and de Jager [8]. The mean flow velocity  $\bar{v}$  is 4.7 mm/s. The values of  $G$  (in G/m) are: 3.3(a), 7.6(b), 12.3(c), (to be continued at next page)



17.0(d), and 0.0(e). The pulse period  $\tau$  is 1.6 ms. The spin-spin relaxation time  $T_2$  of the water sample is 2.4 s. (B). Computer simulations of the effect of  $G$  as calculated in [8]. All parameters and conditions used in the calculations are identical to those in the experiment (see A). (C) Computer simulations of the effect of  $G$  on  $S(t)$  based on eqns. 4.19 through 4.22. For  $\tau$ ,  $T_2$ ,  $G$  and  $\bar{v}$  the experimental values have been used as in A. The value of the length of the rectangular  $B_1$ -field distribution  $l$  was determined to be 27 mm (see text). The value of  $\phi$  (eqn. 4.19) for all four curves equals 0.5 rad. The amplitude-ratio  $E_0^0/S_0$  was taken to be 0.05.

In (B) and (C) laminar flow is simulated using 20 calculated plug flow NMR signals. The vertical scales are given in arbitrary units. The vertical scaling factor of the simulations are for (B) the same as in Figs. 7B and 8B, and for (C) as in Figs. 7C and 8C. Figs. A and B reproduced from [8] by permission of the authors and Academic Press.

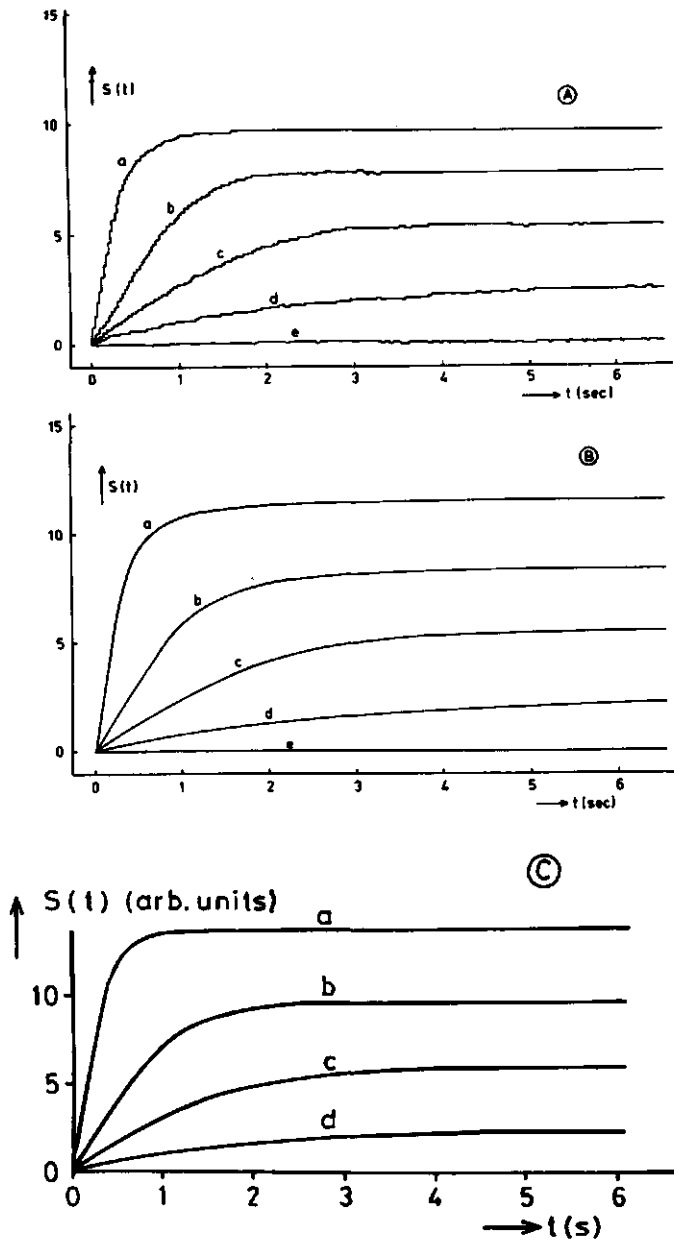


Fig. 7 Effect of flow velocity  $\bar{v}$  on experimental (A) and calculated (B) NMR signals both from [8]. The field gradient  $G$  is 3.3 G/m. The values of  $\bar{v}$  (in mm/s) are: 25.4(a), 7.0(b), 3.0(c), 1.0(d), and 0.0(e). (C) Computer simulations based on eqns. 4.19 through 4.22. See caption of Fig. 6 for other conditions.

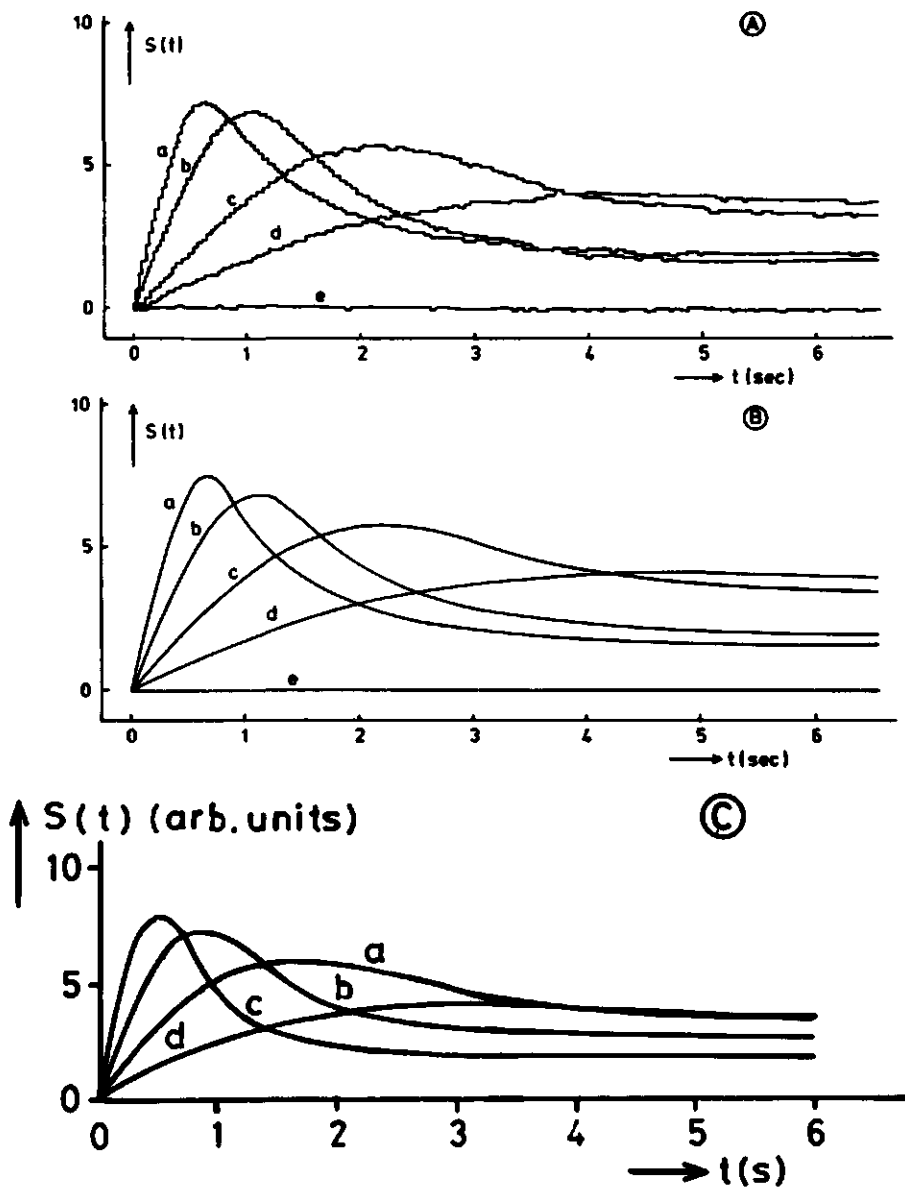


Fig. 8 Effect of flow velocity  $\bar{v}$  on experimental (A) and calculated (B) NMR signals as given in [8].  $G = 6.7$  G/m. The values of  $\bar{v}$  (in mm/s) are: 15.5(a), 8.8(b), 4.3(c), 2.0(d), and 0.0(e). (C) Computer simulations based on eqns. 4.19 through 4.22. See caption of Fig. 6 for other conditions.



Packer [3] has also devised multipulse sequences which allow a "one-shot" determination of  $v$  and  $T_2$ . He has discussed the effect of flow along a magnetic field gradient using two different pulse sequences: (i)  $\frac{1}{2}\pi_{x',-\tau}(-\pi_{y',-\tau})_n$  and (ii)  $\frac{1}{2}\pi_{x',-\tau}(-\pi_{y',-\tau'})_n$ , with  $\tau' > \tau$ . In the theoretical analysis Packer has only considered the liquid already present in the r.f. coil at the beginning of the pulse sequence. The effect of  $\pi$  pulses on the magnetization of fluid moving into the r.f. coil and the loss of magnetization of fluid moving out of the coil volume have been neglected. The time dependence of the amplitude of the echoes, occurring at time  $2n\tau$ , and resulting from the first pulse sequence is given by [3]:

$$E(2n\tau) = E(0)\cos(nyGvt^2) e^{-2n\tau/T_2} \quad (4.32)$$

This result is similar to our eqns. 4.21a,b taking into account liquid already situated in the coil at  $t=0$ , where the sine-function is replaced by a cosine due to phase sensitive detection along the  $y'$  axis instead of the  $x'$  axis in our method. In Packer's pulse sequences (i) and (ii) there is also a contribution to the signal due to fluid moving into the r.f. coil, where it receives  $\pi$  pulses. This results in a contribution  $S(t)$  to the signal equal to that given in eqns. 4.19. However, due to the first  $\frac{1}{2}\pi$  pulse in the pulse sequences used by Packer, the aforementioned contribution due to liquid already present in the coil, at  $t=0$ , is much larger than in the  $\pi$  pulse sequence used in our experiments. In other words, the value of  $P_0$  using Packer's pulse sequences is higher than in our  $\pi$  pulse sequence (see also the  $E_0/S_0$  ratio in eqn. 4.22). These arguments justify the use of eqn. 4.32 in Packer's case.

In biological tissues Packer's methods are not attractive since stationary fluid also gives rise to a signal due to the first  $\frac{1}{2}\pi$  pulse.

#### 4.4 EXPERIMENTAL

The experiments have been performed on a 15 MHz single coil pulsed NMR spectrometer with a 7-in. electromagnet. Details of the spectrometer have been described elsewhere [9]. Several home-made sample probes have been used with transmitter/receiver coils of the Helmholtz-

or the solenoid type. The Helmholtz type coil has a length and diameter of 10 mm, whereas the solenoid type coils have various dimensions. The field homogeneity is optimized using a shim unit. A gradient in the y direction (direction of flow) is produced using the y-shim control. The center of the transmitter/receiver coil is positioned exactly in the middle of the shim coils. Prior to each experiment the magnetic field  $B_0$  is set on-resonance (i.e. no beats in the free induction decay).

To measure flow, a pulse sequence of 4096  $\pi$  pulses is given directed along the x' axis of the rotating frame. The reference phase of the phase-sensitive detector is adjusted to detect the x' component of the magnetization. The receiver was used in combination with a circuit, which integrates the signal between pulses. One data point of the NMR signal contains the integrated signal resulting from 16 pulses, so that experimental signals are built up from 256 data points. Further experimental details are given in [8].

Two types of simulation systems for a plant stem have been constructed. Both contain stationary water in a glass tube with an inner diameter of 7 mm. In the single capillary system a capillary containing flowing water with a diameter of 1.25 mm is fitted in the center of the glass tube. This results in a flowing water fraction of 5%, as calculated from the dimensions of the system. A four-capillary system has also been used, containing four capillaries with inner diameter of 1 mm, which are positioned in the glass tube at the four edges of a square at equal distances (1.7 mm) from the center of the glass tube. The flowing water fraction in this system is 8%. The capillaries are connected to a reservoir, from which water flows through the capillaries under an adjustable hydrostatic pressure. The mean flow velocity  $\bar{v}$  is calculated from the flow quantity and the area of the inner capillaries. The length of the capillary systems is about 6 mm. The system is symmetrically positioned within the NMR sample probe.

The flow velocity  $\bar{v}$  can be obtained from the position  $t_{\max}$  of the extremum in the NMR signals of flowing fluid. Previously it has been shown (Fig. 8 and ref. [8]) that  $t_{\max}$  is inversely proportional to  $\bar{v}$  :  $\bar{v} = C/t_{\max}$  (see eqn. 4.27). The calibration constant C depends on the value of G. At a particular value of G, C can be found by plotting  $\bar{v}$  versus  $t_{\max}^{-1}$ , where  $\bar{v}$  can be calculated from the

measured flow quantity and the known internal diameter of the capillaries of a capillary calibration system [8,10]. To perform this calibration method it is not necessary to know the exact value of the field gradient  $G$ . Therefore we have only estimated the actual value of  $G$ . If necessary, calibration of  $G$  can be carried out more accurately using the free induction decay  $F(t)$  by measuring the time  $t_{1/2}$  at which  $F(t_{1/2}) = \frac{1}{2}F(0)$  [8].  $t_{1/2}$  is related to  $G$  by

$$(\gamma/2\pi) G t_{1/2} = C_1 \quad (4.33)$$

where  $G$  is expressed in gauss per meter,  $t_{1/2}$  in seconds and  $\gamma/2\pi$  in hertz per gauss.  $C_1$  is a constant (in  $m^{-1}$ ) for a particular transmitter/receiver coil, and reflects the spatial distribution  $B_1(y)$  of the r.f. field. For the various transmitter/receiver coils used we have assumed that  $B_1(y)$  may be approximated by a Gaussian function (see Section 4.2.3). In this way  $C_1$  can be calculated for a given transmitter/receiver coil. The value of  $G$  calculated in this way has a maximum deviation of 25% from the actual value.

## 4.5 RESULTS AND DISCUSSION

In this Section we presents the results of a series of NMR-experiments on water flow in glass capillary systems designed to model the use of the  $\pi$  pulse sequence for the measurement of the flow velocity of water in plant stems.

### 4.5.1 Calibration

#### 4.5.1.1 Necessity of a linear field gradient

Flow velocities can in principle be obtained from the NMR signals of flowing water from either the initial slope  $(\frac{\partial S}{\partial t})_0$  (eqns. 4.26 and 4.28), which has been shown experimentally to be proportional to  $\bar{v}$  [8], or, if the signal reaches a maximum or minimum, from the position  $t_{\max}$  of that extremum via  $\bar{v} = C/t_{\max}$  [8,10]. The initial slope depends on the gain of the aplifiers of the pulsed NMR spectrometer and on the amount of flowing water (eqns. 4.26 and 4.28). The second method is independent of these experimental variables

and is therefore preferable for practical applications. Unknown flow velocities can now be determined after calibration of the spectrometer, yielding C for a particular value of G.

When  $G=0$  the NMR signal is expected to be zero (eqns. 4.19 and 4.21). Experimentally, NMR signals have been obtained, however, without applying an external field gradient, because the natural gradient in the magnetic field produced by our electromagnet in the direction of flow is already sufficient to produce the signals. So, if the system containing flowing water is always placed at the same position in the magnetic field, then flow velocities can be measured without applying an external field gradient, after calibration at this particular position, yielding C for this local natural  $y$  gradient. This situation applies to all measurements which we carried out on a single capillary system, where the capillary was concentric with a larger glass tube, placed in the center of the transmitter/receiver coil. The outer tube may contain water, thus simulating plant-tissue surrounding xylem transport vessel in a plant stem.

In general water flow in plant stems cannot be considered as being concentrated in a single capillary. Therefore we have investigated the shape of the natural gradient in the  $x,z$ -plane (see coordinate system in Fig. 1) by measuring the NMR signal of a constant water flow through one of the capillaries of the four-capillary system. By rotating the capillary system around the  $y$  axis (Fig. 1) NMR signals of flowing water at different  $x,z$ -coordinates have been measured. Not surprisingly these measurements revealed that the magnitude and direction of the natural gradient strongly depends on the  $x,z$ -coordinates. When water flows through two neighbouring capillaries it has even been observed that at certain  $x,z$ -coordinates of the capillaries virtually no net signal is observed (see Fig. 9). This can be explained by assuming that the signals produced by the water flow in each capillary are nearly equally shaped, but reversed in sign, indicating that the local natural  $y$  gradients at the position of these capillaries have about the same magnitude, but are of opposite sign. Similar results have been obtained with water flow through all four capillaries. Optimizing the homogeneity of the static magnetic field by using the shim unit and applying an external  $y$  gradient results in NMR signals of flowing water which are almost or completely independent of the  $x,z$ -coordinates of the capillaries.

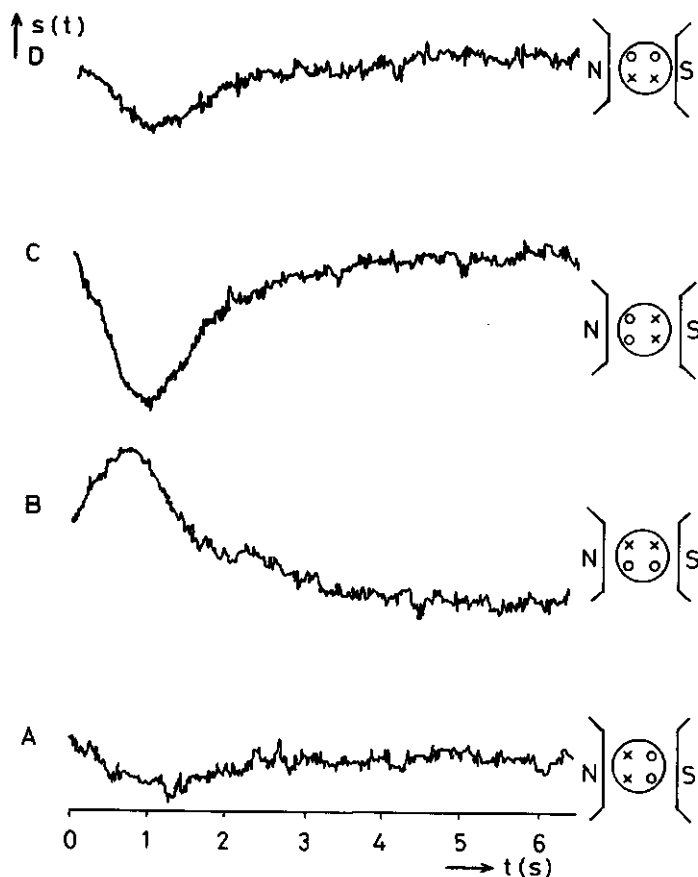


Fig. 9 Experimental NMR signals  $S(t)$  of flowing water vs. time as obtained by the  $\pi$  pulse method as a function of the position in the local natural gradient in the magnetic field. N and S denote the poles of the electro-magnet, x are the flowing water containing capillaries, whereas o are capillaries with stationary water. No external field gradient has been used.

Differences observed in this situation probably are due to inhomogeneities in the  $B_1$ -field distribution.

#### 4.5.1.2 Effect of $T_1$ and $T_2$ relaxation.

Up to now calibration curves of  $\bar{v}$  vs.  $t_{\max}^{-1}$  have been shown for water with  $T_1, T_2 \geq 2.4$  s [8,10]. In Section 4.2.6 we have stated that the contribution  $E(t)$  (see eqns. 4.21) to the total NMR signal of flowing water introduces a  $T_2$  dependence on the position of the

extremum at  $t=t_{\max}$ . In general,  $T_1$  and  $T_2$  of water in biological tissue are shortened with respect to the values for distilled water, and, in addition,  $T_1 \geq T_2$ . In Chapter 5 we demonstrate that  $T_1$  as well as  $T_2$  strongly depend on the diameter of the capillary containing flowing water. For this reason we have investigated the effect of  $T_1$  and  $T_2$  relaxation on the relationship  $\bar{v} = C/t_{\max}$ .

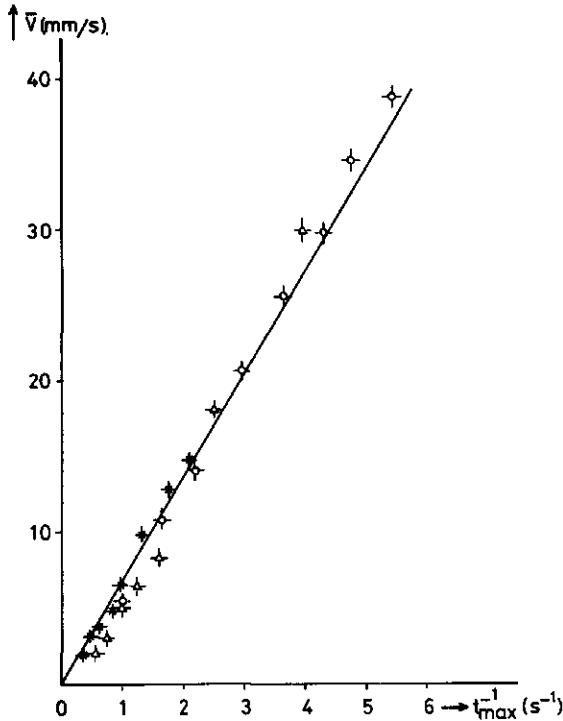


Fig. 10 Plot of  $\bar{v}$  vs.  $t_{\max}^{-1}$  for experimental NMR signals, obtained with the single capillary system.  $G = 7.6 \pm 1.5$  G/m,  $\tau = 1.6$  ms. The transmitter/receiver coil was of the Helmholtz type with length and diameter 10 mm. (O)  $T_1 = T_2 = 2.4$  s, (x)  $T_1 = 2.2$  s,  $T_2 = 1.6$  s, and ( $\Delta$ )  $T_1 = 1.5$  s,  $T_2 = 0.5$  s.

Fig. 10 presents the results of calibration-measurements using the single capillary system containing pure water, and two  $\text{Mn}^{2+}$  solutions with different  $T_1$  and  $T_2$  values, respectively. For both the samples with  $T_1 = T_2 = 2.4$  s, and that with  $T_1 = 2.2$  s,  $T_2 = 1.6$  s, we find that  $t_{\max}^{-1}$  indeed has a reciprocal relationship with  $\bar{v}$  as long as  $\bar{v} < \sim 25$  mm/s, with  $C = 6.7 \pm 0.3$  mm. At higher velocities deviations are found leading to higher values of  $t_{\max}$ . For the sample

with  $T_1 = 1.5$  s,  $T_2 = 0.5$  s the relation  $\bar{v}$  vs.  $t_{\max}^{-1}$  clearly deviates from a straight line.

With the aid of calculated NMR signals we were able to investigate the effects of  $T_1$  and  $T_2$  relaxation on the relationship  $\bar{v} = C/t_{\max}$ , separately. Due to the assumed rectangular r.f. field distribution our theoretical treatment is insensitive for variations in  $T_1$  (see Section 4.3.1.4). Therefore, the calculations have been performed with the computer program based on the formalism of Hemminga and de Jager [8]. The results of these calculations (see Fig. 11) show that as long as  $\bar{v} < 20$  mm/s the relationship  $\bar{v} = C/t_{\max}$  holds. For higher values of  $\bar{v}$ ,  $t_{\max}$  increases with respect to its value derived from

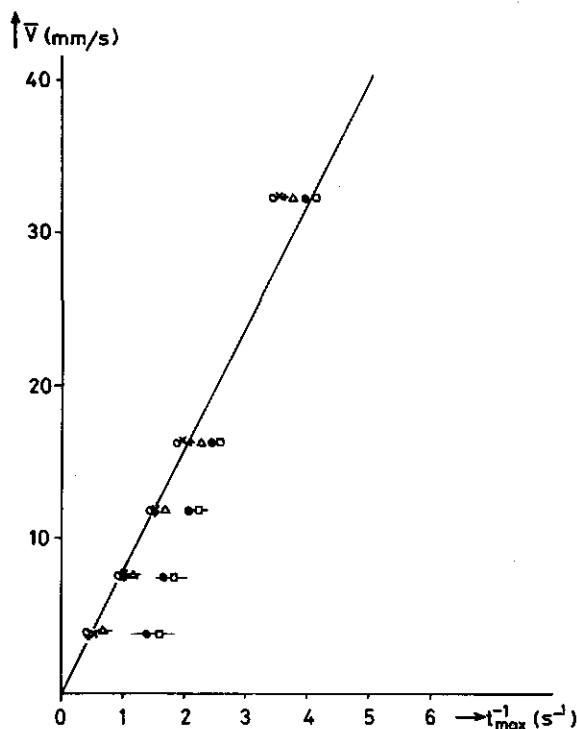


Fig. 11 Plot of  $\bar{v}$  vs.  $t_{\max}^{-1}$  for calculated NMR signals. Calculations have been performed based on the formalism as given in [8].  $G = 7.6$  G/m,  $\tau = 1.6$  ms. The shape of  $B_1(y)$  was chosen as in [8], based on the  $B_1(y)$  distribution of a solenoid with length 3.5 mm and diameter 13.2 mm (o)  $T_1 = T_2$ , (x)  $T_1 = 2.4$  s,  $T_2 = 1.2$  s, ( $\Delta$ )  $T_1 = 2.4$  s,  $T_2 = 0.5$  s, ( $\square$ )  $T_1 = 2.4$  s,  $T_2 = 0.2$  s, (+)  $T_1 = 1.0$ ,  $T_2 = 0.5$  s, (o)  $T_1 = 1.0$  s,  $T_2 = 0.2$  s.

this relationship. If  $T_1 = T_2$  there is no shift in the position of the maximum. The effect of decreasing  $T_2$  is to shift  $t_{\max}$  to lower values, whereas a decrease of  $T_1$  has the opposite effect. For the optimum conditions to obtain a linear relationship  $\bar{v} = C/t_{\max}$  in the range  $0 \leq \bar{v} < 30$  mm/s, we refer to Section 4.5.3.

#### 4.5.1.3 Effect of flow profile

In Section 4.2.5 we have argued that in general  $S_{\text{plug}}(t)$  and  $S_{\text{lam}}(t)$  have a different shape. Consequently, the value of  $C$  in the relationship  $\bar{v} = C/t_{\max}$  for a particular value of  $G$  depends on the actual flow profile. Theoretically this has been confirmed by comparing the results of the calculations for laminar flow as given in Fig. 11 with analogous plug flow calculations. In the case of laminar flow  $C$  was found to be  $7.8 \pm 0.1$  mm, whereas under identical experimental conditions  $C = 12.0 \pm 0.1$  mm for plug flow. So, calibration must be performed with a calibration system in which the behaviour of the flowing water is identical to that in plant stems. In Chapter 5 we will argue that flow of water in the vascular system in plant stems may be expected to be laminar, implying that the Reynolds number ( $Re$ ) in that system is  $< 2000$  [11]. For flow velocities up to 40 mm/s (the range of flow velocities that may be expected for water flow in plant stems [1])  $Re$  is predicted to be  $< 2000$  in cylindrical systems with a diameter  $\leq 0.05$  m. Thus, for the calibration systems used in our experiments  $Re$  is always  $\ll 2000$ , and therefore we may safely assume, that fluid flow in these calibration systems is laminar. Flow profiles in plant vessels are discussed in Chapter 5.

#### 4.5.2 Determination of $T_2$ and volume flowrate

##### 4.5.2.1 Effect of $T_1$

In Section 4.2.7 we have shown that the spin-spin relaxation time  $T_2$  of the flowing fluid can be found from the slope of a plot of  $\ln[\partial(S(t_{\max}) \cdot t_{\max})/\partial t_{\max}]$  vs.  $t_{\max}$  (see eqn. 4.29).

In Figure 12 we show plots of  $S_{\text{lam}}(t_{\max}) \cdot t_{\max}$  vs.  $t_{\max}$  derived from the experimental NMR curves of flowing water which have been used to obtain Fig. 10, with a)  $T_1 = T_2 = 2.4$  s, b)  $T_1 = 2.2$  s,



$T_2 = 1.6$  s and c)  $T_1 = 1.5$  s,  $T_2 = 0.5$  s, respectively. From the slope of curve a) plotted vs.  $t_{\max}$  we have calculated - via eqn. 4.29 - a value of  $T_2$  of  $2.6 \pm 0.3$  s, whereas from the slope of curve b)  $T_2 = 1.2 \pm 0.2$  s was derived. The slope of curve c) is partly negative and therefore it was not possible to calculate a  $T_2$  value via eqn. 4.2. It seems that the deviation of the  $T_2$  value found with this method from the actual value of  $T_2$  increases both with decreasing  $T_2$  and with increasing  $T_1/T_2$  ratio. To investigate the effect of  $T_1$  on the determination of  $T_2$  according to this method, we have used the calculated flow curves from which Fig. 11 was obtained.

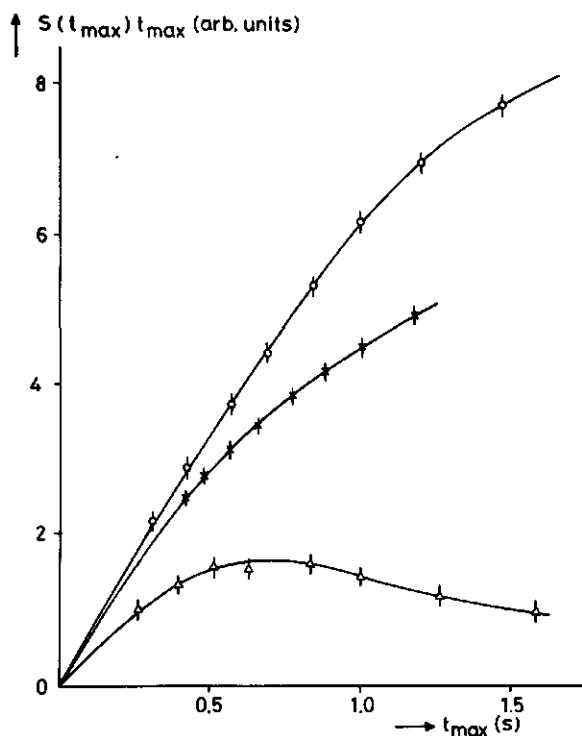


Fig. 12 Plot of  $S(t_{\max}) \cdot t_{\max}$  vs.  $t_{\max}$  from experimental NMR signals. Experimental conditions as given in Fig. 10. (O)  $T_1 = T_2 = 2.4$  s, (x)  $T_1 = 2.2$  s,  $T_2 = 1.6$  s, and ( $\Delta$ )  $T_1 = 1.5$  s,  $T_2 = 0.5$  s.

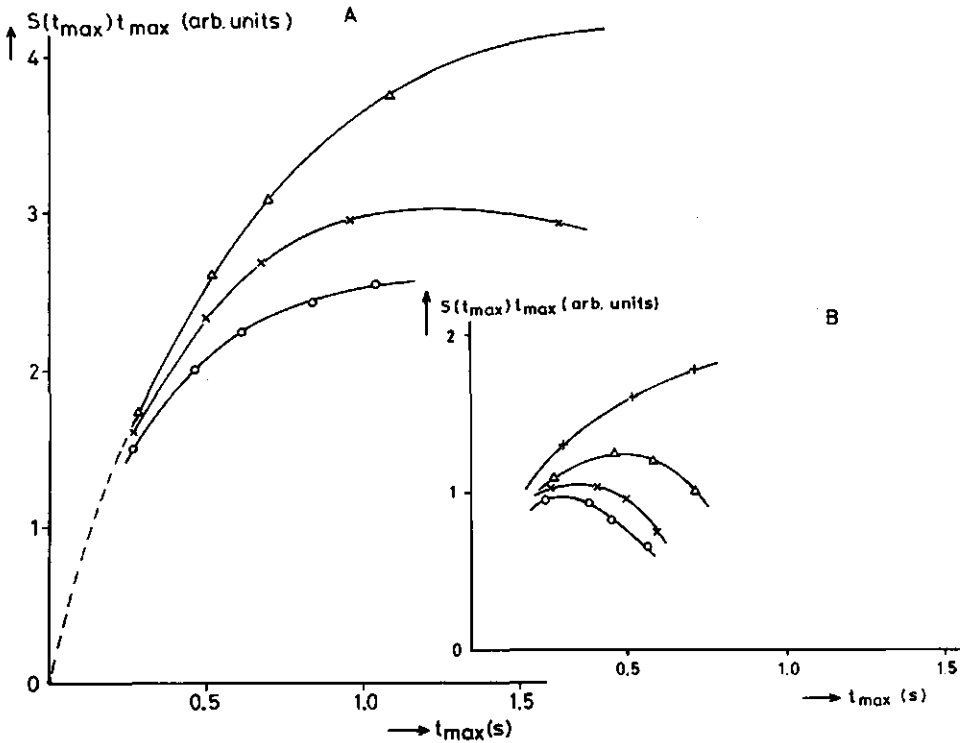


Fig. 13 Plot of  $S(t_{\max}) \cdot t_{\max}$  vs.  $t_{\max}$  from calculated NMR signals. Experimental conditions as given in Fig. 11. A).  $T_2 = 0.5$  s,  $T_1$  (in s) is 2.4 (O), 1.0 (x), 0.5 ( $\Delta$ ), B).  $T_2 = 0.2$  s,  $T_1$  (in s) is 2.4 (O), 1.0 (x), 0.5 ( $\Delta$ ) and 0.2 ( $\square$ ).

Table 4.1 Calculated values of  $T_2$  and  $D_1$  from calculated flow curves with different  $T_1$  and  $T_2$  values.  $T_2$  and  $D_1$  have been calculated via eqn. 4.29.

Actual value of $T_1$ (s)	Actual value of $T_2$ (s)	Calculated value of $T_2$ (s)	Calculated value of $D_1$ (arb. units)
2.4	2.4	$2.3 \pm 0.1$	$78 \pm 4$
2.4	1.2	$1.1 \pm 0.1$	$72 \pm 4$
2.4	0.5	$0.36 \pm 0.04$	$73 \pm 4$
1.0	0.5	$0.40 \pm 0.06$	$75 \pm 5$
0.5	0.5	$0.55 \pm 0.06$	$76 \pm 4$
2.4	0.2	- <sup>a</sup>	- <sup>a</sup>
1.0	0.2	- <sup>a</sup>	- <sup>a</sup>
0.5	0.2	- <sup>a</sup>	- <sup>a</sup>
0.2	0.2	$0.27 \pm 0.07$	$65 \pm 10$

<sup>a</sup> Due to the partly negative slope  $\partial(S_{\text{lam}}(t_{\max}) \cdot t_{\max})/\partial t_{\max}$  (see Fig. 13)  $T_2$  and  $D_1$  cannot be determined.

Fig. 13 demonstrates that the slope  $\partial(S_{\text{lam}}(t_{\text{max}}) \cdot t_{\text{max}}) / \partial t_{\text{max}}$  obtained from these theoretical curves strongly depends on the value of  $T_1$ , in agreement with the experimental results shown in Fig. 12. In Table 4.1  $T_2$  values are presented which were calculated via eqn. 4.29 from these theoretical curves. This Table also contains  $D_1$ , obtained by extrapolating the  $\ln [\partial(S_{\text{lam}}(t_{\text{max}}) \cdot t_{\text{max}}) / \partial t_{\text{max}}]$  vs.  $t_{\text{max}}$  curve to  $t_{\text{max}} = 0$ . Apart from a calibration constant this value of  $D_1$  is equal to  $V$ , the amount of flowing water, which was held constant for all calculated curves.

The results of Table 4.1 clearly show that the calculated  $T_2$  values strongly depend on  $T_1$ . If  $T_1 = T_2$  the calculated value of  $T_2$  corresponds with the actual  $T_2$  value. Increasing  $T_1$  results in an increased deviation of  $T_2$  (calc) from the actual  $T_2$  value. These results also show that  $D_1$  is much less sensitive to variations in  $T_1$  and  $T_2$  and indeed can be used to calibrate and determine the amount of flowing water  $V$ , which in turn can be used to calculate the volume flowrate (see eqn. 4.30).

The deviations of the calculated values of  $T_2$  from the actual values can be explained by considering the contribution  $E(t)$  of the fluid already in the coil at  $t = 0$  to the total signal:  $S_{\text{plug}}$  or  $S_{\text{lam}}$  (see Section 4.2.4, eqns. 4.21). In deriving eqn. 4.29 we have assumed that the contribution of  $E(t)$  is small and can be neglected. However, if  $E(t)$  cannot be neglected it introduces a distortion of the relationship as given in eqn. 4.29. One can rationalize that  $\bar{v} = C/t_{\text{max}}$  holds for  $S(t)$  as well as for  $E(t)$ . If this is so then it can be found from eqn. 4.21a that

$$\partial(E(t_{\text{max}}) \cdot t_{\text{max}}) / \partial t_{\text{max}} = (1 - t_{\text{max}}/T_2) \sin(\frac{1}{2}\gamma G \tau C) e^{-t_{\text{max}}/T_2}, \quad t_{\text{max}} \leq 1/\bar{v} \quad (4.34)$$

Thus,  $E(t)$  introduces a  $t_{\text{max}}$  dependence in the slope  $\partial(S_{\text{plug}}(t_{\text{max}}) \cdot t_{\text{max}}) / \partial t_{\text{max}}$ . A similar dependence is expected for laminar flow. The effect of  $T_1$  in our formalism can now be accounted for by the relative contribution of  $E(t)$  with respect to  $S(t)$ , the signal generated by the  $\frac{1}{2}\pi$  pulse region of our rectangular r.f. field distribution. In Fig. 12B we present the case where  $T_2 = 0.2$  s is held constant and  $T_1$  is varied from 0.2 to 2.4 s. It can be seen that the position at which the slope of the curve becomes zero shifts

towards  $t_{\max} = T_2$  as  $T_1$  increases. For higher values of  $t_{\max}$  this slope becomes increasingly negative. From eqn. 4.34 it follows that for  $E(t)$  the slope  $\partial(E(t_{\max}) \cdot t_{\max})/\partial t_{\max}$  becomes zero at  $t_{\max} = T_2$ , whereas for higher values of  $t_{\max}$  this slope is indeed predicted to be negative. From these observations we conclude that by increasing the  $T_1/T_2$  ratio, the relative contribution of  $E(t)$  increases. If this contribution is much larger than that of  $S(t)$  ( $T_1 \gg T_2$ ) we expect that  $T_2$  can be determined from a plot of  $\ln[S_{\text{plug}}(t_{\max})]$  or  $\ln[S_{\text{lam}}(t_{\max})]$  vs.  $t_{\max}$  (eqn. 4.21). Indeed, from the theoretical curves with  $T_1 = 2.4$  s and  $T_2 = 0.2$  s the slope of  $\ln[S_{\text{lam}}(t_{\max})]$  vs.  $t_{\max}$  yields  $T_2(\text{calc.}) = 0.28 \pm 0.03$  s and  $D_1 = 88 \pm 4$ . On the other hand, such a plot for the curves with  $T_1 = T_2 = 0.2$  s yields  $T_2(\text{calc.}) = 0.72 \pm 0.03$  s and  $D_1 = 66 \pm 4$  and thus is much less satisfactory. These observations support our conclusion mentioned above.

In determining  $T_2$  and  $V$  via  $S(t_{\max})$  we have taken for granted that the nuclei of the flowing fluid have experienced the static magnetic field  $B_0$  long enough to have attained Boltzmann equilibrium before entering the transmitter/receiver coil. However, experimentally this condition is not always met. Suppose we have a fluid with spin-lattice relaxation time  $T_1$ . The time in which the magnetization attains equilibrium is about  $5 \times T_1$ . Let  $d$  be the diameter of the pole face of the electromagnet, and let the transmitter/receiver coil be positioned in the center of the magnet. Now the magnetization of the flowing fluid reaches equilibrium before entering the coil if  $v \leq (d/5T_1)$ . Experimentally we have  $d = 17.5$  cm, meaning that when  $T_1 = 2.4$  s for  $v \gtrsim 7$  mm/s the observed NMR signal does not reach its maximum possible height, but is attenuated by  $T_1$ . This is clearly observed in Figs. 7 and 8, where the calculated curves (B) and (C) are higher than the experimental curves, due to this  $T_1$  effect. In the calculated curves of Figs. 7 and 8 this effect has been neglected.

If  $T_1$  is a known parameter, corrections can be made to the experimental signal height  $S(t)$  using [12]

$$S_0(t) = S(t) \{1 - \exp(-d/2vT_1)\}^{-1} \quad (4.35)$$

where  $S_0(t)$  is the signal at equilibrium magnetization.

#### 4.5.2.2 Off-resonance signal of stationary water.

In Section 4.4 it has been stated that all flow measurements have been performed on-resonance. Under this condition no signal is observed from water with  $v = 0$  (see Figs. 7 and 8). Indeed, using our model systems filled with tap water no signal has been observed from stationary water surrounding the capillaries. However, by making the stationary water fraction inhomogeneous, for instance by using paper tissue or glass beads, it has been observed that this fraction may sometimes give rise to an additional signal, even when the system is on-resonance. This additional signal decays exponentially with a decay time approximately equal to  $T_2$  of the stationary water. Obviously, this signal will introduce errors in  $S(t_{\max})$  and thus in the determination of  $T_2$  and  $V$  of non-stationary water. In plant stems the stationary water fraction can also be considered as an inhomogeneous system and the same additional signals may be expected.

In Fig. 14 the height  $H_0$  of the signal observed from stationary water at  $t = 0$  is presented as a function of the off-resonance frequency  $\omega_c$ ,  $G$ , and  $\tau$ , for the single capillary system with a paper tissue-water system as stationary fraction, where  $\omega_c = \omega_0 - \gamma B_z$ . To obtain the stationary fraction, the outer tube of the single capillary system was filled with an undefined amount of papertissue and with water.

From this Figure it can be seen that  $H_0 = 0$  at  $\omega_c = 0$ . This is valid when the  $B_1$  field and the inhomogeneities in the sample are symmetric with respect to the middle of the r.f. coil. If this symmetry is not present,  $H_0 = 0$  can shift to higher or lower values of  $\omega_c$ . For paper tissue-water systems  $H_0$  may shift up to 60 Hz from  $\omega_c = 0$ .

Theoretically the dependence of  $H_0$  on  $\omega_c$ ,  $G$  and  $\tau$  can be explained by the signal generated by the first pulse, as given in eqn. 4.11. For calculations of  $H_0(\omega_c, \tau, G)$  we have incorporated the off-resonance frequency  $\omega_c$  in this equation, followed by integrating the signal over  $\tau$ , as in the experimental situation. Under these conditions eqn. 4.12 for stationary water ( $v = 0$ ) is transformed into

$$H_0(\omega_c, \tau, G) = \int_0^{\tau} \int_0^{\infty} 2 \sin\{\pi \cdot \exp(-2y_0^2/L^2)\} \cdot \sin(\omega_c x) \cos(\gamma G y_0 x) dy_0 \cdot dx \quad (4.36)$$

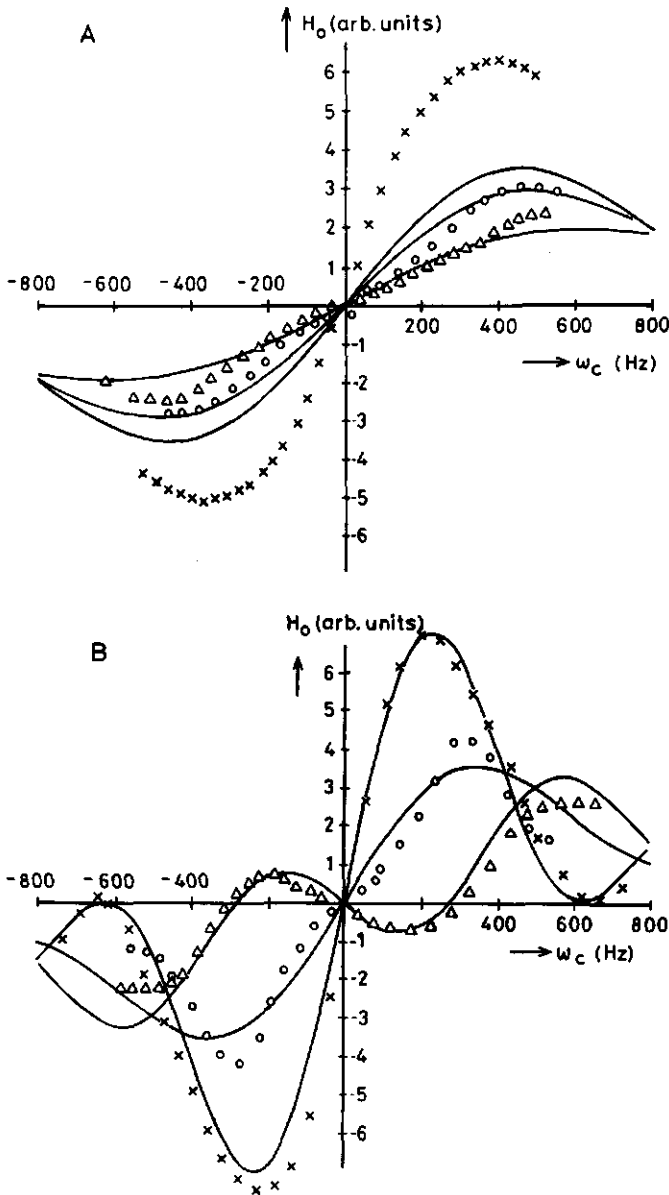


Fig. 14 Height  $H_0$  of the stationary water signal at  $t = 0$  as a function of the off-resonance frequency  $\omega_c$ . Experimental conditions:  $\tau$  (in ms) is 0.8 (A), 1.6 (B);  $G$  (calculated via eqn. 4.33) is (in G/m): 0.7 (x), 8.7 (o) and 15.6 ( $\Delta$ ). The continuous curves have been calculated using eqn. 4.36, with  $L = 7.2$  mm. The vertical scale is given in arbitrary units, but the scale factor is the same in (A) and (B).

By replacing the integral over  $y_0$  by an integral over  $y_0/L$  it can be shown that the cosine-term depends on the product of  $G \times L$ . Thus,  $G$  and  $L$  are strongly coupled and cannot be determined separately from these calculations. Therefore, the continuous curves in Fig. 14 have been calculated by using  $L = 7.2$  mm, taken as being that length of a sample for which the height of the FID becomes insensitive for increasing sample length. The values of  $G$  have been calculated from eqn. 4.33, again using  $L = 7.2$  mm. The shape of the calculated curves is in reasonable agreement with the experimental data. It is clear that experimental data such as given in Fig. 14 can be utilized to determine  $G$  for a particular value of  $L$ .

The dependence of  $H_0$  on  $w_c$  can be used to lock the magnetic field  $B_0$  on the frequency of the rotating frame, particularly at  $\tau = 0.8$  ms, where the shape of  $H_0$  becomes much less sensitive for variations in  $G$ .

#### 4.5.3 Optimum experimental conditions

The optimum conditions to determine  $\bar{v}$  are those where the linear relationship  $\bar{v} = C/t_{\max}$  is valid. This is true whenever  $T_2 \geq \frac{1}{2}T_1$  (see Section 4.5.1.2). Under this condition  $\bar{v}$  can be determined without the need to know the value of  $T_2$ . On the other hand, when  $T_1/T_2 > 2$  and  $T_2 < \sim 1$  s, the calibration curve  $\bar{v}$  vs.  $t_{\max}^{-1}$  strongly depends on the value of the ratio  $T_1/T_2$  and on the value of  $T_2$  (see Fig. 11). Then,  $\bar{v}$  starts to deviate appreciably from  $C/t_{\max}$  and  $\bar{v}$  can only reliably be determined if  $T_1$  and  $T_2$  are known. In addition,  $T_2$  and  $V$  can be reliably determined from the NMR flow curves if  $T_2 \cong T_1$  or  $T_2 \ll T_1$  (see Section 4.5.2.1). From these observations we conclude that  $T_2 \cong T_1$  represents the optimum condition to carry out our experiments.

Unfortunately, in most biological tissues  $T_1 > T_2$ . However, the pulse sequence used to measure flow can be considered as a Carr-Purcell-Meiboom-Gill (CPMG) pulse sequence (Section 3.3.1) minus the first  $\frac{1}{2}\pi$  pulse. Thus, it can be expected that the flowing water curves contain the same value of  $T_2$  as measured using the CPMG pulse sequence. In biological tissue a number of mechanisms may contribute to the spin-spin relaxation (Chapter 3). For the CPMG sequence it is known that the measured  $T_2$  depends on  $\tau$ , the time between the  $\pi$

pulse, if (i) exchange occurs between different sites (see Section 3.2.4 and [13-16]), or (ii) the material is nonhomogeneous, by exhibiting either a distribution of slow diffusion correlation times [17], or inhomogeneity in magnetic susceptibility [18,19], or both. In every case the observed  $T_2$  increases as  $\tau$  decreases, and for very small  $\tau$   $T_2$  approaches the corresponding  $T_1$  value. Due to the inhomogeneous character of the plant xylem vessel system, it may be expected that the same holds for water in that vessels.

Experimentally we have used a pulse spacing  $\tau = 1.6$  ms. Reducing  $\tau$  in order to increase the effective  $T_2$  has two effects on the NMR signal of flowing water: (i)  $t_{\max}$  shifts to higher values and the maximum broadens, resulting in an increase in the lower limit of  $\bar{v}$  that can be measured, and (ii) the signal-to-noise ratio decreases due to the fact that the signal is measured by integrating the  $x'$  component of the magnetization over the time  $\tau$ . The first effect (i) can be compensated by increasing  $G$ . As long as  $G \times \tau$  is held constant the shape of the NMR signal is hardly affected at otherwise constant experimental conditions. The latter effect (ii) is removed by summing over more pulses (see Section 4.4) so that the time between the data points remains unchanged. If we assume that a reduction of  $\tau$  by a factor 10 (160  $\mu$ s) is required to obtain  $T_2 > \frac{1}{2}T_1$ ,  $G$  has to be increased by a factor 10 (50 - 150 G/m) in order to maintain the same shape of the signal as compared with  $\tau = 1.6$  ms. Then, a total of 40960 pulses must be given for the same time-interval and each data point then contains the integrated signal resulting from 160  $\pi$  pulses. These conditions are within experimental reach. The net gain is an effective longer  $T_2$ , resulting in an increase of  $S(t_{\max})$ . In addition, reduction of  $\tau$  has the advantage that the sign of the signal of stationary water becomes insensitive to the magnitude of  $G$  (see Fig. 14), meaning that this signal becomes more suitable as a lock signal to stabilize the magnetic field.

#### 4.6 CONCLUSIONS

The results reported here, demonstrate that the  $\pi$  pulse method can be used to measure the mean linear flow velocity of water in plant stems. Although  $\bar{v}$  can in principle be determined from the initial slope of  $S(t)$ , this slope depends on the amount of flowing



water and amplifier gain; it is also possible that an additional off-resonance signal of the stationary water affects this slope. Therefore, determination of  $\bar{v}$  from  $t_{\max}^{-1}$  is preferable for practical applications. If  $T_2 \geq \frac{1}{2}T_1$ ,  $\bar{v}$  can be determined without a priori knowledge of the value of  $T_1$  and  $T_2$ .

In addition,  $T_2$ ,  $V$ , and consequently the volume flowrate can be determined from the NMR signals. When  $T_1 \gg T_2$ ,  $T_2$  may be determined from the slope of a plot of  $S(t_{\max})$  vs.  $t_{\max}$  in a semilog fashion. For  $T_1 > T_2$  or  $T_1 \cong T_2$  the slope of a semilog plot of  $\partial[S(t_{\max}) \cdot t_{\max}] / \partial t_{\max}$  vs.  $t_{\max}$  yields  $T_2$ . For  $T_1 > T_2$  only that part of the plot with  $t_{\max} < T_2$  is used, whereas for  $T_1 \cong T_2$  the plot is valid for  $t_{\max} < 3T_2$ . The determination of  $V$  is much less sensitive to the value of  $T_1$  and  $T_2$ , and can be found from the intercept at  $t = 0$  from semilog plots of  $S(t_{\max})$  vs.  $t_{\max}$  as well as  $\partial[S(t_{\max}) \cdot t_{\max}] / \partial t_{\max}$  vs.  $t_{\max}$ .

The lower limit of  $\bar{v}$  that can be measured strongly depends on the absolute value of  $T_1$  and  $T_2$  and on the amount of flowing water  $V$ . A typical combination of values for tapwater flowing through a single capillary, surrounded by a 100-fold excess of stationary water, is  $\bar{v} \geq 0.5$  mm/s,  $V \geq 5$   $\mu$ l. For plants, we have measured values as low as 3 mm/s for  $\bar{v}$  and  $V \sim 5$   $\mu$ l.

#### 4.7 ACKNOWLEDGEMENT

We are indebted to Mr. J. Reinders, who has performed part of the experiments and calculations, and to Dr. M.A. Hemminga and Mr. P.A. de Jager for many helpful and stimulating discussions and for making available their computer program for simulating the NMR flow curves.

This work was in part supported by the Netherlands Organization for the Advancement of Pure Research (ZWO).

## REFERENCES

1. B. Slavik, "Methods of Studying Plant Water Relations", Chapter 4 (Springer-Verlag, Berlin, 1974).
2. D.W. Jones and T.F. Child, in "Advances in Magnetic Resonance" (J.S. Waugh, ed.), Vol. 8 (Academic Press, New York, 1976).
3. K.J. Packer, *Mol. Phys.* 17 (1969), 355.
4. K.J. Packer, C. Rees and D.J. Tomlinson, *Advan. Mol. Relaxation Processes* 3 (1972), 119.
5. J.R. Singer, *J. Phys. E: Sci. Instrum.* 11 (1978), 281.
6. A.N. Garroway, *J. Phys. D: Appl. Phys.* 7 (1974), L 159.
7. K. Fukuda and A. Hirai, *J. Phys. Soc. Japan* 47 (1979), 1999.
8. M.A. Hemminga and P.A. de Jager, *J. Magn. Reson.* 37 (1980), 1.
9. M.A. Hemminga, P.A. de Jager, A. Sonneveld, *J. Magn. Reson.* 27 (1977), 359.
10. P.A. de Jager, M.A. Hemminga, A. Sonneveld, *Rev. Sci. Instr.* 49 (1978), 1217.
11. A.T.J. Hayward, "Flowmeters, a Basic Guide and Sourcebook for Users", Chapter 1 (The MacMillan Press, London, 1979).
12. L.R. Hirschel, L.F. Libelo, *J. Appl. Phys.* 32 (1961), 1404.
13. J. Jen, *J. Magn. Reson.* 30 (1978), 111.
14. V.D. Fedotov, F.G. Miftakhutdinova, Sh.F. Murtazin, *Biofizika* 14 (1969), 873 (*Biophysics (USSR)* 14 (1969), 918).
15. H.S. Gutowsky, R.L. Vold, E.J. Wells, *J. Chem. Phys.* 43 (1965), 4107.
16. A. Allerhand, E. Thiele, *J. Chem. Phys.* 45 (1966), 902.
17. J.G. Diegel, M.M. Pintar, *Biophys. J.* 15 (1975), 855.
18. R. Cooke, R. Wien, *Biophys. J.* 11 (1971), 1002.
19. B.M. Fung, T.W. McGaughy, *J. Magn. Reson.* 43 (1981), 316.

## 5 FLOW MEASUREMENTS IN PLANTS

### 5.1 INTRODUCTION

In biology and agriculture knowledge of the water balance of plants is of crucial interest. Uptake, transport, storage and transpiration of water contribute to this balance and are strongly mutually coupled: transport in the xylem vessels is determined by soil- and leaf water potential [1,2,3]. The latter is controlled by stomatal transpiration, which in its turn is governed by plant water status,  $\text{CO}_2$  concentration, light intensity and air humidity [1,2]. Thus, sap stream velocity can be used as an indicator of the transpirational process [4]. Several indirect methods have been used to study water transport by measuring the mean linear flow velocity  $\bar{v}$  or the volume flowrate  $Q$  of the sap stream [5]. None of these methods detects the movement of water itself, however, and many are invasive.

In Chapter 4 we have discussed a pulsed nuclear magnetic resonance (NMR) method, based on a pulse sequence of equidistant  $\pi$  pulses and a linear magnetic field gradient [6], based on measurements in glass capillary model systems, as applied to measure flow in plant stems. In that Chapter we have shown that these flow measurements yield the mean linear flow velocity  $\bar{v}$ , the volume flowrate  $Q$ , the effective cross-section  $A$ , and the spin-spin relaxation time  $T_2$  of the flowing water, without observing the stationary fluid, such as the non-flowing water in the tissue of the plant stem.

In this Chapter we report the use of this pulsed NMR method to measure linear flow velocity of water in the vascular system of stem segments. These measurements have been successful in stem segments of Cucurbitaceae (e.g. cucumber, gherkin, pumpkin) and tomato. On the other hand, for several other plant stem segments no signal of flowing water could be detected under our experimental conditions. These observations can be explained on the basis of the relationship between the radius  $R$  of the transport vessels and  $T_2$  of the water in these vessels.

NMR flow measurements in intact cucumber and gherkin plants have been published recently in a preliminary note [7]. In an earlier communication [8] (see Chapter 7) the effect of plant water content on the  $^1\text{H}$   $T_2$  of the tissue water has been discussed. Here we report simultaneous NMR flow and  $T_2$  measurements in an intact gherkin plant in response to light intensity and soil water potential, showing that the combination of these two pulsed NMR measurements provide a new approach in studying important parts of the plant water balance.

## 5.2 EXPERIMENTAL

### 5.2.1 NMR flow measurements

For the experiments we have used a 15 MHz  $^1\text{H}$  pulsed NMR spectrometer as described in Chapter 4. The linear flow velocity  $\bar{v}$  was obtained from the position  $t_{\text{max}}$  of the extremum in the NMR signal (see Chapter 4), via the relationship  $\bar{v} = C/t_{\text{max}}$ . Calibration of  $C$  has been carried out with a single capillary system, consisting of a capillary containing the flowing water, with a diameter of 1.25 mm, fitted into a glass tube with an inner diameter of 7 mm, filled with stationary water ( $T_2 = 2.4$  s). At the particular value of the linear field gradient  $G$  (in the direction of the flow) used in the experiments,  $C$  was found to be  $6.3 \pm 0.3$  mm. The flowing water used for calibration was tapwater with relaxation times  $T_1 = T_2 = 2.4$  s.

A total of 4096  $\pi$  pulses has been given, with pulse period  $\tau = 1.6$  ms. Each datapoint represents the integrated signal over 25.6 ms (16 pulses). The results reported in this Chapter have been obtained from single trace experiments. The magnetic field  $B_0$  was adjusted to such a value that no signal was observed from stationary water. This was obtained on-resonance (no beats in the free induction decay) or slightly off-resonance, depending on the sample measured (see Section 4.5.2.2). For intact plants it is difficult to control this condition, because the condition  $v=0$  cannot easily be realized, in contrast to the situation in cut stem-segments. In practice the NMR signal of flowing water at  $t=0$  is made coincident with zero signal level for model systems. Further experimental conditions are as given in Section 4.4.

A Helmholtz-type r.f. coil has been used with  $L=1.1$  and  $R=0.5$  cm. In order to perform measurements on intact plants, the r.f. coil was

constructed in such a way that it can be opened and folded around the plant stem (see Fig. 1). The quality factor of this coil was ~50.

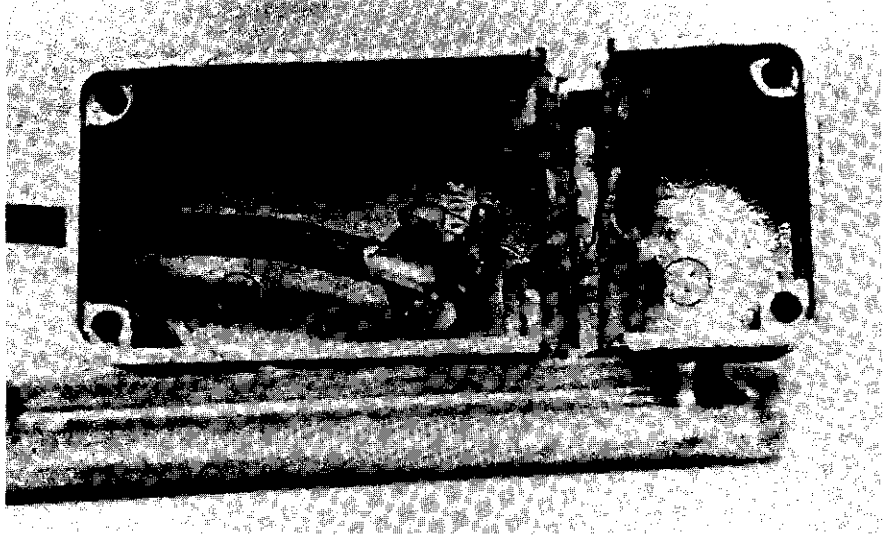


Fig. 1 Helmholtz-type r.f. coil used for measurements in intact plant stems.  $L=1.1$  cm,  $R=0.5$  cm. The coil has been constructed in such a way that it can be opened and folded around the plant stem.

### 5.2.2 NMR $T_2$ measurements

The spin-spin relaxation time  $T_2$  was measured by the Carr-Purcell-Meiboom-Gill (CPMG) method [9], carried out with the same 15 MHz  $^1\text{H}$  pulsed spectrometer and r.f. coil as used for the flow measurements. Because of the internal inhomogeneity and the size of the samples a time-dependent baseline ("baseline drift") must be expected [10,11]. A first order correction for this phenomenon was made by the following pulse sequence:

$$\frac{1}{2}\pi_x - \tau - (-\pi_y - 2\tau)_n - W (=5T_1) - \frac{1}{2}\pi_x - \tau - (-\pi_y - 2\tau)_n,$$

where  $W$  is the waiting time between the two CPMG sequences. By subtracting the two CPMG-decays, the effect of missettings in the  $\pi$  pulses was diminished. The CPMG  $T_2$  decay was measured by sampling the height of the echoes. The time  $2\tau$  was chosen to be 1.6 ms. The echo decays have been analysed by use of a non-linear least squares fit [12] on a total of 1960 datapoints. Due to a considerable scatter in echo heights

the first datapoints of the decay have been rejected before analysing. Invariably, a non-exponential  $T_2$  decay was observed. Least squares fitting has been performed to a maximum of four exponentials. The best solution contains the sum of three exponentials. We define a mean effective relaxation rate  $\bar{R}_2$ ,

$$\bar{R}_2 = \sum_{i=1}^3 P_i T_{2i}^{-1} \quad (5.1)$$

where  $P_i$  denotes the fraction of component  $i$ .  $T_2$  measurements as well as flow measurements were made at probe temperature (29°C).

### 5.2.3 Plant material

Freshly excised stem segments have been used with length 10 cm. Flow velocity has been varied by hydrostatic pressure. Plant stem segment and tube have been connected using an universal variable-bore connector (Omnifit Inc., Cedarhurst, New York).

## 5.3 RESULTS AND DISCUSSION

### 5.3.1 Stem segments

Fig. 2 represents NMR signals of water flowing through an excised segment of cucumber stem (*Cucumis sativus* L.) The mean linear flow velocity  $\bar{v}$  was varied by hydrostatic pressure. In Chapter 4 we have shown for glass capillary systems that  $\bar{v}$  can be determined from the time  $t_{\max}$  at which the NMR signal  $S(t)$  reaches a maximum, by the relationship

$$\bar{v} = C/t_{\max} \quad (5.2)$$

This relationship is valid whenever  $T_2 \geq \frac{1}{2}T_1$  (see Section 4.5.1.2). In Fig. 3 the signals of Fig. 2 have been represented as a plot of the volume flowrate  $Q$  (as volumetrically determined) vs.  $t_{\max}^{-1}$ . Assuming that the effective cross-section is independent of volume flowrate (or hydrostatic pressure) we conclude from Fig. 3 that eqn. 5.2. is equally valid for this stem segment.

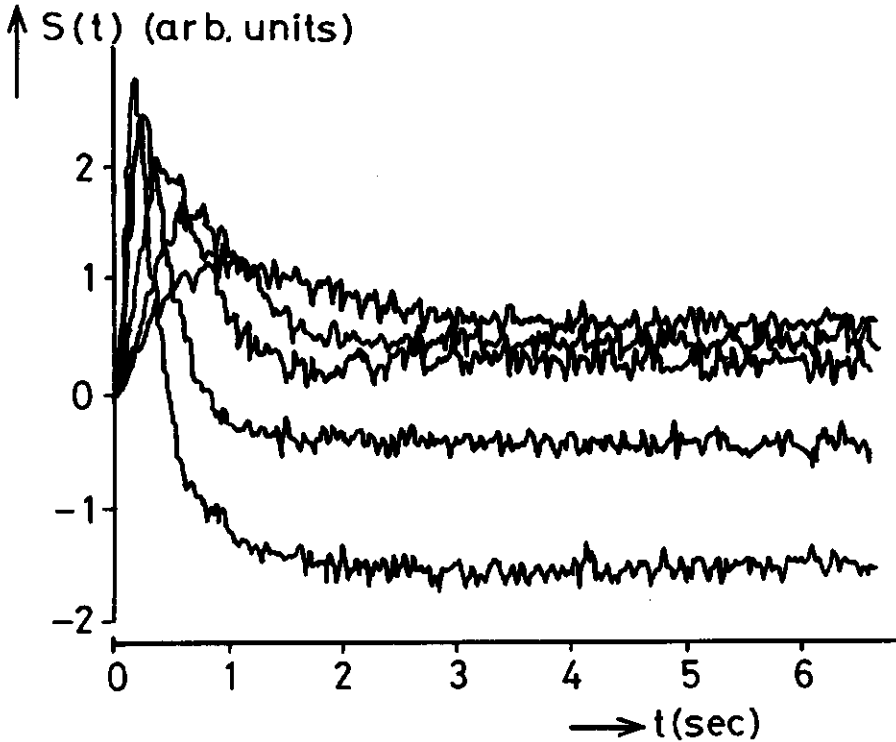


Fig. 2 Single scan 15 MHz NMR signal height  $S(t)$  vs. time for water flowing through an excised stem segment of a cucumber plant. Water flow was varied by hydrostatic pressure. A total of 4096  $\pi$  pulses has been applied, with pulse period  $\tau=1.6$  ms. Each point of the curve represents the integrated signal over 25.6 ms (16 pulses).  $G=13 \pm 3$  G/m.

The validity of eqn. 5.2. for this stem segment suggests that  $T_2 \geq \frac{1}{2}T_1$ . As stated in Chapter 4 when this condition holds,  $T_2$  can be determined from the NMR signals as given in Fig. 2 by plotting  $\partial[S(t_{\max}) \cdot t_{\max}] / \partial t_{\max}$  vs.  $t_{\max}$  in a semilog fashion. For  $T_1 > T_2$  only that part of the plot with  $t_{\max} < T_2$  is used, whereas for  $T_1 \cong T_2$  the plot is valid for  $t_{\max} < 3T_2$ . The slope of such a plot for the curves of Fig. 1 yields  $T_2 = 250 \pm 20$  ms for  $t_{\max} < 400$  ms.

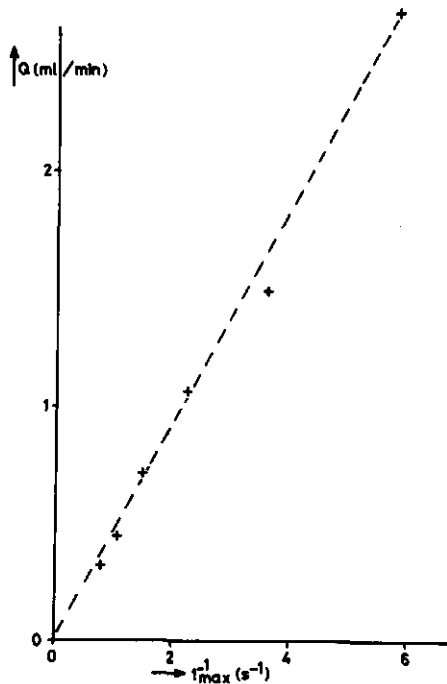


Fig. 3 Plot of volume flowrate  $Q$  (ml/min) vs.  $t_{\max}^{-1}$  for the measurements shown in Fig. 1

If  $T_1 = T_2$  the decay time obtained from a semilog plot of  $S(t_{\max})$  vs.  $t_{\max}$  must be  $>3T_2$  (see Section 4.5.2.1). From the results of Fig. 2  $S(t_{\max})$  vs.  $t_{\max}$  yielded a decay time that equals  $610 \pm 40$  ms, only slightly less than three times the previously calculated  $T_2$  of  $250 \pm 20$  ms. When  $T_1 = 2T_2$  the decay time obtained from a semilog plot of  $S(t_{\max})$  vs.  $t_{\max}$  is about  $2T_2$ . Here, we have the intermediate case, in agreement with the validity of eqn. 5.2. (As noted in Section 4.5.2.1, the shape of the plot  $S(t_{\max}) \cdot t_{\max}$  vs.  $t_{\max}$  strongly depends on the value of the ratio  $T_1/T_2$ , and thus the position at which the slope of this plot becomes zero. For  $T_1 \gg T_2$  this position equals the time  $T_2$ , whereas for decreasing  $T_1/T_2$  ratio this position shifts to higher values of  $t_{\max}$ . For the curves of Fig. 2 the position at which the slope of  $S(t_{\max}) \cdot t_{\max}$  vs.  $t_{\max}$  becomes zero was found to be  $\sim 1.0$  s, equal to  $4T_2$  (calculated). This is an additional argument that  $T_2 > \frac{1}{2}T_1$  for this stem segment (see Fig. 13, Chapter 4.)).



Similar signals of flowing water have been observed in stem segments of gherkin (*Cucumis sativus*), pumpkin (*Cucurbita ficifolia*) and tomato (*Lycopersicon esculentum*). On the other hand, for several other plant stem segments, such as papyrus (*Cyperus alternifolius*), sweet pepper (*Capsicum annum* L.) and seedlings of tomato, cucumber and bean (*Phaseolus vulgaris*), we have tried to obtain NMR signals of flowing water without success, although for some of these the amount of flowing water (volumetrically determined) should have been sufficient for observation with our NMR apparatus.

These negative results may be explained by (i) a flow velocity which is too low, and/or (ii) the value of  $T_2$  (and  $T_1$ ) of the flowing water. Concerning (i): the lower limit of  $\bar{v}$  that can be measured strongly depends on the absolute value of  $T_1$  and  $T_2$  and on the amount of flowing water (Chapter 4). Calculations of the linear flow velocity from the measured volume flowrate based on estimates of the amount of xylem vessels and their diameters revealed that in e.g. the papyrus stem segments the flow velocity was in the range 2-10 mm/s. At the value of the linear field gradient used these flow velocities can be measured if  $T_2 > \sim 175$  ms. At lower values of  $T_2$  the NMR signal broadens and the maximum disappears. The resulting signal then can be easily misintepreted as being an off-resonance signal of the stationary water (see Section 4.5.2.2.), which has about the same shape. Knowledge of the values of  $T_2$  and  $T_1$  of water in these xylem vessels is therefore of prime importance.

As stated above, in the cucumber segment of Fig. 2 we found  $T_2 = 250 \pm 20$  ms. The flowing water fraction used was tap water ( $T_2 \cong 2.4$  s). Thus, the  $T_2$  of water flowing through the xylem vessels is considerably shortened. This behaviour can be explained in a first approach in terms of a two-state fast-exchange model [13,14]. In the framework of this model we may assign one state to water in a xylem vessel ("free" water) with  $T_{2f} \cong 2.4$  s and water, bound on the vessel wall, with  $T_{2b} \ll 1$  ms to the second state. There is fast exchange of water between both states. The observed single relaxation rate  $R_2$  is the weighted average of the separate relaxation rates of the two exchanging fractions:

$$R_2 (\cong T_2^{-1}) = T_{2f}^{-1} + P_b (T_{2b}^{-1} - T_{2f}^{-1}) \quad (5.3)$$

where  $P_b$  is the mole fraction of the "bound" water. Let us assume that we have a thin layer of bound water with thickness  $dr$  and  $dr \ll R$ , the radius of the vessel. Now eqn. 5.3 can be written in terms of  $dr$  and  $R$ , resulting in

$$R_2 = T_{2f}^{-1} + \frac{2dr}{R} (T_{2b}^{-1} - T_{2f}^{-1}) \quad (5.4)$$

showing that  $R_2$  is expected to be inversely proportional with  $R$ . This approach can be extended for intermediate and slow exchange by use of the equations as given by [15] (see also Chapter 3, eqns. 3.16 - 3.20). Comparable results have been obtained by Brownstein and Tarr [16,17]. Using a simple theory based on a diffusion equation using the bulk diffusivity of water, these authors have derived expressions for the relaxation times  $T_1$  as well as  $T_2$  in biological cells in terms of the diffusion constant  $D$  and the dimensions of the cell [17]. These authors have shown that multiexponential decay of the spin relaxation can arise as a consequence of an eigenvalue problem associated with the size and shape of the cell. Brownstein and Tarr have also considered relaxation in a cell with cylindrical geometry [17]. We will use their results to explain relaxation in an xylem vessel. In deriving their equations for relaxation Brownstein and Tarr have neglected relaxation of free water (i.e.  $T_{2f}^{-1} = 0$ ). The surface of the cylinder is considered as an active surface, with surfacelike sinks for the magnetization. At the active surface the sink strength density  $M$  (in cm/s) is assumed to be constant. (Note that  $M$  has the same dimension as flow. Indeed, flow can also be incorporated in their integral theorem [16], resulting in the equations as derived by Hemminga et al [18] for the difference decay curve of stationary and flowing water). Now, the longest decay time  $T_0$  of the spin relaxation is given by

$$T_0 = R^2 / D\eta_0^2 \quad (5.5a)$$

where  $\eta_0$  is the positive root of

$$\eta_0 J_1(\eta_0) / J_0(\eta_0) = MR/D \quad (5.5b)$$

and  $J_0$ ,  $J_1$  are cylindrical Bessel functions.

Brownstein en Tarr discernes three qualitatively different regions of behaviour according to the value of  $MR/D$ :

(i)  $MR/D \ll 1$ . This can be considered as the region that corresponds to the fast-exchange limit of discrete multiphase analysis [13-15]. The corresponding decay time is given by  $T_0 = V/Ms$  where  $V$  is the sample volume and  $s$  is the active surface area. For a cylinder this results in

$$T_0 = \frac{1}{2}R/M \quad (5.6)$$

For  $T_2$ , here again we find that  $R_2 (=T_0^{-1})$  is inversely proportional to  $R$ , in agreement with eqn. 5.4.

(ii)  $1 < MR/D < 10$ . This is called the "intermediate-diffusion" region.  
 (iii)  $10 \ll MR/D$ . This can be called the "slow diffusion" region. In this region the decay time for a cylinder is given by

$$T_0 = R^2/D(0.75 \pi)^2 \quad (5.7)$$

showing a quadratic relationship between  $R$  and  $T_0$ .

In Fig. 4 we have plotted  $T_0$  vs.  $R$  as a function of  $M$ . We have assumed  $D = 2.5 \times 10^{-5}$  cm<sup>2</sup>/s. When  $MR/D \gg 10$  than the relationship between  $T_0$  and  $R$  becomes independent on  $M$  (eqn. 5.7).

Values of  $M$  in biological tissue have not yet been published in literature. However, the diffusional formalism developed by Brownstein en Tarr can be used to explain the spin relaxation behaviour of water protons in rat gastrectonemius muscle [17] and of water in milled Northern white-cedar wood chips [19]. In the first case the relaxation behaviour has been explained with an annular cylinder geometry. The outer surface at  $R=a$  has a sink strength density  $M$  that satisfies  $Ma/D=4.9$ . With the data given in [17] we were able to calculate  $a$ , resulting in  $a=14.7$   $\mu$ m. With  $D=2.5 \times 10^{-5}$  cm<sup>2</sup>/s this yields  $M=8 \times 10^{-2}$  cm/s. In the study of wood chips [19] Brownstein used a surface layer of macromolecules containing water of thickness  $dr \approx 0.26$   $\mu$ m and  $T_2 \approx 1$  ms to explain the relaxation behaviour of water adsorbed on wood [19]. Sinks in the bulk volume have been neglected.

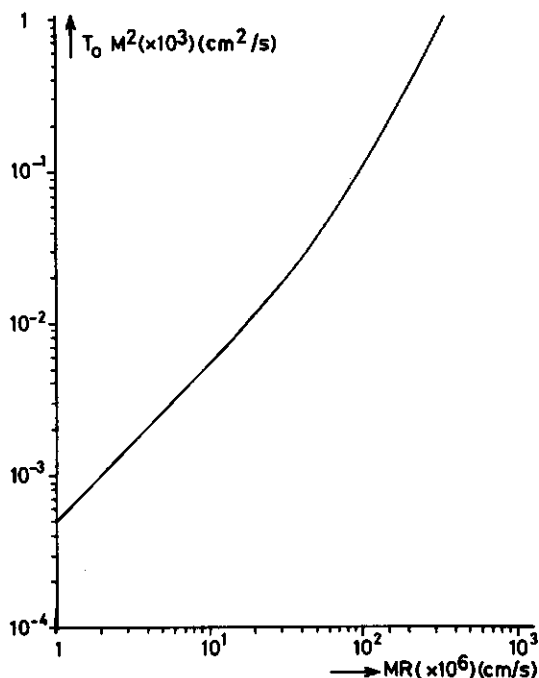


Fig. 4 Calculated plot of  $T_0 M^2$  vs.  $MR$ , based on eqns. 5.5. The diffusion constant  $D=2.5 \times 10^{-5}$   $\text{cm}^2/\text{s}$ .

The initial slope of the observed relaxation decay curve is governed by  $1/T_2$  of this surface layer. In [17] it has been explained that this initial decay is related by  $M$  via  $T_2=V/Ms$ , where  $V$  is the sample volume and  $s$  is the active surface area. For a planar geometry with thickness  $dr$  this results in  $T_2=dr/M$ . For the surface layer of wood [19] this results in  $M < 2.6 \times 10^{-2}$   $\text{cm/s}$ , only a factor three lower than the value of  $M$  in rat muscle. Taking the lowest value of  $M$  calculated above ( $2.6 \times 10^{-2}$   $\text{cm/s}$  in wood) as a representative of xylem vessel walls, we can make an estimation of the xylem vessel radius of the cucumber stem segment of Fig. 2. Using our experimental value of  $T_2=250 \pm 20$   $\text{ms}$  for such a segment we find  $R \approx 60$   $\mu\text{m}$  from Fig. 4. In cucumber stems xylem vessels have been found with  $R \leq 300$   $\mu\text{m}$ .

With the results of Fig. 4 we can also explain why no signal of flowing water has been observed in stem segments of a number of other plants. In these plant stems the maximum vessel radius  $R$  is less than that found in cucumber, and, according to Fig. 4,  $T_2$  is expected

to be  $< 250$  ms. Thus, observation of flowing water NMR signals strongly depends on the maximum vessel radius.

In the diffusional formalism presented by Brownstein and Tarr [16,17] the expected dependence of  $T_2$  on the pulse period  $\tau$  (see Section 4.5.3) is not incorporated. As stated in Section 4.5.3 we expect an increase of the measured  $T_2$  upon a decrease of  $\tau$  allowing the measurement of flow in smaller xylem vessels.

### 5.3.2 Intact plants

Fig. 5 A1 and A2 represent flowing water signals in an intact cucumber stem before and after adding water to the soil, respectively, resulting in an increase of  $\bar{v}=9.9 \pm 0.8$  mm/s to  $14.3 \pm 1.1$  mm/s.

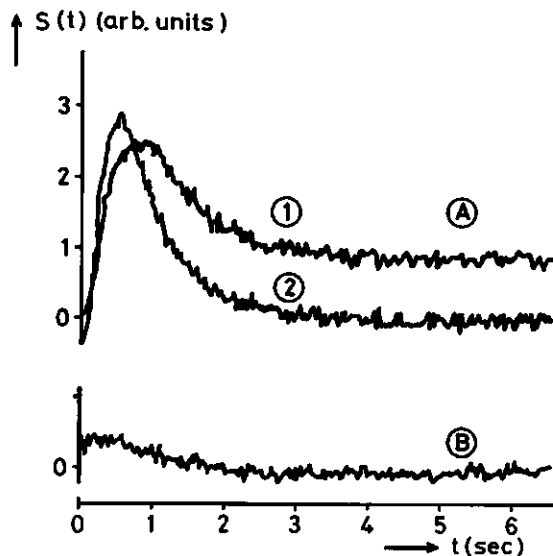


Fig. 5 15 MHz NMR signal (single trace) amplitude  $S(t)$  vs. time for water flowing in the stem of an intact cucumber. (A) Signal of flowing water under illumination with two Na-lamps at 1 m mean distance from the leaves, zero air velocity, ambient temp.  $23^\circ\text{C}$ .

1.  $\bar{v}=9.9$  mm/s 2.  $\bar{v}=14.3$  mm/s

before and after adding water to the soil, respectively.

(B) Signal 15 min. after cut-off of flow closely below stem section in the r.f. coil; all other conditions identical to those in A.

The performance of the method can be judged in Fig. 5B, where, after interrupting the supply of water to the measuring region of the stem, no signal is observed, not even of the stationary tissue-water (90% of the total water content).

The effect of soil water potential and illumination intensity on  $\bar{v}$  and the average spin-spin relaxation rate  $R_2$  have been measured in the stem of an intact gherkin plant. (Figs. 6 and 8). Fig. 6 shows that the soil containing plant is well watered at the moment of measurement: a further addition of water does not alter the mean linear flow velocity, in contrast to what is observed in Fig. 5.

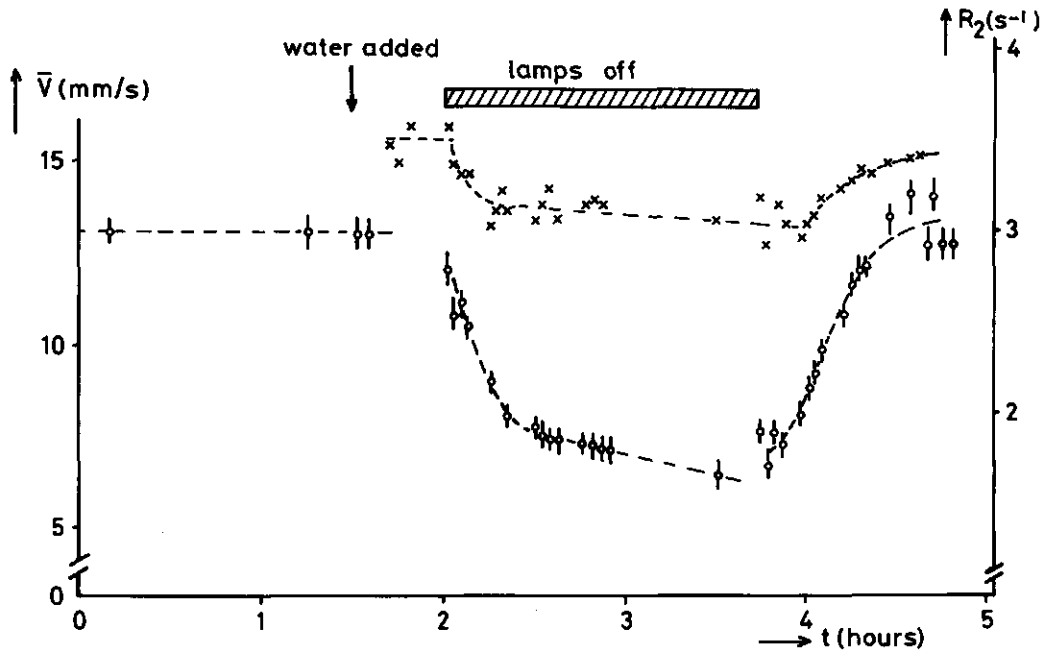


Fig. 6  $^1\text{H}$  pulsed NMR measurements of mean linear flow velocity  $\bar{v}$  (o) and spin-spin relaxation rate  $R_2$  (x) in an intact gherkin plant, measured in the stem at  $\sim 0.5$  m above soil surface. The response of the NMR signals to the addition of water and to variation in light intensity is shown.

Under this condition it is expected that the flow velocity is controlled by the transpiration process in the leaves. Under the actual environmental conditions (relative air humidity: 44 %, temperature:

24.5 °C, illumination with two 400 W Na-lamps at about 2 m above the soil surface, zero air velocity) a maximum flow velocity of 13 mm/s was found. After turning off the lamps,  $\bar{v}$  decreases from 13 mm/s to  $\sim 7$  mm/s over a period of  $\sim 30$  min. At longer times after turning off the lamps the decrease in  $\bar{v}$  is much slower. The decrease in  $\bar{v}$  when the light is turned off is due to closure of stomata. As suggested by Slatyer [1] at that moment the upward movement of water to the leaves, due to a mild water stress in the leaves and stem, begins to exceed the rate of loss due to transpiration, and the differences in water potential between soil, root and leaf decreases (see also [22]). Consequently, the leaf apoplast and cells and stem cells are rehydrated. This is reflected in the decrease of  $R_2$ . As shown in [8]  $R_2 (\equiv 1/T_2)$  is inversely proportional with water content. The slight change in  $R_2$  at turning off illumination indicates that the cells in the stem were only mildly dehydrated during the light-on period due to the well watered soil (low resistance between soil and root). After turning on illumination,  $\bar{v}$  and  $R_2$  increase again and approach about the same value as at the beginning of the experiment. ( $\bar{v} \approx 13.0$ -13.5 mm/s,  $R_2 \approx 3.4$  s $^{-1}$ ). The response of  $T_2$  on dark/light periods has been measured in the stem of an intact papyrus plant (Fig. 7). This is in fair agreement with the data of Fig. 6.

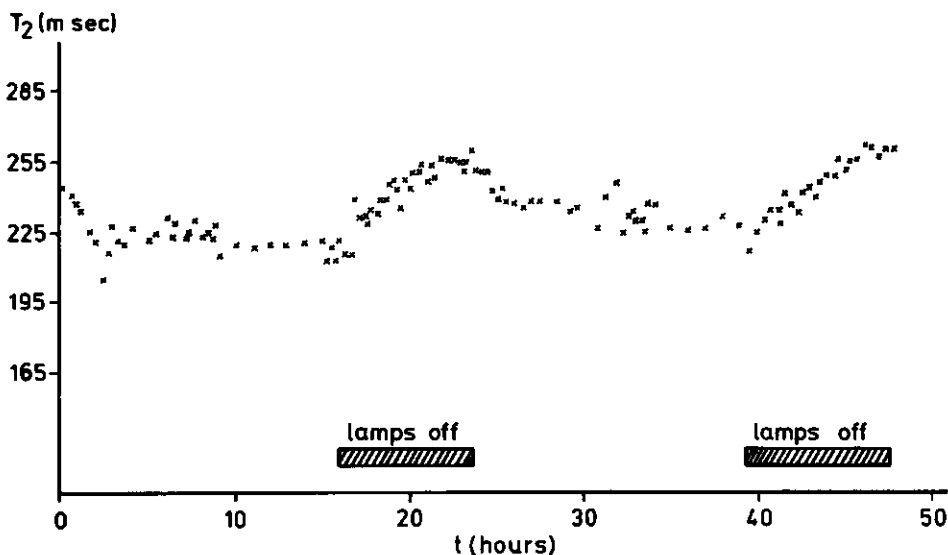


Fig. 7 Change in  $^1\text{H}$  spin-spin relaxation time  $T_2$  (taken as the time at which the value of the decay curve reaches  $1/e$  of its initial value) measured in the stem of an intact papyrus plant in response to light/dark periods.

The effect of a decrease in soil water potential on  $\bar{v}$  and  $R_2$  in the stem of the same gherkin plant is represented in Fig. 8. At  $t=0$  we have measured the flow velocity, two days after adding water to the soil. The measured value,  $\bar{v}=17.5 \pm 1.2$  mm/s, is higher than that measured in Fig. 6. This may be due to an increase in relative air humidity and temperature (65 % and 26 °C, resp.) with respect to the conditions for Fig. 6 (44 % and 24.5 °C, resp.). The following day the flow velocity was found to be decreased considerably, in agreement with the dry soil and the wilting of the lowest leaf on the stem.

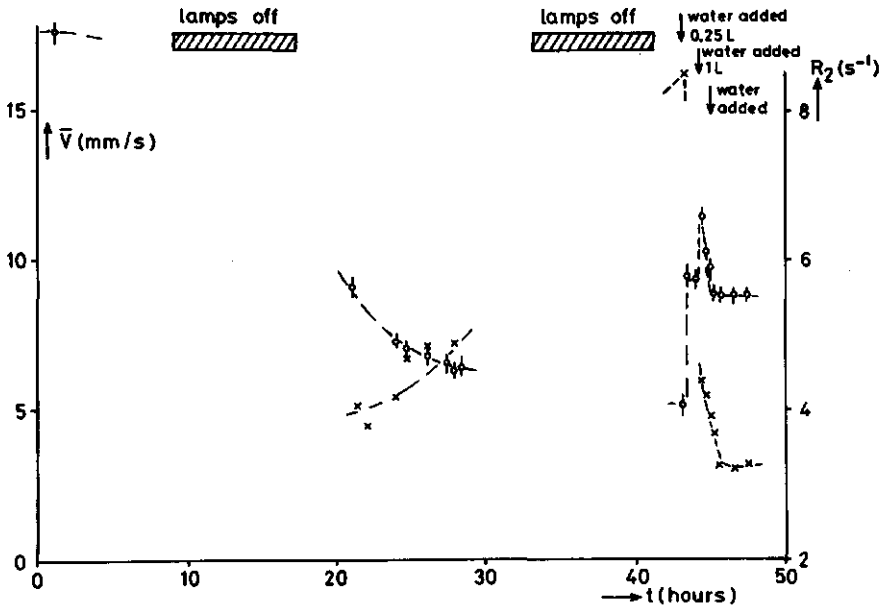


Fig. 8.  $^1\text{H}$  pulsed NMR measurements of  $\bar{v}$  (o) and  $R_2$  (x) in the stem of an intact gherkin, demonstrating the effect of dehydration and rehydration of the soil. For further experimental conditions: see text.

Under these conditions the soil resistance increases and root water potential decreases, resulting in dehydration of cells in root, stem and leaves [1]. This is reflected by the increasing value of  $R_2$ . At the beginning of the third day  $R_2=8.5$  s $^{-1}$ , twice the value measured at the beginning of the second day, indicating a strong decrease in hydration of the stem tissue. The flow velocity is also decreased



with respect to that on the second day. Now, adding a small amount of water to the soil results in an increase in  $\bar{v}$  (measured after a few seconds after the water gift) and a decrease in  $R_2$ . Adding a second and third larger amount of water to the soil,  $\bar{v}$  increases shortly, and next reaches a steady state at  $\bar{v}=8.9 \pm 0.6$  mm/s. This value is lower than the maximum value  $\bar{v}=17.5 \pm 1.2$  mm/s (at  $t=0$ ), reached under the same environmental conditions. The supply of water results in a decrease of  $R_2$ , which after about three hours reaches approximately the same value ( $R_2 \approx 3.2$  s $^{-1}$ ) as measured under well watered conditions with lamps off (see Fig. 6).

As has been stated in Chapter 4, the amount of flowing water (in mm $^3$ ) is found by either plotting  $\partial[S(t_{\max}) \cdot t_{\max}] / \partial t_{\max}$  vs.  $t_{\max}$  or  $S(t_{\max})$  vs.  $t_{\max}$  and extrapolating to  $t_{\max}=0$ . In Fig. 9 the data of Fig. 6 are shown in the form of a semilog plot of  $S(t_{\max})$  vs.  $t_{\max}$ .

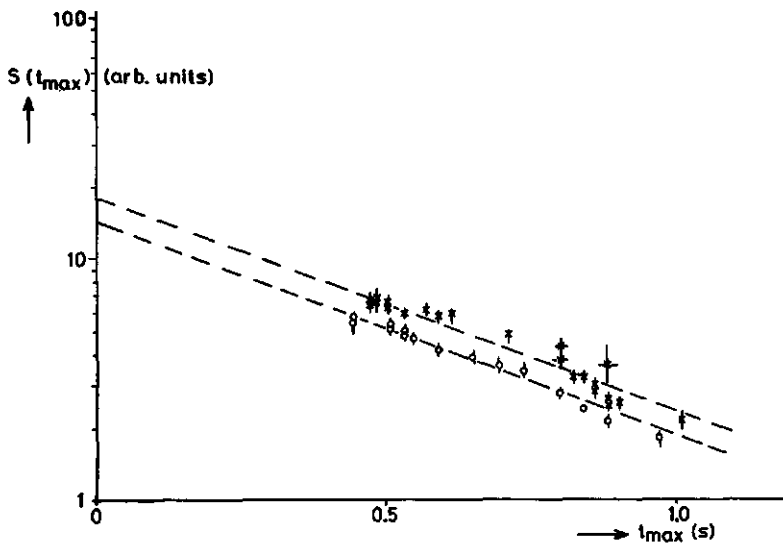


Fig. 9 Semilog plot of  $S(t_{\max})$  vs.  $t_{\max}$  of the data of Fig. 6. (x) data obtained in the dark period following the turning off of lamps, (o) data obtained in the light period, after turning lamps on.

Fig. 9 clearly shows that there is a systematic deviation between the values of  $S(t_{\max})$  during a dark period following the turning off of lamps and those during a light period, after turning lamps

on. Though  $t_{\max}$ , and thus  $\bar{v}$ , is within the same time interval for these two processes,  $S(t_{\max})$  measured with lamps off is systematically higher than with lamps on. Extrapolation of the two curves to  $t_{\max}=0$  reveals that the slope of the curves are approximately the same, but  $S(0)$ , and thus the volume flowrate, is significantly larger for the "lamps off" plot than for the "lamps on" plot. (Fig. 9). These findings indicate a hysteresis effect in the volume flowrate between light and dark periods and vice versa.

A plot of  $S(t_{\max})$  vs.  $t_{\max}$  for the processes of dehydration and rehydration of the soil, obtained by using the data of Fig. 8, is presented in Fig. 10. This Figure demonstrates that now systematic deviations between the data points obtained by rehydration and dehydration are absent, in contrast to the phenomenon in Fig. 9.

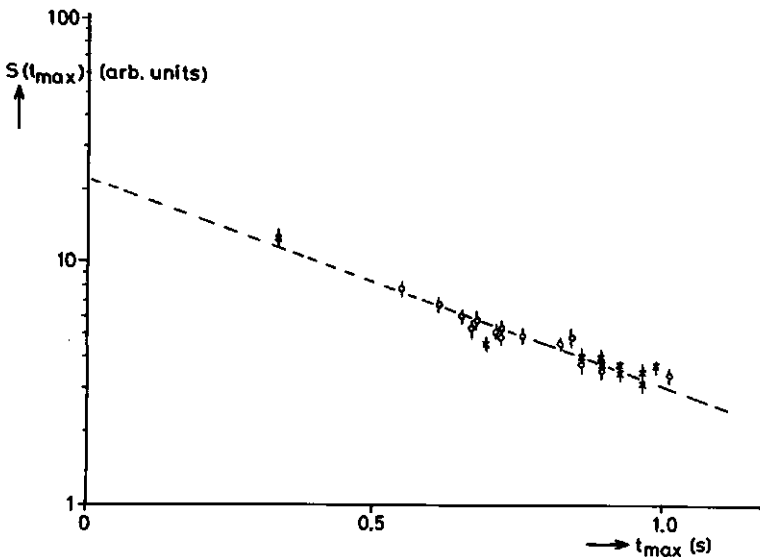


Fig. 10 Semilog plot of  $S(t_{\max})$  vs.  $t_{\max}$  of the data of Fig. 8. (x) data obtained by dehydration of the soil, (o) data obtained after rehydration of the soil.

It is noticeable that  $S(0)$  obtained by extrapolating the curve of Fig. 10 to  $t_{\max}=0$  is significantly higher than  $S(0)$  obtained from the "lamps off" curve in Fig. 9. It is noteworthy, that the data of Fig. 9 and 10 have been obtained using the same gherkin plant, whereas the time elapsed between measuring the data of Fig. 6 and 9

on one hand and the data of Fig. 8 and 10 on the other hand is one week. This may be the reason for the difference in  $S(0)$  in Fig. 9 and 10. Nevertheless, the slopes of the plots of Fig. 9 and 10 are equal within experimental error: Fig. 9 yields a decay time of  $480 \pm 55$  ms, whereas the decay time obtained from Fig. 10 results in  $520 \pm 50$  ms.

Concerning the reliability of the values of  $\bar{v}$  in Fig. 6 and 8, we note first that calibration has been performed with a glass capillary model system (Section 5.2.1) in which the flow may be considered as laminar (Section 4.5.1.3). From measurements in isolated strands of xylem vessels of *Plantago major* L it has been demonstrated that the flow in these vessels is essentially laminar, even though flow resistance in these vessels strongly depends on the wall surface sculptures [20]. The Reynolds numbers ( $Re \approx 10^6 Q/R$ , where  $Q$  is the volume flowrate and  $R$  the vessel radius) found in xylem vessels of *Plantago major* L are in the range  $\sim 0.1$  [20]. From our measurements in cucumber and gherkin the maximum value of  $Re$  calculated from volume flowrate and estimated vessel radius is  $\sim 1$ . Also the effect of surface sculptures and curvature of the vessels may not be expected to introduce turbulence [21]. As has been stated elsewhere the shape of the NMR signals of flowing water are sensitive for the flow profile (Chapter 4 and [6]). Indeed, the shape of the NMR signals support the expected laminar flow pattern.

Secondly, flow velocity has been obtained via eqn. 5.2, which is valid if  $T_2 \geq \frac{1}{2}T_1$  (Section 4.5.1.2). In Section 5.3.1 we have shown that this conditions holds for a particular cucumber stem segment, which is not necessarily true for every type of plant stem. In Chapter 6 we show by comparing flow measurements with the NMR- and balance method that in a particular cucumber plant eqn. 5.2 results in systematic deviations, indicating that for water in the xylem vessels of that plant stem  $T_2 < \frac{1}{2}T_1$  (see Section 4.5.1.2). This has been verified by the NMR results alone. We cannot exclude that for the measurement of the flowing water in the xylem vessel of the gherkin plant presented in Figs. 5-10 also  $T_2 < \frac{1}{2}T_1$ . When  $T_2 < \frac{1}{2}T_1$  the values of  $\bar{v}$  must be corrected according to the data presented in Fig. 11 of Chapter 4. This has no effect on the shape of the response of  $\bar{v}$  on variations in light intensity and soil water potential, however (see also Figs. 6 and 8 of this Section).

#### 5.4 CONCLUSIONS

The value of  $T_2$  of the water in the xylem vessels in plant stems has been shown to be strongly related to the vessel radius  $R$ . Depending on this value, linear flow velocities ( $\bar{v}$ ) and volume flowrates ( $Q$ ) have been obtained by use of the NMR  $\pi$  pulse method.

Combination of these flow measurements with NMR  $T_2$  measurements of the stationary water (tissue water surrounding the vascular system) in intact plants turn out to be useful to study the effects of environmental factors, such as light intensity, temperature, relative air humidity, soil water potential, etc., on  $\bar{v}$ ,  $Q$  and, via  $T_2$ , water content of xylem water and tissue water, respectively. The effects of changes in these environmental conditions on  $\bar{v}$ ,  $Q$  and  $T_2$  can be measured with a time resolution of a few seconds. This study demonstrates that these pulsed NMR measurements provide a new approach to the study of parts of the plant water balance.

#### 5.5 ACKNOWLEDGEMENT

We are indebted to Dr. A.P.M. den Nijs of the Institute of Plant Breeding (IVT) for his kindly gift of the plant material.

## REFERENCES

1. R.O. Slatyer, "Plant-Water Relationships" (Academic Press, New York, 1967).
2. A.H. Fitter, R.K.M. Hay, "Environmental Physiology of Plants" (Academic Press, London, 1981).
3. C.R. Black, *J. Exp. Bot.* 30 (1979), 235.
4. J. Balek, O. Pavlik, *J. Hydrol.* 34 (1977), 193.
5. B. Slavik, "Methods of Studying Plant Water Relations", *Ecological Studies*, Vol. 9, p.p. 223-235 (Springer-Verlag, Berlin, 1974).
6. M.A. Hemminga, P.A. de Jager, *J. Magn. Reson.* 37 (1980), 1.
7. H. Van As, T.J. Schaafsma, *Bull. Magn. Reson.* 2 (1981), 359.
8. H. Van As, W.P.A. van Vliet, T.J. Schaafsma, *Biophys. J.* 32 (1980), 1043 (Chapter 7 this Thesis).
9. S. Meiboom, D. Gill, *Rev. Sci. Instrum.* 29 (1958), 688.
10. R.L. Vold, R.R. Vold, H.E. Simon, *J. Magn. Reson.* 11 (1973), 283.
11. D.G. Hughes, G. Lindblom, *J. Magn. Reson.* 26 (1977), 469.
12. S.W. Provencher, *J. Chem. Phys.* 64 (1976), 2772.
13. R. Cooke, R. Wien, *Biophys. J.* 11 (1971), 1002.
14. J.R. Zimmerman, W.E. Brittin, *J. Phys. Chem.* 61 (1957), 1328.
15. J. Jen, *J. Magn. Reson.* 30 (1978), 111.
16. K.R. Brownstein, C.E. Tarr, *J. Magn. Reson.* 26 (1977), 17.
17. K.R. Brownstein, C.E. Tarr, *Phys. Rev. A.* 19 (1979), 2446.
18. M.A. Hemminga, P.A. de Jager, A. Sonneveld, *J. Magn. Reson.* 27 (1977), 359.
19. K.R. Brownstein, *J. Magn. Reson.* 40 (1980), 505.
20. A.A. Jeje, M.H. Zimmermann, *J. Exp. Bot.* 30 (1979), 817.
21. T.R.F. Nonweiler, in "Transport in Plants. I: Phloem Transport", *Encyclopedia of Plant Physiology*, New Series, Volume I (M.H. Zimmermann, J.A. Milburn, eds.), p.p. 474-477 (Springer-Verlag, Berlin, 1974).
22. M.H. Behboudian, Thesis, Wageningen, The Netherlands, 1977.

## 6 COMPARISON OF FLOW MEASUREMENTS WITH NMR, HEAT PULSE AND BALANCE METHOD

### 6.1 INTRODUCTION

In Chapters 4 and 5 of this Thesis we have presented the use of a non-destructive pulsed NMR method to measure flowing water in plant stem xylem. In Chapter 4 we have shown that this NMR method, based on a pulse sequence of equidistant  $\pi$  pulses in combination with a linear magnetic field gradient in the direction of flow [1], is very suitable to determine the mean linear flow velocity  $\bar{v}$ , as well as the volume flowrate  $Q$ , the effective cross-sectional area  $A$  available for flow, and the spin-spin relaxation time  $T_2$  of the flowing water. In Chapter 5 we reported the results of this method when applied to plant stem segments and intact plants. It has been observed that, using the experimental parameters, this method is successful when applied to plant stems with large diameter xylem vessels, due to the relationship between the vessel radius and  $T_2$  of water in these vessels (Chapter 5). In Chapter 4, however, we have pointed out that the observed value of  $T_2$  depends on the pulse period  $\tau$ . In fact, the effective  $T_2$  increases with decreasing  $\tau$ , thus allowing measurements in smaller diameter xylem vessels.

The combination of  $T_2$  measurements of stationary tissue water and flow measurements in a particular section of a plant stem has been shown to provide a new approach for the non-destructive analysis of important parts of the plant water balance, with a time resolution of a few (4-12) seconds (Chapter 5).

Up to here the NMR flow measurements in plants have been compared and calibrated with the results of measurements in glass capillary model systems. To avoid in-breeding, in this Chapter we compare the results of NMR flow measurements in the stem of an intact cucumber with those obtained by the weight balance method and the microscopically determined cross-sectional area of the xylem elements. A linear relationship between  $\bar{v}$  as measured with NMR and  $Q$  obtained by the balance method is shown. From the slope of  $\bar{v}(Q)$  the effective cross-sectional area  $A$  available for flow has been determined. The

cross-sectional area can also be determined from NMR measurements alone, and is shown to be in good agreement with the previous value of the slope of  $\bar{v}(Q)$ . In addition, the results of flow measurements with a heat pulse method [2] are compared with the results of the balance- and NMR method.

## 6.2 EXPERIMENTAL

### 6.2.1 NMR flow measurements

NMR flow measurements have been carried out by the pulse technique as described in Chapter 4 and [1]. For the experiments we have used a 15 MHz  $^1\text{H}$  pulsed NMR spectrometer as described in Chapter 4. The linear flow velocity  $\bar{v}$  was obtained via the relationship

$$\bar{v} = C/t_{\max} \quad (6.1)$$

where  $C$  is a calibration constant and  $t_{\max}$  the position of the extremum in the NMR signal (see Chapter 4). Calibration has been carried out as described in Chapter 5, using flowing and stationary water with  $T_1=T_2=2.4$  s. Calibration of  $C$  at the particular value of the linear field gradient  $G$  used in the experiments yields  $C=7.5 \pm 0.2$  mm. With the same capillary system used to calibrate  $C$  (see Chapter 5) at the particular value of  $G$  used here we have also calibrated the amount of flowing water  $V$  (in  $\text{mm}^3$ ) via  $S(0)$ , the height of the maximum at  $t_{\max}=0$ , obtained by plotting  $S(t_{\max})$  vs.  $t_{\max}$  and extrapolating to  $t_{\max}=0$  (Chapter 4). For the capillary system  $V$  has been calculated from the cross-sectional area  $A$  of the capillary and the effective length of the r.f. coil  $L_{\text{eff}}$  (defined as that length of a sample for which the height of the free induction decay becomes insensitive for increasing sample length) via  $V=A/L_{\text{eff}}$ . The volume flowrate in a plant is obtained from  $\bar{v}$  and  $V$  (as measured in that plant) via

$$Q = \bar{v} V/L_{\text{eff}} \quad (6.2)$$

whereas the cross-sectional area of the xylem vessels in a plant has been found by

$$A = V/L_{\text{eff}} \quad (6.3)$$

To prevent radio frequency interference from surrounding equipment (e.g. microcomputer, etc.) reaching the receiver through the plant (working as an aerial), the soil has been grounded via the NMR apparatus. In this way a considerable reduction of the noise level is obtained.

Other experimental conditions were the same as in Chapter 5.

### 6.2.2 Heat pulse flow measurements

Heat pulse flow measurements have been carried out with a thermoelectric method as described elsewhere [2]. Heat is applied locally to the stem during a few seconds. The heat flows into the stem in all directions. Part of the heat reaches the xylem vessels and is transported downstream with the moving water. Thus the temperature rise (measured by a pair of integrated circuit temperature sensors) will be higher downstream than it is upstream. Time of occurrence (b) and magnitude (c) of the maximum in the temperature between points upstream and downstream both depend on the flowrate. We have taken  $tg \alpha = c/b$  as a measure of flowrate. A sensor design has been used with a flat surface and a distance between heater and each of the two i.c.'s is 10 mm. The sensing element is mounted on one leg of a thermally isolating clip. The other leg of the clip bears a V groove for correct positioning of the sensor on the stem. To reach an optimum heat transfer between heater and flowing water, the sensor was positioned as near as possible at a xylem vessel bundle (This is easily accomplished in the case of a cucumber).

Duration of heating was 10 s, with a current of 0.5 A in a heating element with 0.5 ohm resistance, allowing a repetition time of about 4 min. at the observed flowrates. Other experimental conditions were the same as in [2].

### 6.2.3 Balance transpiration flowrate measurements

The transpiration rate of the pot plant has been measured by weighing on an electrical differential top balance (Mettler, type



PE-11 in combination with BE-13). The output of the balance was recorded on a strip chart recorder. The transpiration rate at a particular time was determined from the slope of the record at that time. To prevent evaporation of water from the soil in the pot, the soil surface was covered with aluminium foil.

#### 6.2.4 Cross-sectional area

Cross-sectional areas  $A$  of the flow conducting elements have been calculated from microscopic measurements assuming the vessels to be unobstructed capillaries. Measurements have been carried out in radial sections taken from those stem parts which were positioned in the NMR r.f. coil and in the heat pulse sensor.

#### 6.2.5 Plant material

Measurements have been carried out on an intact cucumber plant, potted in a plastic container, placed on the top balance. The plant was illuminated with two 400 W Na-lamps at about 2 m above soil surface. The NMR r.f. coil was situated on the plant stem at 0.75 m above the soil surface, whereas the heat pulse sensor was clamped on the stem at  $\sim 1.25$  m above the soil surface.

### 6.3 RESULTS

Figs. 1 and 2 presents respectively the mean linear flow velocity  $\bar{v}$  as measured with NMR and  $\tan \alpha$  as obtained by the heat pulse method, both plotted versus the volume flowrate  $Q_B$  measured with the weight balance and defined as the weight loss per unit time. In these Figures we will take  $Q_B$  as the reference. As has been shown in Chapter 5, flowrate and water content of the plant tissue are mutually coupled. However, deviations of  $Q_B$  from the true actual volume flowrate due to these variations in the water content have not been considered.

To obtain variations in  $\bar{v}$  and  $Q_B$  the illuminating Na-lamps have been switched off and on, warm water has been added to the soil and, at last, leaves have been cut off from the stem. In Fig. 1 as well as Fig. 2 we have indicated from which procedure the data points have been obtained. The response of  $\bar{v}$  as measured with NMR on each process has the same shape as that given in Chapter 5 (Figs. 6 and 8).

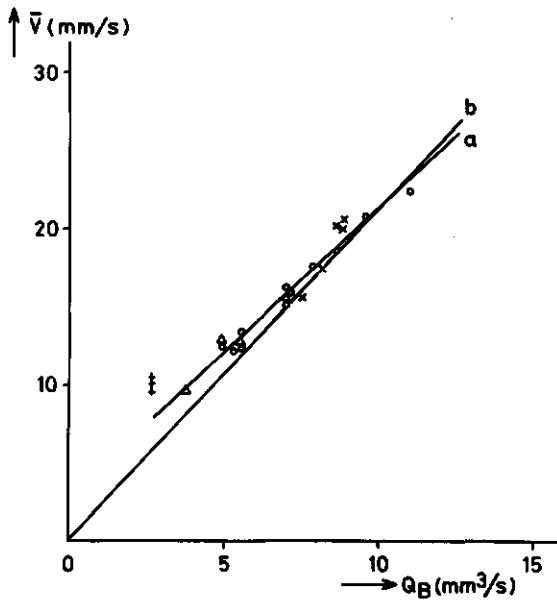


Fig. 1 Plot of  $\bar{v}$  as obtained by NMR method versus  $Q_B$  as measured with the balance method for an intact cucumber plant. For the explanation of curves a and b see text. The flow has been varied by: (o) lamps off, (x) lamps on again plus adding warm water, ( $\Delta$ ) lamps off again, and (+) cutting off leaves from plant stem.

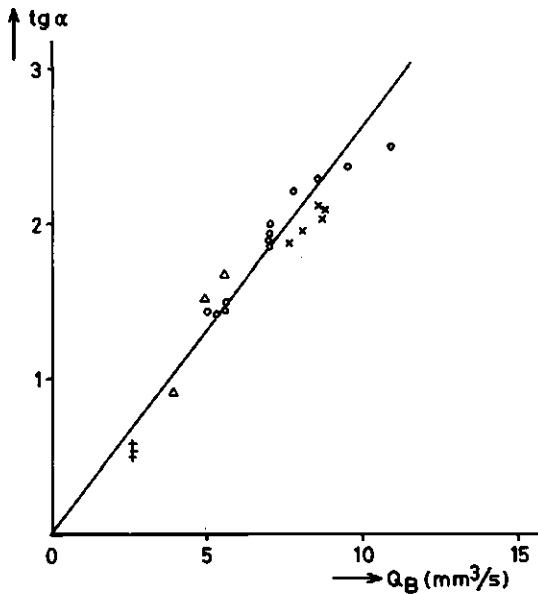


Fig. 2 Plot of  $\text{tg } \alpha$  as obtained with the heat pulse method versus  $Q_B$  as measured with the balance method. See legend of Fig. 1 for other conditions.

As has been stated in Chapter 4 (Section 4.5.2.1) the amount of flowing water  $V$  ( $\text{mm}^3$ ) in the r.f. coil is obtained from the NMR flow measurements by either plotting  $S(t_{\text{max}})$ , the signal height of the maximum, versus  $t_{\text{max}}$  or via a plot of  $\partial[S(t_{\text{max}}) \cdot t_{\text{max}}] / \partial t_{\text{max}}$  versus  $t_{\text{max}}$ . In Fig. 3 the NMR signals of flowing water in the cucumber plant are represented as a plot of  $S(t_{\text{max}})$  vs.  $t_{\text{max}}$ . In this Fig. the difference in  $S(t_{\text{max}})$  between the "lamps off" and "lamps on" data points, as has been observed in a gherkin plant (Chapter 5, Fig. 9) is absent. This may be due to the time lag between the moment of switching the lamps on again and the first flow measurement after switching the lamps on, which has been  $\sim 15$  min. Apart from the data points obtained after cutting off leaves from the stem, denoted with (+) in Fig. 3, the data points show a linear relationship between  $S(t_{\text{max}})$  and  $t_{\text{max}}$ , when plotted in a semilog fashion. Extrapolation of this plot to  $t_{\text{max}}=0$  yields  $S(0)=9\pm 0.5$  (arb. units), which has been found by calibration (Section 6.2.1) to correspond with an amount of flowing water in the coil  $V=3.2\pm 0.4$   $\text{mm}^3$ . Via  $L_{\text{eff}}=7.24$  mm, it is possible to calculate the effective cross-sectional area available for flow via eqn. 6.3, and via eqn. 6.2 the volume flowrate  $Q$ . From eqn. 6.3 we found  $A_{\text{NMR}}=0.44\pm 0.06$   $\text{mm}^2$ .

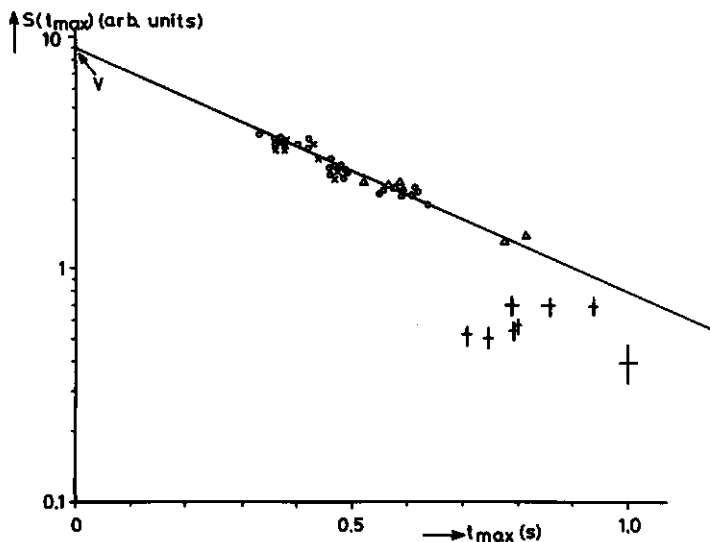


Fig. 3 Semilog plot of  $S(t_{\text{max}})$  vs.  $t_{\text{max}}$  of flowing water in cucumber plant stem as measured with the NMR method.  $V$  denotes the amount or volume of flowing water measured in the r.f. coil. See legend of Fig. 1 for other conditions.

The slope of the plot in Fig. 3 yields a decay time  $T=0.38$  s. In Chapter 4, Section 4.5.2.1 we have pointed out that (i)  $T \approx 3T_2$  if  $T_1 \approx T_2$ , or (ii)  $T=T_2$  if  $T_1 \gg T_2$ , or (iii)  $T_2 < T < 3T_2$  when  $T_1 > T_2$ , where  $T_1$  and  $T_2$  are the spin-lattice and spin-spin relaxation times, respectively. From a plot of  $S(t_{\max}) \cdot t_{\max}$  vs.  $t_{\max}$  (in combination with the value of  $T$ , the decay time obtained from  $S(t_{\max})$  vs.  $t_{\max}$ ) the ratio  $T_1/T_2$  can be estimated from the point where the slope  $\partial[S(t_{\max}) \cdot t_{\max}]/\partial t_{\max}$  becomes zero (Chapter 4, Section 4.5.2.1). For the data of Fig. 3 this point in such a plot is found to be  $\sim 0.5$  s (The curve is rather flat). This value is  $\sim 1.4$  times the decay time  $T$ , indicating that  $T_1 > 2T_2$  and  $T_2$  is therefore only slightly larger than  $T$  (Chapter 4, Section 4.5.2.1). When  $T_1 > 2T_2$  eqn. 6.1 is not longer valid, and  $\bar{v}$  has to be corrected according to the values of  $T_1$  and  $T_2$ . From the above mentioned considerations we estimate  $T_2 \sim 0.4-0.45$  s and  $T_1 \sim 1.0-1.5$  s. Corrections on  $\bar{v}$  in agreement with these values of  $T_1$  and  $T_2$  (see Fig. 11 of Chapter 4) results in Fig. 1 in a transition of the straight line a to b. Line b is given by  $Q_B = 0.49 \bar{v}$ , yielding an effective cross-sectional area for flow  $A_{B-N} \approx 0.49 \text{ mm}^2$ , where B-N denotes that the cross section has been obtained from combined balance and NMR measurements.

The relative large deviation of the data points denoted with (+) in Fig. 1 from line a can be explained using Fig. 3. These points have been obtained by cutting off leaves from the stem. Fig. 3 clearly shows that this results in a decrease of  $S(t_{\max})$  for these points, indicating that at that moment the amount of flowing water in the coil has decreased, due to a decrease in conducting xylem vessels. Thus, the deviation of these points in Fig. 1 from line a reflects a decreased value of the effective cross-sectional area for the flowing water, just as expected.

The microscopically determined cross-section of the xylem vessels yields  $A_m = 0.92 \pm 0.04 \text{ mm}^2$ . Though the distribution of vessel radii at the position of the NMR r.f. coil (Fig. 4) and at the position of the heat sensor are slightly different, the cross-sectional areas are equal within experimental error.

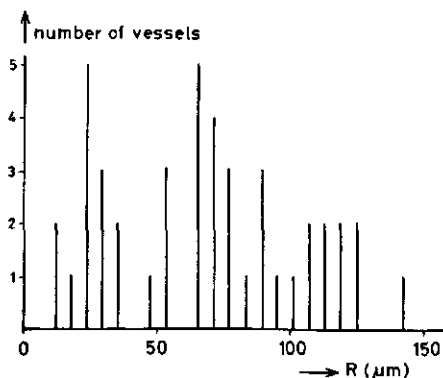


Fig. 4 Distribution of xylem vessel radii in the cucumber plant stem at the position of the NMR r.f. coil.

#### 6.4 DISCUSSION

When we compare the value of the cross-sectional area of the xylem vessels as found from inspection by a microscope ( $A_m = 0.92 \pm 0.04 \text{ mm}^2$ ) with the values of the effective cross-sections as found from  $\bar{v}(Q_B)$  (Fig. 1) ( $A_{B-N} \approx 0.49 \text{ mm}^2$ ) and the value found with NMR alone ( $A_{NMR} = 0.44 \pm 0.06 \text{ mm}^2$ ) we observe good agreement between the latter values, whereas the former is about two times higher. This is not very surprising, because the cross-section for flow may not be the same as the microscopically measured area, due to e.g. a stationary boundary layer of water at the walls of vessels [3], or due to non-conducting vessels [4-8]. The agreement between  $A_{B-N}$  and  $A_{NMR}$  is an argument in favor of the reliability of this value of the effective cross-sectional area available for flow. That  $A_{NMR}$  tends to be slightly lower than  $A_{B-N}$  may be expected from the following considerations: as has been stated in Chapter 5 the value of  $T_2$  of flowing water in a particular xylem element strongly depends on the radius  $R$  of that element; by decreasing  $R$  the value of  $T_2$  will also decrease. This results in a decrease of the height of the NMR signal at  $t_{\max}$ . In addition, when we assume Poiseuille flow, the mean linear flow velocity depends on  $R^2$ . Thus, there is a distribution of values for  $\bar{v}$ , resulting in a spread of  $t_{\max}$  (eqn. 6.1). However, the spread in  $t_{\max}$  is partly compensated by the correlation between  $\bar{v}$  and  $T_2$  via

R: when  $\bar{v}$  is small due to a small value of R,  $T_2$  is decreased and the shift of  $t_{\max}$  to higher values due to smaller  $\bar{v}$  is partly compensated due to the shift in  $t_{\max}$  to lower values by the decrease of  $T_2$  (see Chapter 4, Fig. 11). Indeed, it has been observed that the NMR signals of flowing water in plant stems are hardly broadened with respect to the signals of flowing water in a glass capillary. This may also be caused due to the fact that the volume flowrate Q depends on  $R^4$ , resulting in the largest contribution to the signal of water in the vessels with the largest values of R,  $\bar{v}$  and  $T_2$ .

Comparing the data of Fig. 1 with those of Fig. 2 (keeping in mind that the data points in Fig. 1 have to be considered as grouped around curve b, as argued above), we find a linear relationship between  $\bar{v}$  and  $Q_B$  in Fig. 1, whereas the plot of  $\text{tg } \alpha$  vs.  $Q_B$  exhibits somewhat more scatter, in particular for higher values of  $Q_B$  ( $Q_B > 7 \text{ mm}^3/\text{s}$ ). For these larger values of  $Q_B$  the water flow can be considered as a flow of coolant, resulting in a smaller increase of the magnitude of the heat pulse signal as compared to that at lower flow velocities. Fig. 2 also shows a strong correlation between the relationship of  $\text{tg } \alpha$  and  $Q_B$  and the process by which the flow velocity has been varied. This may be explained by the additional variation in the water content when varying the water flow (see Chapter 5).

The results obtained with the heat pulse method can be presented in terms of time of occurrence of the maximum (b), magnitude of the maximum (c) in the temperature difference or  $\text{tg } \alpha (=b/c)$  [2]. In either case only a relative difference in signal parameter can be achieved. Whether these signal parameters are related to  $\bar{v}$  or Q is presently unclear. By considering the striking agreement in the behaviour of  $\bar{v}$  and  $\text{tg } \alpha$  in Figs. 1 and 2 respectively, at  $Q_B \cong 7 \text{ mm}^3/\text{s}$  and at  $Q_B \cong 5.5 \text{ mm}^3/\text{s}$ , we expect that  $\text{tg } \alpha$  is probably closely related to the linear flow velocity. However, we should note that the heat pulse method generates signals that mainly reflect the water flow in the xylem elements or xylem vessel bundle near the sensor and thus changes in e.g. the effective cross-sectional area and Q are not necessarily reflected by these signals.

## 6.5 ACKNOWLEDGEMENT

We are indebted to Mr. J. Reinders who has performed the NMR experiments and to Mr. J.G. Kornet of the Technical and Physical Engineering Research Service (TFDL), who has performed the heat pulse measurements. The top balance was made available by Dr. H.C.M. de Stigter of the Centre for Agro-Biological Research (CABO). The plant material was a gift of Dr. A.P.M. den Nijs of the Institute of Horticultural Plant Breeding (IVT). The microscope was made available by Dr. R.W. den Outer of the department of Plant Cytology and -Morphology.

## REFERENCES

1. M.A. Hemminga, P.A. de Jager, J. Magn. Reson. 37 (1980), 1.
2. K. Schurer, H. Griffioen, J.G. Kornet, G.J.W. Visscher, Neth. J. Agric. Sci. 27 (1979), 136.
3. B. Huber, in "Handb. Pflanzenphysiol." (W. Ruhland, ed.), Vol. III, p.p. 511-513 (Springer-Verlag, Berlin, 1956).
4. M.H. Zimmermann, C.L. Brown, "Trees: Structure and Function" (Springer-Verlag, New York, 1971).
5. M.H. Zimmermann, J. McDonough, in "Plant Disease" (J.G. Horsfall, E.B. Cowling, eds.), Vol. 3, p.p. 117-140 (Academic Press, London, 1978).
6. M.H. Zimmermann, Can. J. Bot. 56 (1978), 2286.
7. J.A. Petty, J. Exp. Bot. 29 (1978), 1463.
8. A.A. Jeje, M.H. Zimmermann, J. Exp. Bot. 30 (1979), 817.

## BRIEF COMMUNICATION

7. [<sup>1</sup>H]SPIN-ECHO NUCLEAR MAGNETIC RESONANCE  
IN PLANT TISSUE

## I. THE EFFECT OF Mn(II) AND WATER CONTENT IN WHEAT LEAVES

H. VAN AS, W. P. A. VAN VLIET,† AND T. J. SCHAAFSMA, *Department of  
Molecular Physics, Agricultural University, De Dreijen 6, 6700 EP  
Wageningen, The Netherlands*

**ABSTRACT** The effect of age-dependent Mn(II)-gradients, as observed by electron paramagnetic resonance (EPR), on the [<sup>1</sup>H]NMR spin-spin relaxation time ( $T_2$ ) was studied in wheat leaves. A non-exponential  $T_2$  spin-echo decay was always observed, revealing the presence of at least two different fractions of non- (or slowly) exchanging water in the leaves. No effect of the Mn(II)-concentration on  $T_2$  of the separate water fractions (covering ~90% of the total water content) has been found. From these observations we conclude that Mn(II) is present in bound form. The dependence of  $T_2$  on water content can be explained with a two-state model, demonstrating the occurrence of fast exchange within each of the two slowly exchanging water fractions.

## 7.1 INTRODUCTION

Proton-spin-lattice ( $T_1$ ) and Proton-spin-spin ( $T_2$ ) relaxation times have been widely used for the study of the physical properties of water in biological systems (1-4) and a relationship between  $T_1$ ,  $T_2$  and water content has been demonstrated (1, 5, 6, 7). The interpretation of the results is complicated by the complexity of the specimen. The main difficulties arise from the fact that to the measured parameters ( $T_1$ ,  $T_2$ ) contributions may be made by factors not directly related to the physical properties of water. It is well-known, that plants contain Mn(II) and other paramagnetic metalions as a constituent of the photosynthetic unit (8). These paramagnetic centers may shorten the relaxation time of water protons, obscuring the correlation between  $T_1$ ,  $T_2$  and water content.

Fedotov et al. (4) have shown that there is no, or only a small, effect of paramagnetic ions on  $T_1$  of water in intact tissues of bean and crinum leaves, nor is there one in potato tuber. Samuilov et al. (9), using the Overhauser effect have found no effect of paramagnetic ions in seeds of Welsh onions, peas, broad beans and sunflower. According to Hazlewood et al. (2)

†H. van As and T. J. Schaafsma were deeply saddened by the death of W. P. A. van Vliet on July 5, 1980.



the relaxation mechanism in skeletal muscle is insignificantly affected by paramagnetic impurities. Stout et al. (10) suggest, however, that in ivy bark  $T_2$  of extracellular water is shortened by paramagnetic ions in the cell walls. In aqueous suspensions of chloroplasts Wydrzynski et al. (19) concluded that  $T_1$  and  $T_2$  are largely determined by manganese, bound in the chloroplast membrane.

Here, we report the results of measurements on leaves of summer wheat, type SELTEP. Using EPR, we detected Mn(II)-gradients in the leaves, changing sign upon maturation. The effect of these gradients on the spin-spin relaxation time  $T_2$  of tissue water was investigated as a check on the correlation between  $T_2$  and water content. This research is part of a program aimed at the use of spin-echo NMR techniques to measure transport and exchange of water in plant stems (11, 18) and tissues.

## 7.2 MATERIALS AND METHODS

### *Plant Material*

Wheat variety SELTEP, was grown under a 16-h light (23°)/8-h dark (20°C) cycle. No special culture was used. Proton spin-spin relaxation measurements were carried out using leaves in different stages of maturation and at different positions in the plants. Leaves were cut transversally in ~2 cm sections for NMR and EPR measurements. EPR signal amplitudes were not affected by waiting periods of ~2 h after segmentation.

### *EPR Measurements*

Room temperature EPR spectra were obtained using a Varian E-3 spectrometer (Varian Associates, Instrument Div., Palo Alto, Calif.). Samples were contained in a quartz tube, 0.8 mm i.d., permitting reproducible sample positioning. Using standard precautions, the EPR signal amplitude of a 0.175 mM MnCl<sub>2</sub> solution was reproducible within 3%. Instrument settings: 100 kHz modulation amplitude, 10 G; microwave power, 40 mW; time constant, 0.3 s; scan rate, 250 G/min.

### *NMR Measurements*

The experiments were carried out with a home-built 15-MHz spin-echo spectrometer, equipped with a Newport 7-in electromagnet (Newport Laboratories, Inc., Santa Ana, Calif.) (11), a home-made transmitter/receiver coil of the solenoid-type, with a length of 5 mm and a diameter of 11 mm. The spin-spin relaxation time  $T_2$  was measured by the Carr-Purcell-Meiboom-Gill (CPMG) method (12). Because of the inhomogeneity and the size of the samples a time-dependent baseline ("baseline drift") must be expected (13, 14). A first order correction for this phenomena was made by the following pulse sequence:

$$90^\circ - \tau - (-180^\circ - 2\tau)_n - 5T_1 - 90^\circ_x - \tau - (-180^\circ - 2\tau)_n - 5T_1.$$

By subtracting the two CPMG-decays, the effect of missettings in the 180° pulses was diminished. The CPMG  $T_2$  decay was measured by sampling the height of the echoes. The time  $2\tau$  was set on 1.6 ms. A graphical method as outlined by Hazlewood et al. (2) was used to analyze the data. The error in  $T_2$  was evaluated at ±8%. All NMR experiments were made at probe temperature (29°C).

### *Water Content*

Water content was determined by weighing freshly excised samples, drying until constant weight in an oven at 90°C, followed by reweighing.

### *Manganese Determination*

The total manganese content in the wheat leaf segments was determined by atomic absorption spectroscopy. Measurements were made with a Perkin-Elmer HGA-74 type 460 atomic absorption

spectrophotometer (Perkin-Elmer Corp., Instrument Div., Norwalk, Conn.). Dried leaf segments were digested with 100  $\mu$ l concentrated  $\text{HClO}_4$  at  $\approx 150^\circ\text{C}$ . Digested samples were evaporated and dissolved in 100  $\mu$ l concentrated  $\text{HCl}$ . The final volume was brought to 100 ml by adding distilled water. Standards at 0.02, 0.06, and 0.10 ppm Mn were prepared in an acidified water medium.

### 7.3 RESULTS AND DISCUSSION

EPR signals are easily detected in wheat leaves. Two types of spectra can be discerned: (a) a sextuplet hyperfine structure, typical for  $\text{Mn(II)}$ , and (b) a weak peak close to the center of the manganese multiplet.

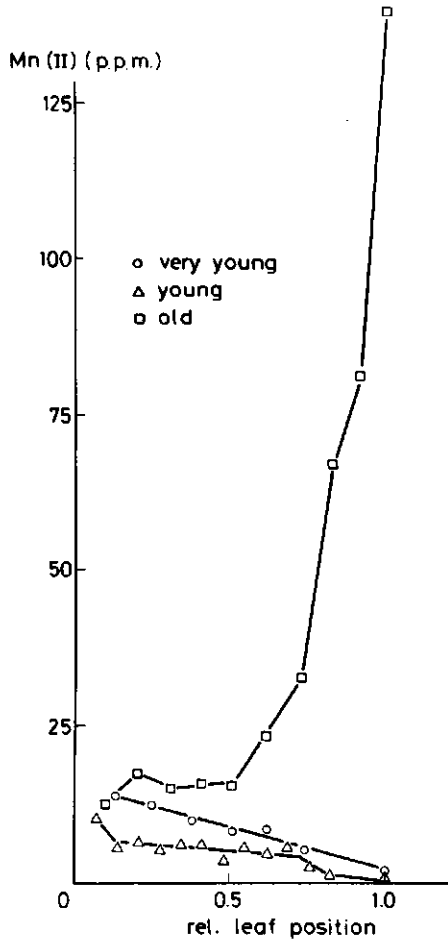


FIGURE 1 Mn(II) in ppm of dry matter vs. the position in the leaf. The relative position is defined as the ratio of the distance from the base of the leaf and the total leaf length. The results are given for three wheat leaves in different stages of maturation: (○) very young, not full-grown (eighth leaf of a total of eight, growth stage of the wheat, after the decimal code of Zadoks et al. (20, 17); (△) young, nearly full-grown (ninth of a total of ten, growth stage 19); (□) old, full-grown (sixth of a total of ten, growth stage 19). Mn(II) is measured by EPR.

Fig. 1 represents the results of Mn(II) EPR measurements for three wheat leaves in various stages of growth. For very young leaves the Mn(II) signal decreases from base to top; upon maturation this Mn(II) gradient reverses sign.

We measured  $T_2$ , Mn(II), and water content of wheat leaves at various positions between the base and the top of the leaf, using spin-echo NMR, EPR, and drying to constant weight, respectively (Fig. 2). Invariably, a nonexponential  $T_2$  decay was observed, indicating that there are several fractions of tissue water with distinguishable  $T_2$ -values. Because of the limited signal-to-noise ratio we have used two water fractions, constituting 90% of the total tissue water for data fitting. The resulting  $T_2$ -values of the two fractions differ by a factor of 3. The ratio between the amplitudes of the slowest and the fastest relaxing water fractions varies from 1 to 2 for young vs. old leaves. Considerable scatter in the  $T_2$ -values of the two separate fractions occurs due to a strong correlation between the fitting parameters (amplitudes and relaxation times). A mean effective relaxation rate  $\bar{R}_2$  is defined by:

$$\bar{R}_2 = P_a T_{2a}^{-1} + P_b T_{2b}^{-1} \quad (1)$$

Here  $P_a$  and  $P_b$  designate the two fractions of tissue water. In solution,  $R_2$  is linearly dependent on the Mn(II)-concentration, but such linear relationship does not obtain in either type of leaf (Fig. 2) for  $R_2$  of the separate fractions.

In older leaves, the sign of the Mn(II) gradient is reversed compared with younger leaves (Fig. 1), but the dependence of the  $\bar{R}_2$  curve on the position in the leaf does not change. Evidently, the effect of the Mn(II) gradient measured by EPR is not reflected in the  $R_2$  values of tissue water determined by NMR. This indicates that Mn(II) is present in bound form inaccessible to water on the timescale of our experiments. This is not in conflict with the fact Mn(II) has been detected by EPR by Meirovitch and Poupko (15) and by other authors. Siderer et al. (16) have observed Mn(II) EPR signals in lettuce chloroplasts similar to our experimental results on intact tissue. Mn(II)-concentrations (Figs. 1 and 2) are calculated from the EPR spectra using aqueous MnCl<sub>2</sub> solutions for calibration. Whether these Mn(II) signals in wheat leaves have the full possible intensity or only 9/35 of the total intensity ( $M_s = \pm 1/2$  transitions) (15, 16) cannot be decided from the observed spectra.

When all manganese is present as Mn(II) in a bound form, allowing the observation of only the  $-1/2 \rightleftharpoons 1/2$  EPR transitions, the amount of manganese deduced from atomic absorption and EPR measurements should be in a ratio of  $\sim 4$ . We observed a ratio of  $\sim 8$ . However, manganese is not necessarily present as Mn(II). In dark-adapted chloroplasts Wydrzynski et al. (19) have found that only part of the bound manganese is present as Mn(II).

Because Mn(II) had no effect on the spin-spin relaxation time of  $>90\%$  of the total water, we will now consider the relationship between  $T_2$  of the water protons and the total water content in the two fractions. Separate  $R_2$ -values for the two fractions indicate that 90% of the total water is present in two slowly exchanging fractions. For a model with two states  $a$  and  $b$ , slow exchange is defined by the condition:

$$\tau_a^{-1} + \tau_b^{-1} \ll (T_{2a}^0)^{-1} + (T_{2b}^0)^{-1}, \quad (2)$$

neglecting the chemical shift difference between the two states;  $\tau_a, \tau_b$  are the lifetimes of water molecules in states  $a$  and  $b$ , and  $T_{2a}^0, T_{2b}^0$  are the spin-spin relaxation times of water in the

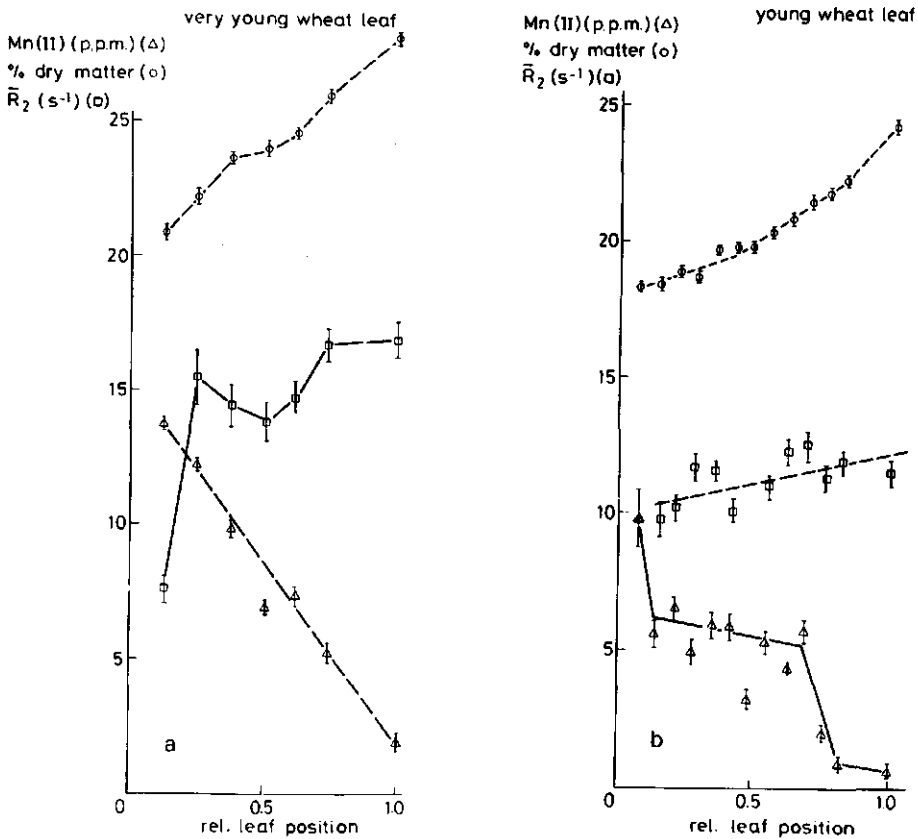


FIGURE 2 Mn(II), percent of dry matter, and spin-spin relaxation rate  $\bar{R}_2$  as function of the leaf position for the very young (a) and the young (b) wheat leaf of Fig. 1. Mn(II) is measured by EPR. The spin-spin relaxation rate is given as the weighted average.

absence of exchange. The existence of fast exchange between two subfractions within each fraction is indicated by the dependence of  $R_2$  on the dry matter/water ratio (Fig. 3).

For a two-state, fast-exchange model (1, 17), the observed single relaxation rate  $R_2$  is the weighted average of the separate rates of two fractions consisting of "bound" and "free" water, yielding:

$$R_2 (\equiv T_2^{-1}) = T_{2f}^{-1} + P_b (T_{2b}^{-1} - T_{2f}^{-1}), \quad (3)$$

where subscripts  $b$  and  $f$  refer to "bound" and "free," respectively;  $P_b$  is the mole fraction of the "bound" fraction. The magnitude of  $P_b$  is proportional to the ratio between the tissue dry weight and the water weight, at least in the high water content region. Thus, in the two-state, fast-exchange model there is a linear dependence of  $R_2$  on the ratio between tissue dry weight

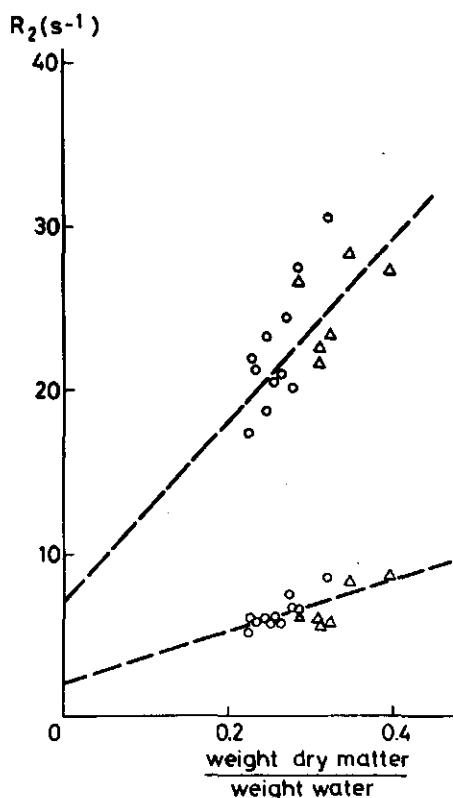


FIGURE 3 Proton relaxation rate  $R_2$  in the wheat leaves of Fig. 2 A ( $\Delta$ ) and B (O) as a function of water content. A nonexponential  $T_2$  decay was observed. The two fractions given here account for >90% of the tissue water.

and water weight in the high water content region as experimentally observed for both separate  $R_2$ s in wheat leaves (Fig. 3).

Therefore, we conclude that >90% of the total water is present in two slowly exchanging fractions within which there are fast-exchanging subfractions. Since the relaxation rate of the separate fractions varies inversely with water content, in this system the water content may be measured using  $T_2$  values. This is not always possible (5) since variations of the exchange rate between different water fractions and of the dry matter structure may disturb the predicted linear dependence of  $R_2$  on the ratio dry tissue weight and water weight.

#### 7.4 CONCLUSIONS

(a) Wheat leaf contains age-dependent Mn(II) gradients. Part of the manganese is observable by EPR. (b) The Mn(II)-concentration does not affect the spin-spin relaxation time  $T_2$  of water fractions representing >90% of the total water content of the leaf. (c) From a and b we conclude that the measured Mn(II) is present in bound form. (d) >90% of the total water is

present in two fractions exhibiting slow exchange on the  $T_2$  timescale. Within these fractions there are fast-exchanging subfractions. (e) The relaxation rate of these two separate fractions varies inversely with water content, in agreement with the predictions from a simple two-state fast-exchange model.

We are indebted to Mr. P. A. de Jager for general technical assistance and to Mr. R. M. J. Penners of the Institute for Atomic Sciences in Agriculture for making available the atomic absorption spectrometer. Stimulating discussions with Mrs. I. van Leeuwen are gratefully acknowledged.

Received for publication 10 June 1980

## REFERENCES

1. COOKE, R., and R. WIEN. 1971. The state of water in muscle as determined by proton nuclear magnetic resonance. *Biophys. J.* **11**:1002-1017.
2. HAZLEWOOD, C. F., D. C. CHANG, B. L. NICHOLS, and D. E. WOESSNER. 1974. Nuclear magnetic resonance transverse relaxation times of water protons in skeletal muscle. *Biophys. J.* **14**:583-606.
3. SAMUILOV, F. D., I. V. NIKIFOROV, and E. A. NIKIFOROV. 1976. Use of nuclear magnetic resonance to study the state of water in germinating seeds. *Fiziol. Rast.* **23**:567-572.
4. FEDOTOV, V. D., F. G. MIPTAKHUTDINOVA, and Sh. F. MURTAZIN. 1969. Investigation of proton relaxation in live plant tissues by the spin-echo method. *Biofizika.* **14**:873-882.
5. FUNG, B. M. 1977. Correlation of relaxation time with water content in muscle and brain tissues. *Biochim. Biophys. Acta.* **497**:317-322.
6. BAČIĆ, G., B. BOŽOVIĆ, and S. RATKOVIĆ. 1978. Proton magnetic relaxation in plant cells and tissues: effect of external ion concentration on spin-lattice relaxation time ( $T_1$ ) and water content in primary roots of *Zea mays*. *Studia Biophysica.* **70**:31-43.
7. RAAPHORST, G. P., P. LAW, and J. KRUIV. 1978. Water content and spin-lattice relaxation times of cultured mammalian cells subjected to various salt, sucrose, or DMSO solutions. *Physiol. Chem. Phys.* **10**:177-191.
8. HOFF, A. J. 1979. Applications of ESR in photosynthesis. *Phys. Rep.* **54**:75-200.
9. SAMUILOV, P. D., V. N. FEDOTOV, V. I. NIKIFOROVA, B. M. OHINTSOV, and E. A. NIKIFOROV. 1975. Study of the effect of paramagnetic impurities on relaxation of protons of tissue water with the use of the Overhauser effect. *Dokl. Akad. Nauk. SSSR.* **224**:730-732.
10. STOUT, D. G., P. L. STEPONKUS, and R. M. COTTS. 1978. Nuclear magnetic resonance relaxation times and plasmalemma water exchange in ivy bark. *Plant Physiol.* **62**:636-641.
11. HEMMINGA, M. A., P. A. DE JAGER, and A. SONNEVELD. 1977. The study of flow by pulsed nuclear magnetic resonance. I. measurements of flow rates in the presence of a stationary phase using a difference method. *J. Magn. Reson.* **27**:359-370.
12. MEIBOOM, S., and D. GILL. 1958. Modified spin-echo method for measuring nuclear relaxation times. *Rev. Sci. Instrum.* **29**:688-691.
13. VOLD, R. L., R. R. VOLD, and H. F. SIMON. 1973. Errors in measurements of transverse relaxation rates. *J. Magn. Reson.* **11**:283-298.
14. HUGHES, D. G., and G. LINDBLOM. 1977. Baseline drift in the Carr-Purcell-Meiboom-Gill pulsed NMR experiment. *J. Magn. Reson.* **26**:469-479.
15. MEIROVITCH, E., and R. POUPKO. 1978. Line shape studies of the electron spin resonance spectra of manganese protein complexes. *J. Phys. Chem.* **82**:1920-1925.
16. SIDERER, Y., S. MALKIN, R. POUPKO, and Z. LUZ. 1977. Electron spin resonance and photoreaction of Mn(II) in lettuce chloroplasts. *Arch. Biochem. Biophys.* **179**:174-182.
17. ZIMMERMAN, J. R., and W. E. BRITTIN. 1957. Nuclear magnetic resonance studies in multiple phase systems: lifetime of a water molecule in an adsorbing phase on silica gel. *J. Phys. Chem.* **61**:1328-1333.
18. HEMMINGA, M. A., and P. A. DE JAGER. 1980. The study of flow by pulsed nuclear magnetic resonance. II. Measurements of flow velocities using a repetitive pulse method. *J. Magn. Reson.* **37**:1-16.
19. WYDRZYNSKI, T. J., S. B. MARKS, P. G. SCHMIDT, GOVINDJEE, and H. S. GUTOWSKY. 1978. Nuclear magnetic relaxation by the manganese in aqueous suspensions of chloroplasts. *Biochemistry.* **17**:2155-2162.
20. ZADOKS, J. C., T. T. CHANG, and C. F. KONZAK. 1974. A decimal code for the growth stages of cereals. *Weed Res.* **14**:415-421.

## 8 APPLICATION OF NMR FLOW MEASUREMENTS

Based on the results reported in Chapters 4-7, we suggest for the combination of the pulsed NMR measurements of flow and water content the following applications in agriculture and in particular horticulture for use as:

- controlling device for irrigation of cropfield and glasshouse cultures.
- warning device for development of stress phenomena due to drought, frost or diseases.
- monitoring device for screening in plant breeding experiments to select plants with low energy (low temperature) or low water requirements.
- laboratory device for, e.g. study of the water balance in relation to the effects of environmental factors and study of the blocking phenomenon of water transport in cut-flowers, relevant to tenability.

In all these cases the water flow in the stem xylem vessels can serve as a parameter for characterizing the water uptake, transport and storage (fructification).

The results discussed in Chapters 4-7 have been obtained with a home-built NMR spectrometer, operating at 15 MHz, and equipped with an air-cooled electromagnet with a square yoke (total weight  $\pm$  200 kg), and either a single solenoid or Helmholtz r.f. coil. The working dimensions determined by magnet and coil dimensions permit the use of objects with  $\leq$  15 mm cross-section.

In view of the applications suggested above, a more practical NMR instrument should be:

- portable for horticulture and field applications. This can be achieved by using small permanent magnets (e.g. [1]), keeping in mind, however, that the water protons must be able to have reached Boltzmann equilibrium before entering the r.f. coil (Section 4.5.2.1). For parameter settings see Section 4.5.3.

- able to measure  $T_2$  as well as flow velocities. This requires two different trains of pulses, which only differ in the first pulse.
- able to compensate for drift. This can be achieved by making use of the response of the off-resonance signal of stationary water (Section 4.5.2.2).

The method has some distinct advantages also in medical applications, in comparison with existing NMR methods measuring blood-circulation (see Section 3.5.1 and 3.5.2). The main advantage is that the method is insensitive for a large amount of stationary tissue water. Preliminary results of steady-state measurements in fingers of adults have shown the following results:

- the method is sensitive enough to measure the effect of the two-chamber heart contraction in the profile of the NMR signal (see Fig. 1).

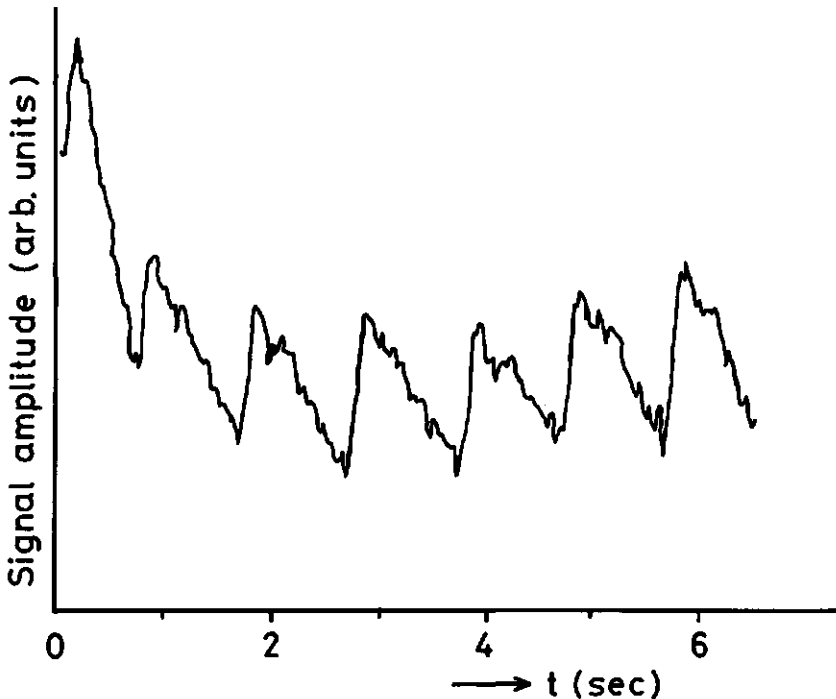


Fig. 1 NMR signal of pulsed blood flow in finger of adult during the first seconds after starting a  $(\pi-\tau)_n$  pulse-train. Note structure of heart-beat signal and the shape of the back-ground curve, which is similar to that of steady-state flow. (See e.g. Fig. 5, Chapter 5). This signal may also be due to stationary water in finger-tissue, observed off-resonance (Section 4.5.2.2).



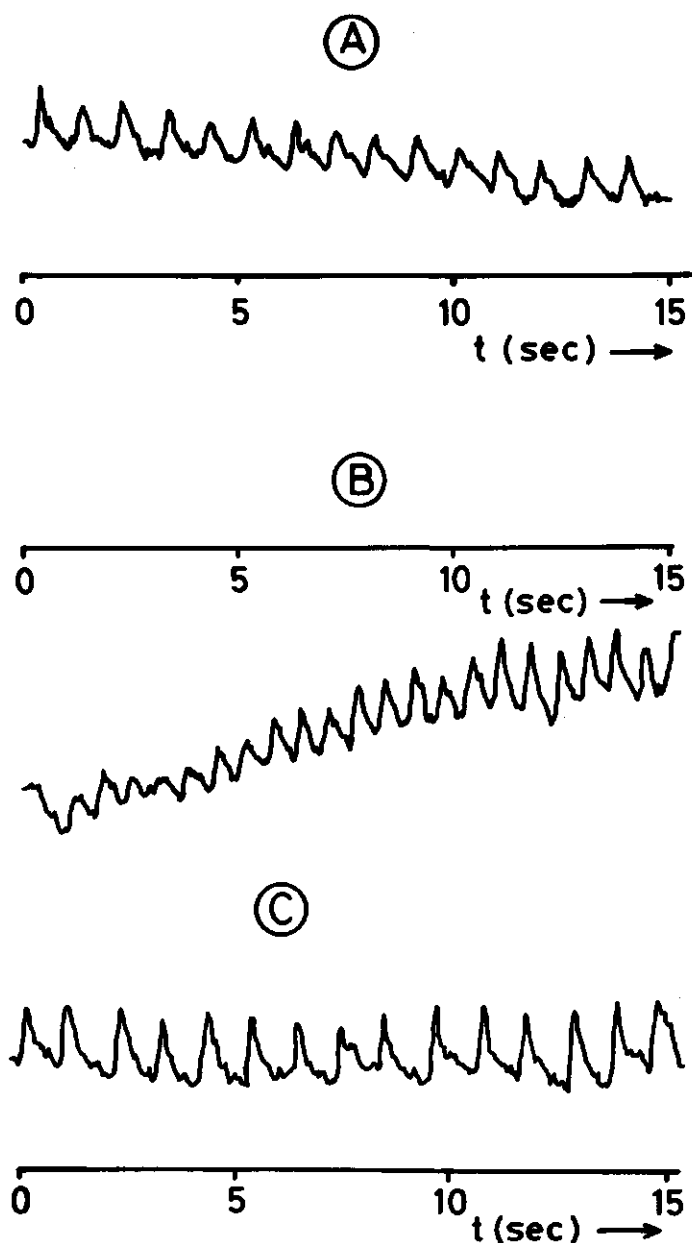


Fig. 2 A Steady state  $^1\text{H}$  pulsed NMR signals of blood flowing through index finger of adult, obtained by a pulse sequence of equidistant  $\pi$  pulses in combination with a linear magnetic gradient in the direction of flow. Time  $t=0$  coincides with the  $n^{\text{th}}$  pulse, where  $n > 4000$ .

B Same signal after 10 times knee-flexing. The DC-level changes sign due to change in net flow and/or blood oxygenation.

C Same signal as in B after  $1\frac{1}{2}$  min. resting period.

- as shown in Fig. 2, both heart-beat frequency, net flow and flow during a heart-cycle can be measured. Changes in net flow and/or blood oxygenation cause an off-set in DC-level, observed when comparing Fig. 2A and B.
- since oxygenation results in changes in  $T_2$  of blood [2], which in its turn affects the steady state level of the flowing fluid signal, effects of e.g. breathing and smoking have easily been detected.
- since the  $T_2$  of the fluid is strongly related to the vessel radius, physiological processes resulting in a change of R will be detectable. This applies to defects in the blood circulation system.

In addition, the pulsed NMR method to measure flow as used in this Thesis [3] can easily be combined with the "sensitive-line" imaging method [4] to measure spatially resolved flow patterns in various objects.

Obviously, for medical applications, the NMR method would be of considerably more interest if the instrument would permit the use of objects with large diameters. Preferably the magnet gap should admit legs and arms. This does not seem to prevent application in the medical field, since instruments would be laboratory-bound.

#### REFERENCES

1. J.G. Shanks, F.-D. Tsay, W.K. Rhim, Am. J. Phys. 48 (1980), 620.
2. K.R. Thulborn, J.C. Waterton, P. Styles, G.K. Radda, Biochem. Soc. Trans. 9 (1981), 233.
3. M.A. Hemminga, P.A. de Jager, J. Magn. Reson. 37 (1980), 1.
4. W.S. Hinshaw, P.A. Bottomley, G.N. Holland, Nature 270 (1977), 722.

## SUMMARY

This Thesis describes the application of a non-destructive pulsed proton NMR method mainly to measure water transport in the xylem vessels of plant stems and in some model systems. The results are equally well applicable to liquid flow in other biological objects than plants, e.g. flow of blood and other body fluids in human and animals (Chapter 8). The method is based on a pulse sequence of equidistant  $\pi$  pulses in combination with a linear magnetic field gradient G.

Following a general introduction and a survey of the properties of water in plants (Chapters 1 and 2), the basic NMR theory as well as reviews on the application of pulsed NMR to the determination of flow, diffusion and water content are presented in Chapter 3.

A mathematical treatment has produced analytical expressions for the shape of the signal  $S(t)$ , based on a model in which the flowing fluid is thought to receive a  $\frac{1}{2}\pi - \tau - (\pi - \tau)_{n-1}$  pulse train: a  $\frac{1}{2}\pi$  pulse upon entering the r.f. coil followed by a sequence of equidistant  $\pi$  pulses until the fluid leaves the coil; simultaneously, this movement of the fluid along a magnetic field gradient applied in the direction of flow produces a phase shift of the nuclear magnetization with respect to the rotating frame of reference (Chapter 4). Although this model does not lead to perfect agreement between the experimental and theoretical signal shape  $S(t)$ , it correctly predicts the effects of experimental parameters on  $S(t)$  via analytical expressions. The main results from this theoretical treatment in combination with computer simulations, which have been experimentally verified in glass capillary systems, are:

- as long as  $T_2 \geq \frac{1}{2}T_1$ , the mean linear flow velocity  $\bar{v}$  can be found from the time  $t_{\max}$  at which a maximum appears in the signal shape:  $\bar{v} = C/t_{\max}$ , where C is a calibration constant, depending on G,  $\tau$  and the flow profile. If  $T_2 < \frac{1}{2}T_1$   $\bar{v}$  can only be reliably determined when both  $T_1$  and  $T_2$  of the flowing fluid are known.
- $T_2$  and the amount of flowing water in the coil V, and consequently the volume flowrate Q, can be determined from the height of the maximum  $S(t_{\max})$  and  $t_{\max}$ . Depending on the value of  $T_2$  and the value of the ratio  $T_1/T_2$ ,  $T_2$  and V are found from a semilog plot

of either  $S(t_{\max})$  vs.  $t_{\max}$  ( $T_1 \gg T_2$ ) or  $\partial[S(t_{\max}) \cdot t_{\max}] / \partial t_{\max}$  vs.  $t_{\max}$  ( $T_1 \approx T_2$ ).

Based on flow measurements in plant stem segments (Chapter 5) it has been suggested that  $T_2$  strongly depends on the vessel diameter for the narrow xylem capillaries. This behaviour of  $T_2$  can explain negative results in plant stems with small vessel diameter. Under the present experimental conditions the method has been successfully applied to Cucurbitaceae (cucumber, gherkin, pumpkin) and tomato plants.

$T_2$  measurements in wheat leaves have been shown to be insensitive to the presence of cell-bound paramagnetic ions (Chapter 7). The magnitude of  $T_2$  of two separate water fractions (covering ~90% of the total water content) has been found to be inversely proportional to water content. Measurements of flow and water content have been combined for an intact gherkin plant (Chapter 5), demonstrating that the combination of both NMR methods results in a powerful non-invasive method to study important parts of the plant water balance simultaneously. The results strongly suggest that the method can be used as an early warning for development of stress phenomena in plants, due to drought and other factors. From the flow measurements it has been shown how in a plant system the values of  $T_2$  and  $T_1$  of the water in the xylem vessels can be determined and estimated, respectively.

A comparison between the results obtained with NMR, heat pulse and weight balance flow measurements is presented in Chapter 6. A linear relationship between the linear flow velocity obtained by NMR and the volume flowrate determined by the balance method yields an effective cross-sectional area available for flow of ~50% of the cross-sectional area of the xylem vessels measured by using a microscope. NMR measurements alone yield a slightly lower value of the effective cross-sectional area. Compared with the NMR method, the heat pulse method monitors only relative changes in the flow velocity. A plot of the flow velocity obtained by the heat pulse method versus the volume flowrate obtained by the balance method exhibits some unwanted experimental scatter.

Chapter 8 suggests some applications of the pulsed NMR flow method, also to other systems than plants, and defines important instrumental requirements for these applications.

## SAMENVATTING

In dit proefschrift wordt een niet-destructieve proton puls NMR-methode beschreven, voor de meting van met name het watertransport in het xyleem van plantestengels en in modelsystemen van een plant. De methode is even goed toe te passen op de meting van vloeistofstroming in andere biologische systemen dan planten, b.v. stroming van bloed en andere lichaams-vloeistoffen in mens en dier (hoofdstuk 8). De methode is gebaseerd op een pulstrein van equidistante  $\pi$  pulsen in combinatie met een lineaire magneetveldgradient  $G$  in de stroomrichting.

Na een algemene inleiding (hoofdstuk 1) en een overzicht van de fysisch-chemische eigenschappen van water in planten (hoofdstuk 2) wordt in hoofdstuk 3 de theorie van puls NMR behandeld. Dit hoofdstuk bevat tevens een bespreking van de tot nu toe bekende puls NMR-methoden om stroming, diffusie en watergehalte in biologische systemen te meten.

Analytische uitdrukkingen voor de vorm van het NMR signaal  $S(t)$  werden verkregen uitgaande van een model waarin de stromende vloeistof de pulstrein  $\frac{1}{2}\pi - \tau - (\pi - \tau)_n$  ondervindt, zodanig dat de vloeistof een  $\frac{1}{2}\pi$  puls ondervindt op het moment dat het de r.f. spoel instroomt, gevolgd door een reeks  $\pi$  pulsen totdat de vloeistof de spoel verlaat; gelijktijdig heeft de stroming van de vloeistof in de richting van de magnetische veldgradient tot gevolg dat er een fase verschuiving ontstaat van de magnetisatie ten opzichte van het roterend assenstelsel (hoofdstuk 4). Hoewel dit model niet tot volmaakte overeenstemming leidt tussen de experimentele en theoretische vorm van de signalen  $S(t)$ , voorspellen de analytische uitdrukkingen wél goed de effecten van de experimentele parameters op  $S(t)$ . De voornaamste resultaten, die ook experimenteel in glascapillair systemen zijn geverifieerd, uit deze theoretische behandeling in combinatie met computersimulaties zijn:

- zolang  $T_2 \geq \frac{1}{2}T_1$ , kan de gemiddelde lineaire stroomsnelheid gevonden worden uit  $t_{\max}$ , de tijd waarop het signaal een maximum bereikt, via  $\bar{v} = C/t_{\max}$ , met  $C$  een calibratieconstante die van  $G$ ,  $\tau$  en het stromingsprofiel afhangt. Indien  $T_2 < \frac{1}{2}T_1$  kan  $\bar{v}$  alleen betrouwbaar

bepaald worden als zowel  $T_1$  als  $T_2$  van het stromende water bekend zijn.

- $T_2$  en de hoeveelheid stromend water in de spoel  $V$ , en dus ook de volumesnelheid  $Q$ , worden gevonden uit de hoogte van het maximum,  $S(t_{\max})$ , en  $t_{\max}$ . Afhankelijk van de waarde van zowel  $T_2$  als de verhouding  $T_1/T_2$ , worden  $T_2$  en  $V$  gevonden door middel van een semilogaritmische grafiek van of  $S(t_{\max})$  tegen  $t_{\max}$  ( $T_1 \gg T_2$ ) of  $\partial[S(t_{\max}) \cdot t_{\max}] / \partial t_{\max}$  tegen  $t_{\max}$  ( $T_1 \cong T_2$ ).

Gebaseerd op stromingsmetingen in segmenten van plantestengels is verondersteld dat de waarde van  $T_2$  van het stromende water sterk afhankelijk is van de diameter van de xyleemvaten (hoofdstuk 5). Deze afhankelijkheid kan een verklaring zijn voor de negatieve resultaten die in stengelsegmenten met kleine vatdiameter zijn gevonden. Onder de huidige experimentele gegevens is de methode tot nu toe met succes toegepast in Cucurbitaceae (komkommer, augurk, pompoen) en tomatenplanten.

In het blad van tarweplanten is gevonden dat de  $T_2$  van het celwater onafhankelijk is van celgebonden paramagnetische ionen (hoofdstuk 7). Voor twee afzonderlijke waterfracties ( $\pm 90\%$  van het totale watergehalte vertegenwoordigend) is gevonden dat de waarde van  $T_2$  omgekeerd evenredig is met het watergehalte. Dit stelt ons in staat om niet-destructief veranderingen in het watergehalte te volgen. Metingen van stroming en watergehalte m.b.v. twee verschillende pulstreinen zijn aan éénzelfde intacte plant (augurk) uitgevoerd (hoofdstuk 5). Uit de resultaten van deze metingen blijkt dat de combinatie van deze twee NMR methoden veelbelovende perspectieven biedt om belangrijke onderdelen van de waterbalans van een plant gelijktijdig te bestuderen op een wijze die de plant niet beïnvloedt. Er zijn bovendien sterke aanwijzingen dat de methode gebruikt kan worden om het ontstaan van stress situaties - b.v. ten gevolge van droogte of andere factoren - in de plant vroegtijdig te signaleren. Met behulp van deze stromingsmetingen wordt tevens aangetoond hoe de waarden van  $T_2$  en  $T_1$  van het xyleem water in een plant respectievelijk kunnen worden bepaald en afgeschat.

In hoofdstuk 6 worden de resultaten van stromingsmetingen verkregen met NMR-, warmtepuls- en balansmethoden vergeleken. Van het lineaire verband tussen de lineaire stroomsnelheid (bepaald met behulp van NMR) en de volumesnelheid (verkregen met behulp van de balansmethode)

werd het effectieve oppervlak van de dwarsdoorsnede, dat beschikbaar is voor stroming, bepaald. Dit oppervlak bleek ~50% te zijn van het oppervlak van de xyleem vaten gezamenlijk zoals gemeten met een microscoop. De NMR resultaten alleen leverden een iets lagere waarde op voor de effectieve dwarsdoorsnede van de vaten. In tegenstelling tot de NMR methode meet de warmtepuls methode alleen relatieve veranderingen in de stroomsnelheid. Een grafiek van de stroomsnelheidsveranderingen gemeten met de warmtepuls methode uitgezet tegen de volume snelheid verkregen m.b.v. de balansmethode, vertoont een onverwachte sterke mate van spreiding van de experimentele meetresultaten.

Hoofdstuk 8 bevat een opsomming van enige mogelijke toepassingen van de puls NMR-methode, zowel in de land- en tuinbouw als in de medische sfeer. Tevens worden in dit hoofdstuk een aantal belangrijke instrumentele eisen voor deze toepassingen geformuleerd.

*CURRICULUM VITAE*

Hendrik Van As werd op 12 september 1952 te Huizen (N-H) geboren. In 1968 behaalde hij het MULO-B diploma aan de Christelijke ULO-school Groen van Prinsterer te Huizen en in 1970 het HBS-B diploma aan het Bijzonder Willem de Zwijger Lyceum te Bussum. Hetzelfde jaar begon hij de studie scheikunde aan de Vrije Universiteit te Amsterdam. Na het afleggen van het kandidaatsexamen S2 in 1973, bereidde hij zich bij de vakgroep Fysische Chemie, afdeling Spectroscopie van prof.dr.ir. C. MacLean, o.l.v. dr. J. Bulthuis voor op het doctoraal-examen. In het kader van het bijvak Klinische Chemie werd een 6-maands doctoraal onderzoek verricht aan het Academisch Ziekenhuis te Utrecht. Na het behalen van het doctoraal-examen in december 1976, trad hij op 1 januari 1977 in dienst bij de Stichting Zuiver Wetenschappelijk Onderzoek. Hij werd te werk gesteld aan de Landbouwhogeschool te Wageningen bij de vakgroep Moleculaire Fysica. Op 1 januari 1978 kwam hij voor hetzelfde onderzoek in dienst van de Landbouwhogeschool. Naast het in dit proefschrift beschreven onderzoek had hij als onderwijstaak het leidinggeven aan de practica Chemische Binding en Molecuulspectroscopie.

Met steun van de Stichting Technische Wetenschappen hoopt hij soortgelijk onderzoek voort te zetten bij de vakgroep Moleculaire Fysica.